Università degli Studi di Bari Aldo Moro

DIPARTIMENTO INTERUNIVERSITARIO DI FISICA
Corso di Laurea in Fisica Teorica

Tesi di Laurea

PHASE TRANSITIONS IN AN ACTIVE DUMBBELL SYSTEM

Relatore:
Chiar.mo Prof.
Giuseppe Gonnella

Laureando:
Pasquale Digregorio

Anno Accademico
2015/2016

A Domenico
A papà, mamma ed Alessandro

Introduction

It is understandably frequent to find in the recent-years statistical mechanics literature that "there are many reasons for studying nonequilibrium phase transitions. First and foremost, equilibrium in nature is more of an exception than the rule, and structural changes (which constitute a significant portion of interesting phenomena) usually take place in nonequilibrium conditions. Thus there is much to be learned about the complex ordering phenomena occurring far from equilibrium."
Despite their fundamental role, a general understanding of the physics of nonequilibrium systems and how phase transitions occur in these systems still lack. Although there is no complete languages for the description of out-of-equilibrium phenomena, many statistical mechanics tools exist, that provide useful opportunities to investigate and describe the behavior of various interesting nonequilibrium features.

Active matter encloses a large class of condensed matter systems, whose constituents consume energy from their environment and use it to displace. This class of systems thus inherently belongs to the out-of-equilibrium purview, and is recently became a topic of intense research for various reasons. Active systems undergo a plurality of new nonequilibrium phenomena, like swimming and clustering, and then provide stuff for a phenomenological description of such features, and for the building of a right theoretical framework for the description of nonequilibrium systems. Moreover active matter, due to the ability of its constituents to move by themselves, often represents a fundamental tool to mimic the collective features of living matter, and allows to deeper understand some of the most intriguing characteristics of living systems.

This thesis follows to numerous studies by Gonnella G., Cugliandolo L.F., Suma A. *et al.* about an interesting model of active matter, whose constituents are auto-propelled dumbbells. Such set of works still leaves some fundamental open question about the phase separation phenomenon that, as in many other active systems, results from the aggregation of the motile dumbbells and the formation of large cluster that stabilize in the

system and eventually rotate. We are interested in a deeper description of the aggregation mechanism, using the language of the disorder-order transitions.
The questions that we will try to answer throughout this thesis are the following ones.
Firstly considering the passive dumbbell system, we will search for a confirmation of some new interesting results, existing for the phase transition scheme of hard-disk systems. In particular, we will investigate about the first-order character of the order-disorder transition, and about the possibility for a coexistence region of the phase-space to exist. We aim thus to relate two different phase separation phenomena: the equilibrium phase separation that settles in the coexistence region for the passive system and the non-equilibrium phase separation induced in the system by the activity.
Furthermore, we aim to understand, at least qualitatively, whether self-propelled dumbbells are allowed to crystallize in an ordered phase, despite the fact that energy is injected incessantly in the system and, if so, how the activity modifies the passive phase transition ordering scenario.
The thesis is organized as follows:

- In the first two chapters we will widely describe active matter, its phenomenology, its experimental usefulness, and the theoretical frameworks according to which active systems are used to be described.
  In the first chapter, we will illustrate which are the distinctive traits that join active matter with systems of living components, within a wide domain of sizes, from bacterial colonies, to insects, bird flocks, fish schools, up to mammals. Then we will outline how active systems can be realized with non-living components that are able to move by themselves, directly extracting energy from the environment.

- In the second chapter we will present three different approaches to the study of active matter: a field-theory approach where the evolution of coarse-graining fields (like density or velocity fields) is considered within a fluid dynamics or kinetic context; an "agent-based" approach in which single active particles evolve with a generalized Brownian dynamics; a hydrodynamic approach that investigates the microscopic interactions of the bodies with the environment, directly dealing with the causes of the active motion.
  The purpose of this first two chapters is to provide an exhaustive

physical frame concerning active matter, in order to present our active dumbbell system within the right perspective.

- In the third chapter we will give a detailed description of the dumbbell model. A summary of the works mentioned before will be made and the main characteristics of the dumbbell system will be outline. A great variety of fascinating behaviors have been found for such system, i.e. very rich translational and rotational diffusive behavior [SGL+14, CGS15], singular behavior of active work fluctuations, motility-induced phase separation and non-trivial cluster dynamics [SGMO14]. Some of the these properties, that are believed to avail to our purposes, will be summarized.

- Finally, in the last two chapters, will be presented the results from Brownian dynamics computer simulations for the passive dumbbell system and its active counterpart. The numerical methods used for the simulation and for the analysis of the data will be described with details and the results will be largely discussed. By means of the results of the simulations, we will delineate a complete phase diagram for the active system in the Pe-ϕ parameter space.

Acknowledgments

Il lavoro svolto in questa tesi nasce, alla luce dei risultati trovati fin ora per i sistemi di dumbbell passive interagenti, dalle discussioni con la Prof.ssa Laticia F. Cugliandolo (*Université Pierre et Marie Curie*, Paris VI), alla quale, perciò, voglio rivolgere un sentito ringraziamento. Il frutto di questo lavoro si deve anche al continuo confronto con la Prof.ssa Cugliandolo, ai suoi suggerimenti e all'impegno diretto che ha dedicato al proseguimento di questa attività di tesi.

Rivolgo un sentito ringraziamento al Dott. Antonio Suma (*SISSA*, Trieste). Oltre ad aver fornito tutto il materiale di partenza da cui abbiamo prodotto i codici numerici per le simulazioni condotte e ad aver messo a disposizione la sua competenza per l'utilizzo dei programmi paralleli di simulazione, ha rappresentato per me un aiuto indispensabile. Devo anche ad Antonio e al confronto costante con lui una sostanziale parte delle cose che ho imparato durante il lavoro di tesi.

Ringrazio infine calorosamente il Prof. Giuseppe Gonnella, relatore di questa tesi. Il suo straordinario impegno e la sua competenza sono state senza dubbio il cardine di questo lungo lavoro. I motivi per cui voglio ringraziarlo però vanno ben oltre tutto ciò. Il Prof. Gonnella è stato un amico e un compagno di viaggio, il cui affetto e la cui attenzione hanno contribuito a rendere il mio percorso universitario un'esperienza insostituibile. Voglio infine ringraziarlo ancora una volta e chiedergli scusa per i continui ritardi, le scadenze mancate e i consigli ignorati. Credo che anche ora, mentre scrivo queste righe, ci sia qualcosa da dovergli mandare, un'altra consegna che arriverà, ancora una volta, in ritardo. Grazie.

Contents

Introduction **v**

Acknowledgments **ix**

1 Active Matter systems **1**
1.1 Living systems 2
1.2 Self-propelled particles 5

2 Modeling Active Matter **9**
2.1 Continuous models and active fluids 11
2.2 Molecule models and mesoscale description 17
2.3 Microscopic dynamics 23

3 The active dumbbell system **29**
3.1 Langevin equations for a single dumbbell 30
3.1.1 A single passive dumbbell 31
3.1.2 How activity enters in the model 35
3.2 Numerical integrator for the Langevin equation 38
3.3 Collective behavior of a homogeneous active dumbbell system 39
3.3.1 MIPS for the dumbbells 40

4 Phase transitions in the passive dumbbell system **47**
4.1 No long-range order in one and two dimensions 47
4.2 Melting scenarios for two-dimensional systems 49
4.2.1 Observables and correlations for the KTHNY melting scenario 51
4.2.2 Two-step first order melting for hard disks 53
4.3 Observables for the dumbbell system 57
4.3.1 Voronoi diagram 57
4.3.2 Local hexatic order 59
4.3.3 Large systems simulation methods 61

4.4 Passive WCA-interacting dumbbells 62
4.4.1 Disordered liquid phase 65
4.4.2 Ordered phase 65
4.4.3 First evidences of liquid-hexatic coexistence 68

5 Phase coexistence in passive and active dumbbell system 73
5.1 Coexistence in passive Mie-interacting dumbbells 74
5.1.1 Passive two-step phase transition 78
5.2 Crystallization in active dumbbells 80
5.2.1 Effects of the activity 81
5.3 Low-density limit of the phase separation region 84
5.4 High-density limit of the phase separation region 88
5.5 Phase diagram 89

Conclusions and perspectives 91

A Two-dimensional positional order 93

Bibliography 97

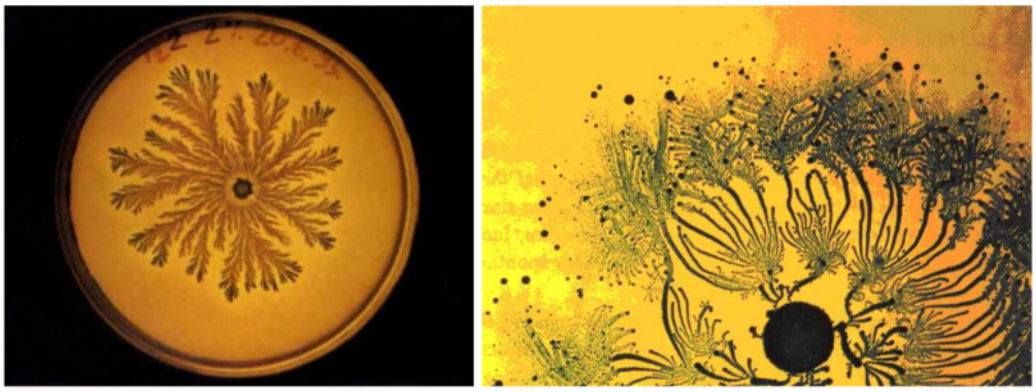
Chapter 1

Active Matter systems

The word *active matter* has become a widely used term to refer to all physical systems in which the constituents are able to displace themselves, extracting the energy for their motion from either internal energy reservoir or external surroundings. A collection of self-propelled particles is intrinsically out-of-equilibrium. However, a subtle difference exists between active matter and classical thermodynamic non-equilibrium systems in how non-equilibrium takes place. In the latters there are specific boundary conditions or external fields that settle, and drive the system out of thermodynamic equilibrium, whereas in active systems non-equilibrium arises at the level of each single active component of the system.

Under the name of active matter is included a large class of systems, mostly in the realm of living organisms, and chemical or mechanical imitations. One of the fundamental ingredients of "activity" is the autopropulsion, and organisms at all lengthscales (from bacteria to birds and fishes) display mechanisms of propulsion of great variety, complexity and beauty. In this chapter and in the following one we mainly review some of these interesting mechanisms that characterize activity in various type of systems, and we describe them from a phenomenological point of view.

For active systems, however, the details of the propelling device are not the single object of study. Researchers are interested as well in the singular collective properties of systems of many self-propelled particles. The most common phenomena observed in active systems is one or more ordering transitions, and, more interesting relative to this work, various aggregation phenomena. These transitions, typically toward a polar or nematic order, occur when parameters such as propulsion velocity or particle density are changed. Beside the description of the main features of active systems, we will then summarize in the present chapter the phenomenology of such phenomena.



(a) (b)

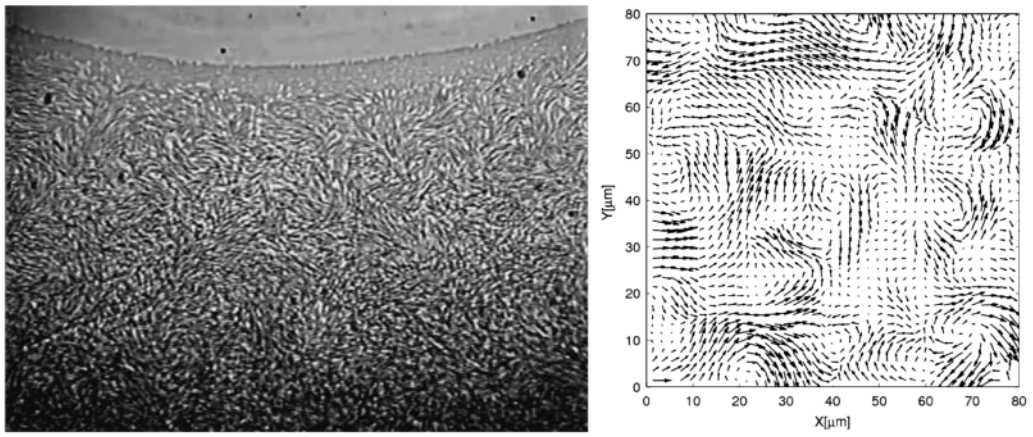
Figure 1.1: (a) - Pattern of colonies grown on a substrate. The *peptone* level (the food) is lowered here from a standard concentration. As the peptone level is decreased, the pattern become more ramified and presents a fractal structure. (b) - A typical colony of *vortex* pattern in a *Bacillus subtilis* colony. The black disks contain thousands of bacteria circling together as the disks themselves glide outward on the surface during colony growth. From [BJST+94]

1.1 Living systems

Living systems, of course, provide the preeminent example of active matter, exhibiting extraordinary properties such as reproduction, adaptation, spontaneous motion, and dynamical organization, including the ability to generate and to respond in a calibrated manner to forces. Moreover it seems that collective motion is displayed by almost every living system consisting of at least dozens of units. The kinds of systems and the types of collective motion patterns have a great variety.

Bacterial colonies

Microorganism colonies, such as bacteria colonies, are one of the simplest systems consisting of many interacting organisms, yet exhibiting a non-trivial macroscopic behavior.
The first works attempting to quantitatively study experimental aspects of colony formation and on related collective behavior is the work of Ben-Jacob *et al.* [BJST+94]. During this investigations, and in the related ones, it has become evident that collective organization in growing colonies of *Bacillus subtilis* is driven by some ambient control parameters. Under standard favorable conditions, colonies do not exhibit a high level of organization. However, as the conditions on the growing surface change, for



(a) (b)

Figure 1.2: (a) - *Bacillus subtilis* cells concentrated at a sloping water-air interface. Near the top of the image bacteria have accumulated. Toward the bottom of the image the fluid becomes progressively deeper; the swimming cells exhibit collective dynamics. The accumulation occurs because bacteria swim up the gradient of oxygen produced by their consumption and by diffusion from the air bubble. (b) - One randomly chosen instant of the bacterial swimming vector field. The turbulent appearance of the flow is evident here. From [CCD+07]

example toward unfavorable distributions of food sources, the complexity of the colony increases, organization phenomena as *cell-differentiation* or *long-range information transmission* appear. Figure 1.1-(a) shows typical self-organization patterns observed in [BJST+94]. Even vortices can form (figure 1.1-(b)), or clusters migration.

If bacterial cells are very concentrates in a nearly close-packed arrangement, another type of collective phase can take place, called *Zooming BioNematics*, as observed from experiments in [CCD+07]. Within this phase bacteria form co-directionally swimming domains that move chaotically, giving the appearance of turbulence. These regions are demonstrated to eventually move at speeds larger than the average speed of the single organisms. Zooming BioNematics behavior is shown in figure 1.2, taken from [CCD+07].

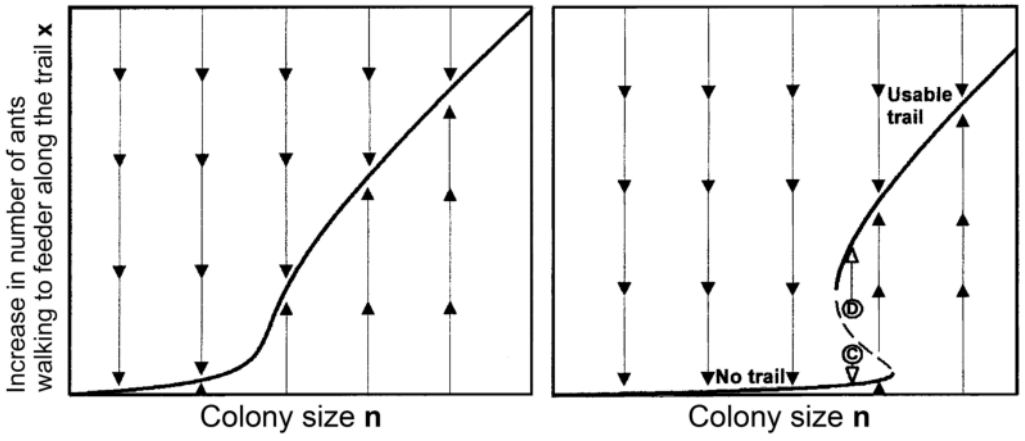
This kind of collective dynamics occurs in response to chemical gradients (oxygen in the case of *Bacillus subtilis* considered in [CCD+07]) and is governed by the interplay between buoyancy, oxygen consumption and hydrodynamic interaction.

Insects, fish schools and bird flocks

Many animal species, such as insects, fishes, birds, up to mammals, exhibit widely investigating social behavior and collective motion. Their social and spatial organization, differently from simple microorganisms, arise from sophisticated principles that involve, for example, production of members with different roles, carrying out specialized tasks in the groups. However such systems can be counted among active matter systems and then their collective dynamics can be successfully studied with the tools of statistical mechanics.
Fundamental questions regarding social animals have still no general answers. One of the major doubts is about how the "common decision" (which direction to take together, where to stop and forage, how to guard against predators) are reached. Possibilities are various: perhaps some kind of leadership is present, or a consensus-based mechanism drives aggregations. Maybe there is no general answer to these questions, but mechanisms vary from a species to another, as the following examples seem to show.

A species of insects exhibiting well known collective behavior are *ants*. Many of them create tracks between the nest and the food sources very efficiently, using pheromone trails (figure 1.3). Largest swarms can reach size of up to 200 thousand individuals forming *trail* systems that are up to 100m long and 20m wide.
Beekman *et al.* [BSR01] have investigated a fundamental question regarding these formations, namely what is the minimum number of "workers" (ants that move from the nest searching widely for food) that are required for this kind of self organization to occur. They have actually discovered that small groups forage in a disorganized way while larger ones are organized. Thus, for the first time, they have provided experimental evidence and a theoretical framework which agree on a first-order phase-transition exhibiting hysteresis between organized and disorganized states.

The largest groups of vertebrates exhibiting a rich set of collective motion patterns are certainly fish schools. In a school fish swim in a tightly organized way considering, from one second to the other, their speed and direction. Both the individual and the collective behavior were studied in fish schools as a function of "fish density", and a transition from disordered to correlated motion was found. It was also discovered that individual fish responded to a "quorum" rule: they only react once they see a threshold number of members of their same species to perform a particular behavior [WSC+08]. Leadership phenomena are also observed to drive the decision making process in some kind of fish [Ree00].



(a) (b)

Figure 1.3: Solutions for a dynamic system for ant trail's formation [BSR01]. On the vertical axis the predicted total increase in the number of ants walking to a single food source as a function of colony size when the feeder is found (a) frequently and (b) infrequently by independently searching ants. The dashed line is the unstable equilibrium. If a small group of ants initially discover the source (point C), then the total increase in foragers will be determined by the lower stable equilibrium branch. However, if the initial discovery is by a larger group (point D), then the increase will be to the upper equilibrium. The arrows visualize where a point in phase space will move to depending on its initial position. From [BSR01]

1.2 Self-propelled particles

Although living systems offer a great variety of interesting active behaviors, briefly outlined back in this chapter in their general characteristics, collective motion and phase transitions also emerge among interacting physical objects. The main difference between living and non-living matter is about which kind of interplay between constituents mediate such collective phenomena. As we have seen in the previous section, living organisms in aggregations, especially the more complex ones, exchange some kind of information. In addiction to their physical, usually of a steric nature, interactions, they can communicate. Whereas in non-living matter, collective dynamics is based on mere physical interactions, either long-range or short-range or of volume-exclusion type.
Various non-living *self propelled particles* (SPPs) as, following the literature, we will call these kinds of objects, possessing diverse features support that the shape and symmetry of the SPPs play an important role in their collective dynamics, and that large-scale inhomogeneity and coherent motion can also appear in a system in which particles do not communicate except

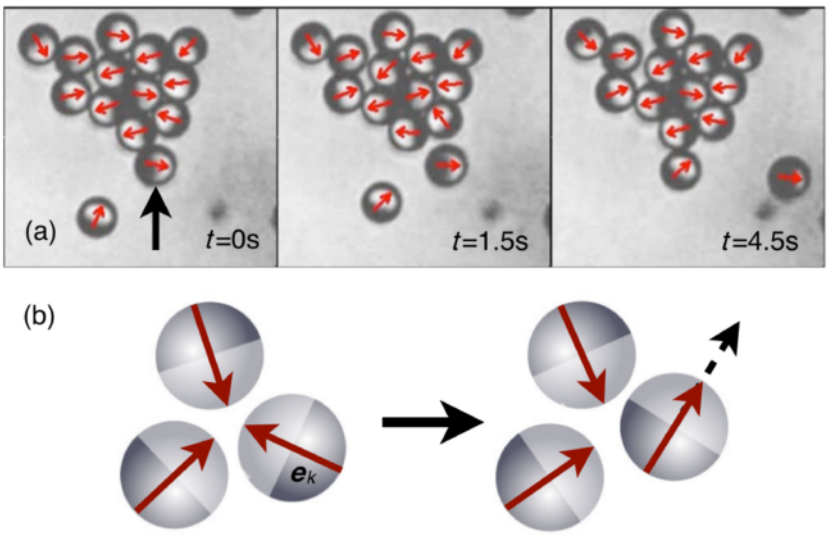


Figure 1.4: (a) - Consecutive close-ups of a cluster, where we resolve the projected orientations (arrows) of the caps. Particles along the rim mostly point inwards. The snapshots show how the indicated particle towards the bottom (left) leaves the cluster (center) and is replaced by another particle (right). (b) - Sketch of the self-trapping mechanism: for colliding particles to become free, they have to wait for their orientations to change due to rotational diffusion and to point outwards. From [BBK+13]

by contact.

In order to give an idea of the reasons for the increasing physical interest in studying such active systems, we address a paradigmatic observation. Following our physical intuition, "agitating" a system by, e.g., increasing the temperature also increases disorder. The most simple example is the well known Ising model of interacting spins on a lattice, which, in two or more dimensions, displays a second-order phase transition from an ordered state to a disordered state as we increase the temperature. Nonequilibrium driven systems, however, may challenge our intuition and show the opposite behavior: increasing the noise strength leads, in certain cases, to the emergence of an ordered state. Some of the numerous examples existing of such behavior will clarify what stated here. In addictions to such examples, we refer to the next chapter for the detailed description of a remarkable model, the so called *Vicsek model*, that displays transitions of these kinds.

Symmetric rods on vibrating surfaces have been observed to form nematic order and, under certain conditions, found to exhibit persistent vortices as well [NMR06]. Narayan *et al.* [NRM07] have also investigated symmetric macroscopic rods and have found giant number fluctuations lasting long, decaying only as a logarithmic function of time.

Periodically, vertically vibrated granular rods form vortex patterns [BNK03]. Above a critical packing fraction, the ordered domains, consisting of nearly vertical rods, spontaneously form and coexist with horizontal rods.
Kudrolli *et al.* [KLVT08] have made experiments with polar (non-symmetric) rods on a vibrating surface. Their rods had a symmetric shape, but a non-symmetrical mass distribution which caused them to move toward their lighter end. They have observed local ordering, aggregation at the side walls, and, in contrast with round-shaped self-propelled particles, clustering behavior.
Simple, very useful, SSPs are the so-called *Janus particles* (JPs). The name comes from the two faced Roman god Janus, because these synthetic, often spherical, particles have two different sides, whose surfaces have two distinct physical or chemical properties. This characteristic allows JPs to have a strictly directional behavior and, in specific conditions, to self-propel. Buttinoni *et al.* [BBK$^+$13] have experimentally and numerically studied a system of JPs and they found what follows. At low densities the driving stabilizes small clusters, whereas at higher densities, the suspension undergoes a phase separation into large clusters and a dilute gas phase. They observe the same qualitative behavior in simulations of a minimal model for repulsive self-propelled particles that mimic the behavior of JPs.

The phenomenon of cluster formation is actual a general behavior of active matter, observed, numerically and experimentally, in numerous active systems. The phase separation that arise because of cluster formations due to the activity is therefore a deeply studied circumstance known as *motility-induced phase separation* (MIPS). The occurrence of such phase separation is rationalized in [BBK$^+$13] in terms of a dynamical instability due to the self-trapping of self-propelled particles, as shown in figure 1.4. We will illustrate in detail the physics of this special kind of phase separation rapidly reviewing, in the next chapter, some other systems in which it arise and various models for its understanding. We will also outline later a description of MIPS in the context of the active system that we have considered for this thesis, because it is of fundamental importance for our purposes.

Chapter 2

Theoretical understanding of Active Matter. From mean field models to microscopic description

A fully theoretical description of the general properties of living matter is not currently achievable because of its overall complexity. As an example one can consider the detailed state of a living cell that is determined by a hopelessly large number of variables. In a given living organism there are at most hundreds of different cell types, which may appear as a relatively small number. The behavior of each cell is, however, affected by a countless number of internal and external signals and stimuli, rendering the accessible parameter space too much large to be described in details. Perhaps, therefore, global principles such as conservation laws and symmetries constrain the possible dynamical behaviors of cells or, indeed, of organisms and populations, such as collections of bacteria, fish schools, and bird flocks. Quantifying the spontaneous dynamical organization and motion of living systems is the first step toward understanding in a generic way some of these principles, by focusing on specific questions that are accessible to theory. Within this aim one can distinguish between two approaches. One generally involves setting up deterministic differential equations at population level, that are often targeted at a quantitative description of specific dataset and sometimes, though not always, involve numerous fitting parameters. A complementary approach, which is the main focus of this chapter, is grounded on statistical physics. This approach emphasizes the role of stochasticity at the ground level of the behavior of living systems, the identification of phase transitions in parameter space and the use of minimal models to explore universal, or at least generic, mechanisms, even when this seriously compromises a model's ability to

quantitatively fit the data.

In this chapter we will focus on identifying generic aspects of the behavior of active systems and characterizing their material properties. Many of the macroscopic properties of active systems are universal, in the sense that systems operating at widely differing length scales, with significant differences in their detailed dynamics at the microscopic level, display broadly similar properties. Visually similar flocking phenomena are seen in fish shoals and collections of keratocytes. Contractile stresses are evident on a subcellular scale in the cytoskeleton, as well as on a scale of many cells in swimming algae.

Before starting to summarize the present-day understanding of the physics of active matter, an important distinction between models has to be underlined. Active particles in a viscous fluid of viscosity η and experiencing a frictional drag γ can in general be described as a system with or without momentum conservation, depending on the physical parameters, such as the density of active particles, and the length scales of interest. If the fluid can be treated as an inert medium, providing only friction, then the collection of active particles that transfer momentum to the fluid can be modeled as a system with overdamped dynamics and no momentum conservation. Systems that can be described by models with no momentum conservation is generally referred to as "dry". In contrast, when solvent-mediated hydrodynamic interactions are important, the dynamics of the suspending fluid must be incorporated in the model and one must develop a description of the suspension of active particles and fluid, with conserved total momentum. Systems described by models with momentum conservation, where fluid flow is important, are usually called "wet". Although one refers to various systems as wet or dry, we stress that this distinction refers to the model used, rather than to the system itself, and also to the length scales of interest, as in general hydrodynamic flows can be neglected only on length scales larger than $\sqrt{(\eta/\gamma)}$. Accounting this general theoretical background, we can start to outline three fundamental class of active matter models:

- macroscopic field models in which hydrodynamic limit is taken discarding from the description the medium where active constituents move;
- particle-scale models in which, still in an inert-medium scheme, a single-particle description is retrieved;
- microscale models that investigate the arise of the activity as a result of the fluid dynamic interactions between each active element and

the medium.

The following, non fully detailed, although quite exhaustive illustration of the theoretical models for active matter is thought to be necessary to correctly frame our active-dumbbells model, that will be completely shown in the next chapter.

2.1 Continuous models and active fluids

A useful theoretical framework to describe the macroscopic properties of active matter is provided by the methods of nonequilibrium statistical mechanics. In a generalized hydrodynamic approach, a coarse-grained description of the large-scale, long-time behavior of the system is given in terms of a small number of continuum fields. The evolution of these fields is written in terms of a set of continuum or hydrodynamic equations that modify the well-known liquid-crystal hydrodynamics to include new nonequilibrium terms that arise from the activity. The word "hydrodynamics" here refers to any continuum model where a system of many interacting constituents can be described at large scales in terms of the dynamics of a small number of fields, generally corresponding to conserved variables and, when applicable, broken-symmetry fields.

One approach to obtain a hydrodynamic theory of active systems is to start from a microscopic model and use the tools of statistical physics to coarse grain the model and obtain the long-wavelength, long-time scale equations. This task is difficult if the microscopic description is realistic and it can be carried out only at the cost of approximations, such as low-density or weak interactions. It allows one to relate the parameters in the macroscopic equations to specific physical mechanisms and to estimate them in terms of experimentally accessible quantities.

An alternative, more pragmatic approach is to directly write hydrodynamic equations for the macroscopic fields including all terms allowed by symmetry as pioneered for dry flocks by Toner and Tu [TT95], [TT98] and extended to the case of self-propelled particles suspended in a fluid by Simha and Ramaswamy [ASR02]. As one might expect in hindsight, novel terms, of a form ruled out for thermal equilibrium systems, appear in these versions of the equations of active hydrodynamics.

A more systematic implementation of the phenomenological hydrodynamic approach is to treat the nonequilibrium steady state of an active system as arising through the imposition of a non-vanishing but small driving force on a well-defined thermal equilibrium state whose existence is not

in question. If this driving force is assumed to be small, the macroscopic hydrodynamic equations can be derived in a systematic way following the Onsager procedure. One identifies thermodynamic fluxes and forces and writes the most general linear relation between them that respects the symmetries of the problem. The novel terms mentioned above that arose by directly writing down the hydrodynamic equations of active matter are then seen to be a consequence of off-diagonal Onsager coefficients and an imposed constant nonzero driving force. Generalized hydrodynamic theories have been very successful in the description of complex and simple fluids. The advantage is that the equations are expanded around a well-defined state. The drawback is that many active systems, biological ones being particularly pertinent examples, are far from equilibrium and one might, for example, miss some important physics by the restriction to the linear nonequilibrium regime.

Regardless of the choice of hydrodynamic framework, the reasons for the choice of variables remain the same. When an extended system is disturbed from equilibrium by an external perturbation, its relaxation is controlled by the microscopic interactions among constituents. It is useful to divide the relaxation processes into fast and slow, and to build a theory of the slow dynamics in which the fast processes enter as noise and damping. Such division is unambiguous when there are collective excitations with relaxation rates that vanish as the wave vector goes to zero; these are the hydrodynamic modes of the systems.

Toner and Tu continuous model of flocking

A continuum effective theory for the flocking model of Vicsek *et al.* [VCBJ+95] was proposed in 1995 by Toner and Tu [TT95]. The Vicsek model, as we will see in detail later in this chapter, describes a collection of self-propelled particles with fixed speed and noisy polar aligning interactions and displays a nonequilibrium phase transition from a disordered state at low density or high noise to an ordered, coherently moving state at high density or low noise strength. Toner and Tu formulated the continuum model phenomenologically solely on the basis of symmetry considerations.

Since the particles are moving on a frictional substrate, the only conserved field is the number density $\rho(\mathbf{r}, t)$ of active particles. In addition, to describe the possibility of states with polar orientational order, one must consider the dynamics of a polarization vector field $\mathbf{p}(\mathbf{r}, t)$. These continuum fields can be defined in terms of the position $\mathbf{r}_n(t)$ of each active particle and a unit vector $\hat{\boldsymbol{\nu}}_n(t)$ denoting the instantaneous orientation of

the velocity of each particle as

$$\rho(\mathbf{r},t)=\sum_n \delta(\mathbf{r}-\mathbf{r}_n(t)),\quad \mathbf{p}(\mathbf{r},t)=\frac{1}{\rho(\mathbf{r},t)}\sum_n \hat{\boldsymbol{\nu}}_n(t)\delta(\mathbf{r}-\mathbf{r}_n(t)). \tag{2.1}$$

The dynamics of ρ and $\mathbf{p}$ is described in the equations below:

$$\partial_t\rho + v_0\boldsymbol{\nabla}\cdot(\rho\mathbf{p}) = 0\,, \tag{2.2a}$$

$$\partial_t\mathbf{p} + \lambda_1(\mathbf{p}\cdot\boldsymbol{\nabla})\mathbf{p} = -\frac{1}{\gamma}\frac{\delta F_p}{\delta\mathbf{p}} + \mathbf{f}\,, \tag{2.2b}$$

where v_0 is the self-propulsion (fixed) speed of the individual active particles, γ is a kinetic coefficient and $\mathbf{f}$ is a white Gaussian noise. The equation for ρ is a continuity equation. In the equation for $\mathbf{p}$ the terms that can be viewed as arising from a free-energy functional of Ginzburg-Landau form F_p are separated out from truly nonequilibrium ones. The parameter λ_1 controls the strength of the advective term on the left-hand side of equation (2.2b), that resembles the familiar advective nonlinearity in the Navier-Stokes equation. In the Toner-Tu picture $\mathbf{p}$ is both a current and an orientational order parameter, and thus acts on itself by advection and flow alignment, both of which contribute to $(\mathbf{p}\cdot\boldsymbol{\nabla})\mathbf{p}$ in the equation for $\mathbf{p}$. In the density equation only the velocity-like character of $\mathbf{p}$ enters.

The free-energy functional used in the equations (2.2) is given by

$$\begin{aligned} F_p = \int \mathrm{d}^d\mathbf{r}\,\Big\{&\frac{\tilde{\alpha}(\rho)}{2}|\mathbf{p}|^2 + \frac{\tilde{\beta}}{4}|\mathbf{p}|^4 + \frac{\tilde{K}}{2}(\partial_i p_j)(\partial_j p_i) + \\ &+\frac{w}{2}|\mathbf{p}|^2\boldsymbol{\nabla}\cdot\mathbf{p} - w_1\boldsymbol{\nabla}\cdot\mathbf{p}\frac{\delta\rho}{\rho_0} + \frac{A}{2}\Big(\frac{\delta\rho}{\rho_0}\Big)^2\Big\} \end{aligned} \tag{2.3}$$

where ρ_0 is the average density and $\delta\rho = \rho - \rho_0$ is the fluctuation in the density about its mean value ρ_0 . Such fluctuations are penalized by the compression modulus A. The first two terms on the right-hand side of equation (2.3) control the mean-field continuous order-disorder transition that takes place as the parameter $\tilde{\alpha}$ goes through zero. A reasonable phenomenological approach to describe the physics near the transition is to take $\tilde{\alpha}(\rho) = a_0(1-\rho/\rho_c)$, changing sign at a characteristic density ρ_c. For stability reasons the coefficient is positive. The ratio $D_r = a_0/\gamma$ is a rotational diffusion rate with dimensions of frequency. The third term in the free energy describes the energy cost for a spatially inhomogeneous deformation of the order parameter. $\tilde{K}$ is a positive constant.

By using equation (2.3) for the free energy, the equation for $\mathbf{p}$ takes the form

$$\begin{aligned}\partial_t \mathbf{p} + \lambda_1(\mathbf{p}\cdot\boldsymbol{\nabla})\mathbf{p} = &-(\alpha(\rho)+\beta|\mathbf{p}|^2)\mathbf{p} + K\nabla^2\mathbf{p} \\ &- v_1\boldsymbol{\nabla}\frac{\rho}{\rho_0} + \frac{\lambda}{2}\boldsymbol{\nabla}|\mathbf{p}|^2 - \lambda\mathbf{p}(\boldsymbol{\nabla}\cdot\mathbf{p}) + \mathbf{f},\end{aligned} \tag{2.4}$$

where $v_1 = w_1/\gamma$, $\lambda = w/\gamma$ and all quantities without tilde are obtained from those with tilde by dividing by γ.

The dynamical model described by equations (2.2) exhibits a continuous transition from a disordered to an ordered state. For $\alpha > 0$, corresponding to an equilibrium density $\rho_0 < \rho_c$, the homogeneous steady state of the system is disordered or isotropic, with $\mathbf{p} = 0$ and a corresponding zero mean velocity. For $\alpha < 0$, corresponding to $\rho_0 > \rho_c$, the system orders in a state with uniform orientational order, with $|\mathbf{p}_0| = \sqrt{-\alpha_0/\beta}$, where $\alpha_0 = \alpha(\rho_0)$. In the ordered state, which is also a moving state with $\mathbf{v} = v_0\mathbf{p}$, continuous rotational symmetry is spontaneously broken.
The built-in non-equilibrium nature of this system allows it to undergo a spontaneous symmetry breaking even in two dimensions, even if such behavior is forbidden, within equilibrium realm, accordingly to the Mermin-Wagner theorem. The latter states that continuous symmetries cannot be spontaneously broken at finite temperature (or, as in this case, at finite noise amplitude) in systems with short-range interactions in dimensions $d \leqslant 2$.

A coarse-grained theory of motility-induced phase separation

Within the context of coarse-grained continuous levels of description, another simple model deserves to be illustrated in this brief review. Starting from a kinetic approach one can establish a hydrodynamic equation for the a self-propelled swimmers system. This theoretical framework allows to easily understand the physics of the mechanism of the well known motility-induced phase separation that we have described in the previous section from a phenomenological point of view. This approach was first suggest by [Sch93] and later presented in [GMST15].

In order to describe a population of swimmers that runs for a time τ with velocity v between two successive tumbles, the relevant continuous variable here is the distribution $f(\mathbf{r}, \mathbf{u}, t)$ of active particles with position $\mathbf{r}$, swimming in the direction $\mathbf{u}$ at the time t. The kinetic Boltzmann-like equation for the evolution of f in d dimension can be written as

$$\partial_t f(\mathbf{r}, \mathbf{u}, t) = -\boldsymbol{\nabla}_{\mathbf{r}} \cdot \Big[v\mathbf{u} f(\mathbf{r}, \mathbf{u}, t) \Big] - \frac{f(\mathbf{r}, \mathbf{u}, t)}{\tau} + \frac{\int \mathrm{d}^{d-1}\mathbf{u} f(\mathbf{r}, \mathbf{u}, t)}{\tau \int \mathrm{d}^{d-1}\mathbf{u}} \tag{2.5}$$

The first term on the right-hand side of the equation is the divergence of the advective current resulting from self propulsion (here $v\mathbf{u}$ is the velocity), whereas the second and the third term are loss and gain (collisional) terms accounting respectively for the particles that "tumble out" and "tumble into" the direction $\mathbf{u}$.

A standard way to analyze equation (2.5) is to consider the so-called hydrodynamic limit in which suitable moments of the distribution functions change smoothly in space and in time. A gradient expansion of equation (2.5) can be performed in such limit and a hierarchy of equations, one for each order of the derivative, results. According to such expansion, the distribution functions is written as

$$f = f^{(0)} + f^{(1)} + f^{(2)} + \dots \tag{2.6}$$

where $f^{(n)}$ is a contribution which is $\sim O(D^n)$, where D denotes derivatives over space or time. In the hydrodynamic limit, every successive derivative applied to f is assumed to make it much smaller, that is:

$$O(D^n) \ll O(D^{n-1}) \ll \dots \ll O(D^1) \ll O(D^0) \equiv \mathbf{I}, \tag{2.7}$$

hence

$$f^{(n)} \ll f^{(n-1)} \ll \dots \ll f^{(1)} \ll f^{(0)}. \tag{2.8}$$

The details of the calculus can be found in [GMST15]. We limit here to present the results pf this approach.

The zero-order equation reads

$$f^{(0)} = \frac{\rho}{\Omega_d} \tag{2.9}$$

where ρ is the density of swimmer at the point $\mathbf{r}$ and is nothing but the integral in (2.5) and Ω_d is the d-dimensional solid angles. From this first equation immediately comes that no term other than $f^{(0)}$ contributes to the coarse-grained hydrodynamic density ρ. From the successive two equations of the gradient expansions, taking the integral over the directions and considering the expression for $f^{(0)}$ from (2.10) one get

$$\partial_t \rho + \frac{1}{\Omega_d} \int \mathrm{d}^{d-1}\mathbf{u}\, \partial_i (v u_i \rho) - \frac{\tau}{\Omega_d} \int \mathrm{d}^{d-1}\mathbf{u}\, \partial_t \partial_i (v u_i \rho) - \frac{\tau}{\Omega_d} \int \mathrm{d}^{d-1}\mathbf{u}\, \partial_i (v u_i \partial_j (v u_j \rho)) = 0 \tag{2.10}$$

Because, for symmetry reasons, the second and the third integral in above expression are zero, from the relation

$$\frac{\int \mathrm{d}^{d-1}\mathbf{u}\, u_i u_j}{\Omega_d} = \frac{\delta_{ij}}{d}, \tag{2.11}$$

one obtains

$$\partial_t \rho = \frac{\tau}{d} \boldsymbol{\nabla} \cdot \Big[v \boldsymbol{\nabla} (\rho v) \Big]. \tag{2.12}$$

Equation (2.12) provides a basis to describe the physics of the phenomenon of self-trapping. The important point here is that running velocity depends on the position, that is $v = v(\mathbf{r})$. Noticing that the distribution $\rho = 1/v(\mathbf{r})$ is a steady-state solution of the equation (2.12), one recovers immediately from this treatment that self-propelled particles accumulate where they go slower, that actually is the leading process from which phase separation arise. In order to deeply understand how this mechanism turns on for active swimmers, an assumption is necessary. Consider for instance the case of a concentrate suspension of active particles, where the swim speed decreases for density, for example, due to crowding. One can suppose for simplicity an exponential decay

$$v \sim v_0 e^{-\lambda \rho / 2} \tag{2.13}$$

where λ measure how steep is this decay. Using this assumption in a 2D-version of the dynamic equation (2.12) one gets

$$\partial_t \rho = \boldsymbol{\nabla} \cdot \left[\frac{\tau v^2}{2} \left(1 - \frac{\lambda \rho}{2} \right) \boldsymbol{\nabla} \rho \right] \equiv \boldsymbol{\nabla} \cdot \Big[D_{eff}(\rho)\, \boldsymbol{\nabla} \rho \Big] \tag{2.14}$$

where the effective diffusion coefficient here is a function of the density. Similar to the Toner Tu picture, this feature is the main difference between this out-of-equilibrium dynamics and a standard equilibrium diffusive dynamic where the diffusion coefficient depends at least on the position. Within this frame, for ρ high enough, $D_{eff} < 0$, so the effective diffusivity becomes negative. Negative diffusion means that an infinitesimally small fluctuation leads to a divergent increase in the density field. In other words, the system phase separates.

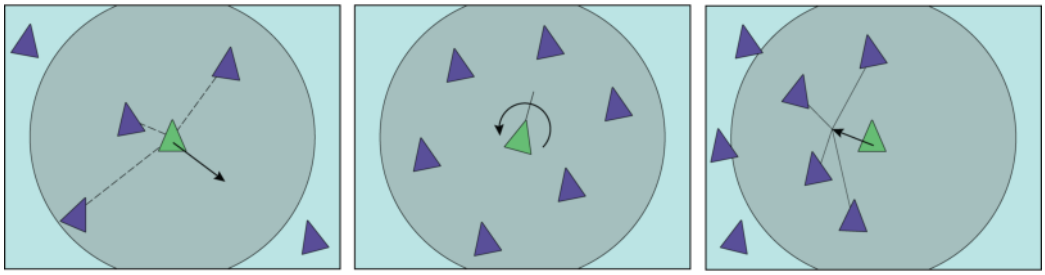


Figure 2.1: The three basic steering behaviors determining the motion of the objects. (a) Separation, in order to avoid crowding local flock-mates. (Each boid reacts only to flock-mates within a certain neighborhood around itself, they are the "local flock-mates".) (b) Alignment: objects steer towards the average heading direction of their local flock-mates. (c) Cohesion: objects move to-ward the average position of their neighboring boids.

2.2 Molecule models and mesoscale description

Beside continuous models quickly described in the previous sections, one can consider another level of coarse graining for the description of the active systems. We refer to a picture at a mesoscale level, in which again the microscopic sources of the activity do not enter in the model, but the constituents of the system, instead of macroscopic fields, are singly considered and their motion is individually described. These "agent-based" models are shown to offer a minimal approach to the study of active systems, clearly with an emphasis on order and fluctuations rather than forces and mechanics. The challenge in building of such picture is preeminently the appropriate choice of the interactions between the bodies in the system. Several attempts exist to date in this context and they offer a really detailed level of comprehension on many of the more fascinating collective behaviors of living active systems.

In order to illustrate the idea at the ground of the models belonging to this class, we present the scheme of one of the first model of *self-propelled particles* (SPP) for flocking simulations published by Reynolds [Rey87]. The objects of his system were moving along trajectories determined by differential equations, taking into account three types of interactions: avoidance of collisions, headings in the direction of the neighbors and finally, trying to stay close to the center of mass of the flock, as illustrated on figure 2.1. This qualitative description provides a representative example in the mesoscale picture that enclose all the models described below in this section, for which a more quantitative description will be give.

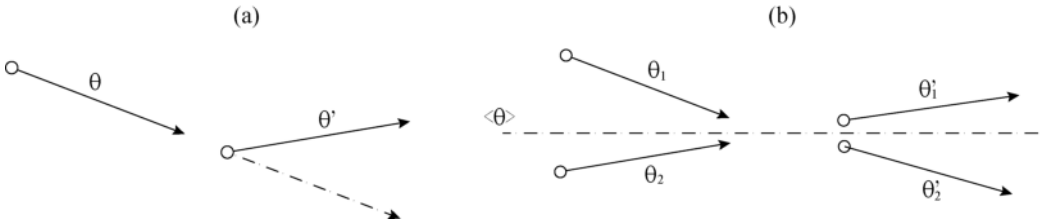


Figure 2.2: Schematic view of the dynamics of the model: (a) self-diffusion events, (b) binary collisions with alignment interactions.

Vicsek-like models

Seminal quantitative studies of flocking as a phase transition were first carried out by Vicsek *et al.* [VCBJ+95], with important successive modifications and extensions. These models describe, within the scheme generally depicted above, point particles with fixed speed moving on an inert background. The direction of motion changes according to a local rule that requires particles to align with their neighbors at each time step. This family of models displays a transition from a disordered to an ordered phase with decreasing noise strength or increasing density.

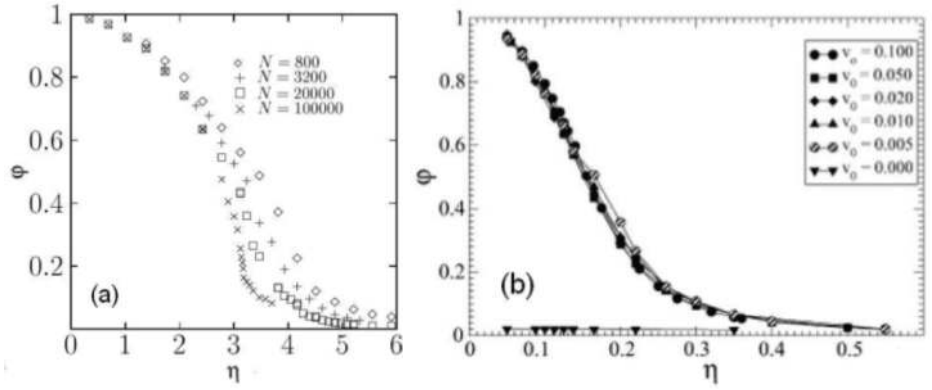
The velocity $\mathbf{v}_i$ (of fixed magnitude v_0) of a particle can be identified simply by the angle θ_i between $\mathbf{v}_i$ and an arbitrary reference direction. Particles evolve ballistically until they experience either a self-diffusion event (a random "kick") or a collision that tends to align the velocities within a given neighborhood. More specifically, the velocity $\mathbf{v}_i$ of any particle is update as follows:

$$\mathbf{v}_i(t+1) = v_0 \frac{\langle \mathbf{v}_j(t) \rangle_R}{|\langle \mathbf{v}_j(t) \rangle_R|} + perturbation \tag{2.15}$$

where the first term is the alignment rule, $\langle \cdot \rangle_R$ denotes averaging over a circular neighborhood of radius R and the second term is the random contribution to the change in the direction of the particle. The scheme described by equation (2.15) is sketched in figure 2.2 for the simple case of a binary collision.
The trajectory of each particle is easily reconstructed by means of the updated velocities:

$$\mathbf{x}_i(t+1) = \mathbf{x}_i(t) + \mathbf{v}_i(t+1) \tag{2.16}$$

The perturbation term in equation (2.15) can be taken into account in various ways. In the standard version of the Vicsek model it is represented by adding a random angle to the direction of motion



(a) (b)

Figure 2.3: Order parameter (φ) versus noise (η) in the Standard Vicsek Model (SVM). (a) The different kind of points belong to different system sizes. (b) The different curves belong to different v_0 velocities, with which each particles move. As it can be seen, the concrete value of v_0 does not effect the nature of the transition (except when $v_0 = 0$, that is, when the units do not move at all).

$$\theta_i(t+1) = \theta_i(t) + \Delta_i(t) \tag{2.17}$$

where Δ_i is actually the random deviation taken from a uniform distribution in the interval $[-\eta\pi, \eta\pi]$ with $\eta < 1$.

Taking as order parameter the normalized average velocity

$$\varphi = \frac{1}{Nv_0} \left| \sum_{i=1}^{N} \mathbf{v}_i \right|, \tag{2.18}$$

this simple model, as shown in figure 2.3, undergoes a continuous phase transition from disorder to an ordered state (that obviously refers to the directions of the particles) as the level of perturbation η decrease.

Models without alignment rule. Active Brownian motion

Although the Vicsek's model is the simplest model of ordering transitions of active particles, several variants of SPP's models have been proposed over the years with the purpose of a more profound understanding of the physics of the active systems. One of the main gap of the Vicsek's model with reference to this aim is the pure phenomenological nature of the alignment rule for the particle's directions on motion. The reason why this could represent a lack in a correct theoretical modeling of the aggregation in active materials is because in some living systems there is no evidence for

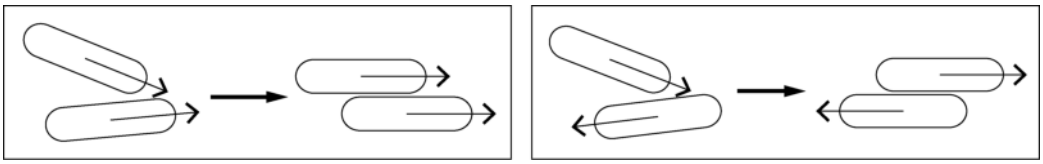


Figure 2.4: Nematic collision means that, if the included angle of the two velocity vectors belonging to the colliding rod-like units was smaller than 180° before they impinge on each other, they would continue their motion in the same direction, in parallel, after the collision. If this angle was bigger than 180°, then they would continue their travel in parallel, but in the opposite direction.

long-range alignment-type interactions and units coordinate their movement by signaling mechanism in which physical contact is needed. We present here some of the most noticeable studies that investigate systems in which the particles do not follow any kind of alignment rule and only collisions occur between them in the presence of some kind of interaction potential.

An attempt in this direction was brought by Ginelli *et al.* [GPBC10] that investigated in great detail the properties of a collection of elongated, asymmetric polar units moving in two dimensions with constant speed, interacting only by "nematic collisions", in the presence of noise. Nematic collision, illustrated on figure 2.4, means the following: if the included angle of the two velocity vectors belonging to the colliding rod-like units was smaller than 180° before they collide, they would continue their motion in the same direction, in parallel, after the collision. If this angle was bigger than 180°, then they would continue their travel in parallel, but in the opposite direction. Disordered and ordered phase were observed for this system that arise depending on the strength of the noise.

The first work in which the relevance of the simultaneous presence of volume exclusion and self-propulsion is shown to give rise to an effective alignment of the particles was published by Peruani *et al.* [PDB06]. They stressed the importance of the particle shape by showing than self-propelled objects moving in a dissipative medium and interacting by inelastic collision, can self-organize into large coherently moving clusters. Furthermore, they showed that self-propelled rods exhibit non-equilibrium phase transition between a monodispersed phase to an aggregate phase that depends on the aspect ratio and density of the self-propelled rods.

Discarding phenomenological alignment rules seems to actually constrain the shape of the particles to be non spherical, to provide some collective behaviors. However a further generalizations is possible in the context

of stochastic dynamics. We complete this section presenting such theoretical approaches for active matter, known as *active Brownian motion* models, that are actually representative of mesoscale-particle class of models. Active Brownian models develop from the idea that the dynamic degrees of freedom of each particle, evolve, as the name suggests, according to Brownian rules. Beside this main feature, there are many ways to account for the autopropulsion.

Including an additional energy input allows to derive a first example of such models for self-propelled (living) motion. The additional inflow of energy, leading to active motion, can be modeled by negative friction, instead of a standard constant friction coefficient γ. The motion of an "active Brownian particle" (ABP) with general velocity- and space-dependent friction in an external potential $U(\mathbf{r})$ can be described by the Langevin equation (with the mass m set to 1 for notation simplicity):

$$\frac{\mathrm{d}\mathbf{r}}{\mathrm{d}t} = \mathbf{v}\,; \quad \frac{\mathrm{d}\mathbf{v}}{\mathrm{d}t} = \mathbf{F}_{diss} - \boldsymbol{\nabla} U(\mathbf{r}) + \boldsymbol{\mathcal{F}}(t) \tag{2.19}$$

where, we stress, the new feature with respect the passive Brownian motion is the dissipative force which now acts in direction of the motion and is given with a position and velocity dependent coefficient

$$\mathbf{F}_{diss} = -\gamma(\mathbf{r}, \mathbf{v})\mathbf{v}\,. \tag{2.20}$$

The term $\boldsymbol{\mathcal{F}}(t)$ is a stochastic force with strength D and a δ-correlated time dependence:

$$\langle \mathcal{F}_i(t)\, \mathcal{F}_j(t')\rangle = 2D\, \delta_{i,j}\, \delta(t-t')\,, \quad i,j = x,y,z. \tag{2.21}$$

But now, due to nonequilibrium, this noise strength is independent of the parameters in the dissipative force and the Einstein relation is therefore considered invalid.

Equation (2.19) gives the basis for the derivation of an energetic balance. From the time derivative of the mechanical energy one obtains

$$\frac{\mathrm{d}E}{\mathrm{d}t} = \mathbf{v}\frac{\mathrm{d}\mathbf{v}}{\mathrm{d}t} + \boldsymbol{\nabla} U(\mathbf{r})\frac{\mathrm{d}\mathbf{r}}{\mathrm{d}t} \tag{2.22}$$

which, averaged over the noise, yields

$$\frac{\mathrm{d}}{\mathrm{d}t}\langle E\rangle = -\gamma(\mathbf{v}, \mathbf{r})\mathbf{v}^2 + D \tag{2.23}$$

One gets immediately that negative values of the friction coefficient lead to an increase of the mechanical energy.

The choice of the velocity-dependent friction coefficient obviously plays an important role in this class of models of active Brownian particles (ABPs). A standard choice comes from certain models of the theory of sound developed by Rayleigh and Helmholtz where the friction coefficient is assumed to have a parabolic behavior:

$$\gamma(\mathbf{r}, v) = -\alpha + \beta \mathbf{v}^2 \equiv \alpha\left(\frac{v^2}{v_0^2} - 1\right) \equiv \beta(v^2 - v_0^2) \tag{2.24}$$

where at low velocities ($v^2 < v_0^2$) the friction is negative and the particle gains energy.

An alternative way to assign a form to the friction coefficient is based on the so-called depot model, for which the Brownian particle is assumed to be capable of taking energy and storing some of this additional energy into an internal energy depot, named $e(t)$. One can consider a balance equation for the internal energy depot of a Brownian particle:

$$\frac{\mathrm{d}}{\mathrm{d}t} e(t) = q(\mathbf{r}) - ce(t) - h(\mathbf{v})e(t) \tag{2.25}$$

where in $q(\mathbf{r})$ are taken into account the energy gathered from the environment, $ce(t)$ is energy loss rate due to the dissipation (assumed to be proportional to e) and $h(\mathbf{v})$ is the rate of conversion of internal energy to kinetic motion. A simple ansatz for q and h is:

$$q(\mathbf{r}) = q_0 \qquad h(\mathbf{v}) = d\mathbf{v}^2 \tag{2.26}$$

One can assume that energy conversion may result in an additional acceleration of the Brownian particle in the direction of movement, including this term in the usual passive friction coefficient in the Langevin equation (2.19) as follows:

$$\mathbf{F}_{diss} = -\gamma_0 \mathbf{v} + de(t)\mathbf{v} \tag{2.27}$$

With such coupling the Langevin equation for the active system reads:

$$\frac{\mathrm{d}}{\mathrm{d}t}\mathbf{v} = -\gamma_0 \mathbf{v} - de(t)\mathbf{v} - \boldsymbol{\nabla} U(\mathbf{r}) + \mathcal{F}(t) \tag{2.28}$$

Regardless of the choice of the phase space dependent friction coefficient, Langevin equations including acceleration terms (eventually resulting from an energy inflow) are shown to be useful to describe the complex dynamics of active particles. Some of the features of such dynamics are for

example non-standard diffusive properties with large mean squared displacements or unusual velocity distribution that, as we have seen before, are as well some of the main typical character of active matter systems.

Before starting to outline the mechanics of auto-propulsion and the microscopic causes of active behavior, we review here another simple model of active Brownian particles, largely used to investigate collective behavior, such as Vicsek-type phase transitions, for self-propelled bodies with no alignment interaction [FM12]. The set of $2N$ Langevin equations (one for each particle) reads:

$$\dot{\mathbf{r}}_i = v_0 \boldsymbol{\nu}_i + \mu \sum_{j \neq i} \mathbf{F}_{ij} + \boldsymbol{\eta}_i \,, \tag{2.29a}$$

$$\dot{\theta}_i = \zeta_i \,, \tag{2.29b}$$

where $\boldsymbol{\nu}_i = (\cos\theta_i, \sin\theta_i)$ are the directions of polarization of the particles, v_0 the self-propulsion speed, μ the mobility and $\mathbf{F}_{ij}$ is the force on i due to interaction with the particle j. Two standard Gaussian white noises $\boldsymbol{\eta}_i(t)$ and $\zeta_i(t)$ explicitly account for the translational and rotational diffusion. They respectively satisfy:

$$\langle \eta_{i,a}(t)\eta_{j,b}(t')\rangle = 2D\delta_{ij}\delta_{ab}\delta(t-t') \,, \quad \langle \zeta_i(t)\zeta_j(t')\rangle = 2D_R\delta_{ij}\delta(t-t') \,, \tag{2.30}$$

where Greeks labels denote Cartesian coordinates. The two diffusion constant are shown to be related as follows:

$$D_R \sim D/\sigma^2 \,, \tag{2.31}$$

for spherical particles of characteristic size σ. In [FM12] this model is observed to provide typical active behavior, such as phase separation, even if there are no explicit alignment interaction. We prefer not to go further in the illustration of the details of such models, since in the next chapter we will describe very accurately our active-particle model, that actually belongs to this class of active Brownian particles models.

2.3 Microswimmers and microscopic swimming dynamics

While the macroscopic equation of motion of active matter can be obtained, as we have seen before, from general considerations of symmetry or appropriate stochastic rules, determination of the magnitude and often even

the sign of the coefficients requires additional physical assumptions about the microscopic self-propelling mechanism and fluid dynamic interactions. The purpose of this section is to review some minimal microscopic descriptions of active matter, particularly regarding to mechanics of swimming motility, that have provided such an insight into the complex physics of these systems.

To keep the scope of this short description simpler, we consider here a "swimmer" to be an object that moves by deforming its body in a periodic way and we discard other mechanisms that could be termed "swimming" as well. Furthermore, in order to have a focus on the most interesting swimming strategies, we confine our discussion to the low Reynolds number fluid dynamics regime.

Flow at low Reynolds number

With the aim to describe the motion of a single body moving in a fluid, we purpose to identify the force distribution acting on it. Therefore we need to solve for the flow field $\mathbf{v}$ and the pressure p in the surrounding fluid. The so-called *no-slip* boundary condition is generally prescribed and it requires that the velocity of the fluid at the boundary is equal to the velocity of the material points on the body surface.

For an incompressible Newtionian fluid ($\boldsymbol{\nabla} \cdot \mathbf{v} = 0$) with density ρ and viscosity μ, the flow satisfies the Navier-Stokes equation

$$-\boldsymbol{\nabla} p + \mu \nabla^2 \mathbf{v} = \rho \frac{\partial \mathbf{v}}{\partial t} + \rho (\mathbf{v} \cdot \boldsymbol{\nabla})\, \mathbf{v} \tag{2.32}$$

The terms on the left-hand side represent pressure and viscous terms, and the terms on the right-hand side correspond to inertial terms.

Considering, on the other hand, a flat body moving on a fluid, the force necessary to keep the object moving at a constant speed v is, roughly speaking, $F \sim \mu A \mathrm{d}v/\mathrm{d}y$, where A is the surface area of the object and $v(y)$ is the velocity, parallel to the direction of motion, of the fluid at a perpendicular distance y from the object. The linear relationship between F and the velocity gradient is characteristic of a Newtonian fluid. Supposing that l is a characteristic size of the object, using dimensional analysis, the viscous force $\mu A \mathrm{d}v/\mathrm{d}y$ will scale as $\mu l v$, whereas the inertial force $m\mathrm{d}v/\mathrm{d}t$ due to the fluid's momentum will scale as $\rho l^2 v^2$. The ratio of these forces is characterized by a single dimensionaless parameter known as the *Reynolds number* (Re):

$$Re = \frac{\rho l^2 v^2}{\mu l v} = \frac{\rho l v}{\mu} \tag{2.33}$$

The value of the Reynolds number sets whether inertial forces dominate the dynamics (Re $\gg$ 1) or viscous forces dominate (Re $\ll$ 1). In order to give numerical reference for this ranges we mention typical orders of magnitude of the Reynolds magnitude for the two extreme regimes: using typical length and velocity scales for humans and bacteria swimming in water, one finds that Re $\sim 10^4$ for humans and Re $\sim 10^{-3} - 10^{-5}$ for bacteria.

Low Reynolds number regime easily translates into a limit case for the form of the Navier-Stokes equation (2.32). After non-dimensionalizing the Navier-Stokes equation, the right-hand side is multiplied by Re, so that for Re $\ll$ 1, equation reduces to the time-independent Stokes equation

$$\mu \nabla^2 \mathbf{v} = \boldsymbol{\nabla} p \tag{2.34}$$

One of the immediate consequences of swimming at low Reynolds number is that the net forces acting on a body must at all times be zero, since they cannot be counterbalanced by an inertial force (mass times acceleration). Consider, for example, a microscopic swimmer that moves by changing its shape. The requirement that there is net motion for the swimmer constrains the allowed sequence of motions, as illustrated by the so-called *scallop theorem* formulated by Purcell [Pur77] and that can be illustrated as follows. Consider a scallop that moves in water opening and closing its shell. The latter action expels a jet of water that propels the scallop in the opposite direction, whereas reopening leads to drag. At low Reynolds number, the flow of water into and out of the scallop over one cycle would be the same, regardless of the speed, implying that a scallop would make no net progress. Fortunately scallops swim at high Reynolds number, in which regime the drag associate to the reopening part of the cycle can be reduced by opening slowly and a net motion can results. This theorem reflects the fact that the Navier–Stokes equation in the limit Re $\to$ 0 (2.34) is time reversal symmetric. The motion is therefore independent of the speed and is determined only by the sequence of body configurations.

A model of dumbbell-shape swimmer

The scallop theorem forces any swimming mechanism of an isolated object at low Reynolds number to be non-reciprocal in time. The helical structure

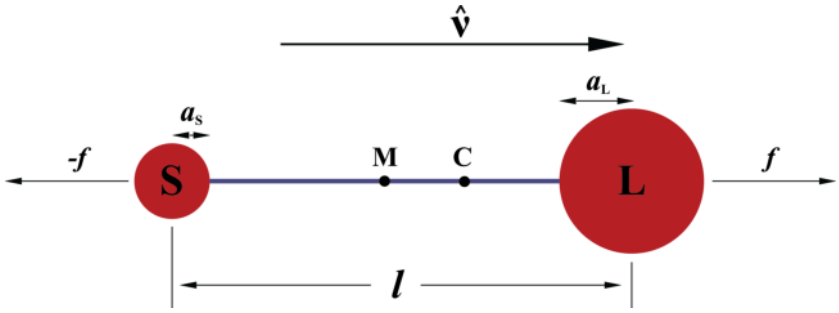


Figure 2.5: Stroke-averaged swimmer is an asymmetric rigid dumbbell composed of a small and a large sphere of radii a_S and a_L , respectively, connected by an infinitely thin rigid rod. The swimmer has length l, and its orientation is characterized by a unit vector $\hat{\boldsymbol{\nu}}$ directed along its axis from the small to the large sphere. Also shown are the equal and opposite forces $\mathbf{f} = f\hat{\boldsymbol{\nu}}$ that the swimmer exerts on the fluid. Propulsion is centered at the hydrodynamic center, denoted by C, which here lies to the right of the swimmer's geometrical midpoint M, which is also the center of the force dipole. From [BM09].

of flagella motors for example breaks time reversal symmetry and thus allows organisms that use a time asymmetric swimming strategy to generate net motion even at low Re.

With reference to the model of Baskaran and Marchetti[BM09] of microswimmers, we describe here how is possible to construct a simple model of interacting swimmers in a fluid, that provides microscopic insights for a coarse-grained stochastic theory of active systems.

Bearing in mind, as a realistic paradigm, that living bacteria propel themselves by a variety of periodic, nonreciprocal movements that involve the motion of flagella or cilia, the details of the mechanism of self-propulsion are handled in this model in a simplified way, approximating the force that the swimmer exerts on the fluid as a static force dipole centered at the swimmer's midpoint. Figure 2.5 shows the prototype of swimmer used in [BM09]. It consists of an asymmetric rigid dumbbell with spherical head and tail of radii a_L and a_S. As indicate in the sketch, $\hat{\boldsymbol{\nu}}$ is a unit vector directed along the molecule's axis, oriented from the small (tail) to the large (head) sphere, $\mathbf{f} = \pm f\hat{\boldsymbol{\nu}}$ are the equal and opposite forces and M is the molecule's midpoint. Due to the rigidity of the molecule, denoting with $\mathbf{r}_L$ and $\mathbf{r}_S$, the position of the large and small sphere and, one has $\mathbf{r}_L - \mathbf{r}_S = l\hat{\boldsymbol{\nu}}$. The position of the point C on the axis will be clarified later. The axial asymmetry of the dumbbell results in an time-asymmetric movement protocol, satisfying the constraint imposed from the scallop theorem.

At low Reynolds number is assumed that the swimmer is convected along with the fluid at the local fluid velocity $\mathbf{u}(\mathbf{r})$. The dynamics of the

i-th rigid swimmer is then described by

$$\begin{aligned} \dot{\mathbf{r}}_{L,i} &= \mathbf{u}(\mathbf{r}_{L,i}) \\ \dot{\mathbf{r}}_{S,i} &= \mathbf{u}(\mathbf{r}_{S,i}) \end{aligned} \tag{2.35}$$

The flow velocity $\mathbf{u}(\mathbf{r})$ of the fluid is determined by solving the Stokes equation

$$\mu \nabla^2 \mathbf{u}(\mathbf{r}) = \boldsymbol{\nabla} p - \mathbf{F}_{active} \tag{2.36}$$

where

$$\mathbf{F}_{active} = \sum_i f \hat{\boldsymbol{\nu}}_i \Big[\delta(\mathbf{r} - \mathbf{r}_{L,i}) - \delta(\mathbf{r} - \mathbf{r}_{S,i}) \Big] \tag{2.37}$$

is the active force exerted by the swimmer to the fluid. The fluid exerts equal and opposite forces on the swimmer and the net force is zero at all times. The effect of fluid fluctuations is described, beside the noise generated by the swimmer itself, after the coarse graining at the level of the Langevin equations, by a random force.

Stokes equation (2.36) are solved for the translation of the hydrodynamic center of the body (indicated in figure 2.5 with C) and the rotation about this point. The hydrodynamic center is the point about which the net hydrodynamic torque (exerted by the fluid) on the body vanishes and its position is shown to be defined by

$$\mathbf{r}_C = \frac{\zeta_L \mathbf{r}_L + \zeta_S \mathbf{r}_S}{\zeta_L + \zeta_S} = \frac{a_L \mathbf{r}_L + a_s \mathbf{r}_S}{a_L + a_S} \,, \tag{2.38}$$

where the second equality comes from the definition $\zeta_{L,S} = 6\pi\mu a_{L,S}$, that is the friction of the two spheres of radii $a_{L,S}$ in a fluid of viscosity μ.

Substituting a formal solution of the Stokes equation (2.36) in the boundary conditions for the two spheres (2.35) and using (2.38) provides a set of equations on motion describing the translational and rotational dynamics of the swimmers in the fluid, in the form

$$\dot{\mathbf{r}}_{C,i} = v_0 \hat{\boldsymbol{\nu}}_i + k \sum_{j \neq i} \mathbf{F}_{i.j} + \boldsymbol{\xi}_i(t) \,, \tag{2.39a}$$

$$\dot{\theta}_i = k_R \sum_{j \neq i} \tau_{i,j} + \xi_{R,i}(t) \,. \tag{2.39b}$$

This is a system of N Langevin-like equations in terms of their hydrodynamic center position $\mathbf{r}_{C,i}$ and their directions θ_i about a certain fixed

reference direction. Here v_0, k and k_R are system dependent constant parameters, $\boldsymbol{\xi}_i(t)$ and $\xi_{R,i}(t)$ are Gaussian white noises, $\mathbf{F}_{i,j}$ and $\tau_{i,j}$ are the force and the torque on the molecule i due to the j-th one. The explicit derivation of such equations is not immediate and goes beyond the aim of this little presentation.
As seen in section 2.2 for the case of the general active Brownian motion, no alignment rule are present in the dynamics of the direction angle, but each of the two degrees of freedom of the molecules evolves according to a Brownian diffusion. Although this model is definitely an ABP-type model, such description comes up from fluid dynamic miscroscopic considerations about the motion of this type of swimmers.

Chapter 3

The active dumbbell system

This chapter is aimed to a detailed illustration of the features of the *active dumbbell model*, an active matter model which is the target model of our analysis in the present thesis. We call "dumbbell" a biatomic molecule built of two identical spherical beads stiffly bonded together.
The reasons for the choice of this model are many, mostly regarding with the shape of the dumbbells. It is clear from the literature that (as mentioned above in section 2.2 and carefully described in [PDB06] and [GPBC10]) active particles with spherical shape seems to need of a phenomenological alignment rule. This rule can be of Vicsek's type (section 2.2) or can be taken into account through a direction-dependent friction coefficient, as in equation (2.20) for active Brownian particle's models. Alternatively to phenomenological alignment, all the other ABP's models account for the angular dynamics with an explicit diffusion equation. Even in the case of dumbbell-shape objects, for a microscopic-based swimming dynamics description [BM09], at the mesoscale coarse-grained level an explicit Brownian-type angular diffusion has to be considered, as in equation (2.39b). As we will see within this chapter, angular diffusion comes in the dumbbell model as a resulting feature, due to the interactions within the system, and not need to be placed by-hand in the equations of motion. Furthermore non-spherical constituents are more appropriate to mimic real swimmers, that are typically rod-like or elongated: a common example are most bacteria.
The dumbbell model is therefore a simple way to realize a careful description for some of the features of the physics of active matter, that has been shown to display singular diffusion behaviors and an *activity-induced* phase separation of the type described in section 1.2 and in section 2.1. Moreover active dumbbell's system has provided a tool to investigate the way these nonequilibrium phenomena are affected by particle shape. For instance,

the elongated shape is demonstrated to introduced some local orientational order that possibly may couple to density fluctuations triggering the phase transition, it can affect the dynamics of the motility-induced clusters or perhaps it can change the kinetics of the phase separation.

We will present here a two-dimensional version of the active dumbbell model and we will describe in details some of the results for it, with particular attentions for the activity-induced phase separation, being this particular phenomenon one of the main elements of our investigation.

3.1 Langevin equations for a single dumbbell

We will base the present description on the previous works by Gonnella, Suma, Cugliandolo *et al.* [SGL+14, SGMO14, CGS15, GLS14], that have largely investigated the characteristic of the dumbbell model.

How summarized in the introduction to this chapter, the constituents of this model are dumbbell, namely dimers formed by two identical colloids of mass m and diameter σ, bonded together as rigidly as possible. For practical reasons in the context of numerical simulations of the model, this bond is implemented with a finitely extensible non-linear elastic (FENE) spring. This is the easiest way to mimic a Hookeian spring-like interaction with elastic constant k between the two beads in the dumbbell, that prevent them to eventually separate more than a certain fixed distance r_0 during the time evolution of the system. The FENE interaction results in a potential

$$U_{FENE}(r) = -\frac{1}{2} k r_0^2 \, \log\left[1 - (r/r_0)^2\right], \tag{3.1}$$

where r is the distance between the two beads centers of mass.
An additional repulsive force between the colloids is added, derived from the repulsive part of a Lennard-Jones potential $U_{LJ}(r)$, that ensures that colloids cannot overlap. This potential is known as Weeks-Chandler-Anderson (WCA) potential and is given by

$$U_{WCA}(r) = \begin{cases} U_{LJ}(r) - U_{LJ}(r_c), & r < r_c \\ 0, & r > r_c \end{cases} \tag{3.2}$$

where

$$U_{LJ}(r) = 4\varepsilon \left[\left(\frac{\sigma}{r}\right)^{12} - \left(\frac{\sigma}{r}\right)^{6} \right] \tag{3.3}$$

is the Lennard-Jones potential with ε an energy scale, σ again the diameter of the colloids and $r_c = 2^{1/6}\sigma$ in (3.2) the minimum of the Lennard-Jones potential.

In order to describe the contact between the dumbbell and a heat bath at temperature T, one can use a mesoscale stochastic Brownian dynamics, in a generalized Langevin approach, according to which the beads in the dumbbell move interacting, within a microscopic time scale, with microscopic particles of the bath, whose dynamics need to be ruled out from the description.

3.1.1 A single passive dumbbell

Langevin equations for a single Brownian dumbbell at temperature T in a d-dimensional space read:

$$m\ddot{\mathbf{r}}_i = -\gamma\dot{\mathbf{r}}_i - \left[\frac{\partial U_{FENE}}{\partial r_{ij}} + \frac{\partial U_{WCA}}{\partial r_{ij}}\right]\hat{\mathbf{r}}_{ij} + \boldsymbol{\eta}_i \,, \tag{3.4}$$

where $i, j = 1, 2$ label the two beads in the dimer, γ is the friction coefficient, $\mathbf{r}_i$ is the position of each bead with respect to a fixed frame of reference, $\mathbf{r}_{ij} = \mathbf{r}_i - \mathbf{r}_j$, r_{ij} is its modulus (the distance between two beads) and $\hat{\mathbf{r}}$ its direction. The Gaussian noise $\boldsymbol{\eta}_i$ has zero mean and is delta-correlated:

$$\langle \eta_{i,a}(t) \rangle = 0 \,, \tag{3.5a}$$

$$\langle \eta_{i,a}(t)\, \eta_{i,b}(t') \rangle = 2\gamma k_B T \delta_{ij}\delta_{ab}\delta(t - t') \,. \tag{3.5b}$$

Here a, b are labels for the Cartesian coordinates in a d-dimensional space, k_B is the Boltzmann constant. The value of the strength of the Gaussian noise is related to the temperature and the friction coefficient in order to correctly satisfy the equipartition principle for the expectation value of the energy.

Having in mind to solve equation (3.4) is useful to recast the dynamics in term of the center of mass of the dumbbell $\mathbf{r}_{CM} = (\mathbf{r}_1 + \mathbf{r}_2)/2$, its elongation r_{12} and its direction.

Center of mass diffusion for a single passive dumbbell

In the equation for the center of mass $\mathbf{r}_{CM}$ the contributes to the force due to the FENE and the repulsive WCA interaction cancels out. The equation (3.4) than reduces to:

$$m\ddot{\mathbf{r}}_{CM} = -\gamma\dot{\mathbf{r}}_{CM} + \boldsymbol{\xi} \,, \tag{3.6}$$

where $\boldsymbol{\xi}(t) = (\boldsymbol{\eta}_1 + \boldsymbol{\eta}_2)/2$ is a white noise with zero mean defined by

$$\langle \xi_a(t) \rangle = 0 \,, \quad \langle \xi_a(t)\, \xi_b(t') \rangle = \gamma k_B T \delta_{ab} \delta(t - t') \,. \tag{3.7}$$

This can be view effectively as the Langevin equation of a pointlike particle with mass m, in contact with a bath with friction γ and temperature $T/2$. It can therefore straightforward to recover several results on the statistic of the center-of-mass position and velocity.

The mean-square displacement of the center of mass between two times t' and t can be calculated as

$$\begin{aligned} \Delta^2(t,t') &\equiv \langle [\mathbf{r}_{CM}(t) - \mathbf{r}_{CM}(t')]^2 \rangle \\ &= d\Bigg[\left(v_0^2 - \frac{k_B T}{2m} \right) \frac{\left(e^{-\frac{\gamma}{m}t'} - e^{-\frac{\gamma}{m}t} \right)^2}{(\gamma/m)^2} + \frac{k_B t}{\gamma}(t - t') - \frac{m k_B T}{\gamma^2}\left(1 - e^{-\frac{\gamma}{m}(t-t')} \right) \Bigg] \,, \end{aligned} \tag{3.8}$$

where v_0^2 is the velocity of the particle at the initial time $t = 0$. Note that a separation between two time scale arise from (3.8). Given the inertial time

$$t_I = m/\gamma \tag{3.9}$$

one immediately obtains two different regimes, with respect to the inertial time reference. At short times $0 \leqslant t' \leqslant t \ll t_I$, by expanding all exponentials at small arguments, a ballistic behavior results:

$$\Delta^2(t,t') = d v_0^2 (t - t')^2 \,. \tag{3.10}$$

At long times $t \geqslant t' \gg t_I$ and short time delay $(t - t') \ll t_I$, ballistic mean-square displacement sets again:

$$\Delta^2(t,t') = d \frac{k_B T}{2m} (t - t')^2 \,. \tag{3.11}$$

For long time delay $(t - t') \gg t_I$, no matter where t and t' are with respect to a fixes temporal reference, a diffusive regime takes place:

$$\Delta^2(t,t') = d \frac{k_B T}{\gamma} (t - t') \equiv 2d D_{CM}^{p.d.} (t - t') \,, \tag{3.12}$$

where we have defined the passive-dumbbell (*p.d.*) diffusion constant for the center of mass motion as:

$$D_{CM}^{p.d.} = k_B T/(2\gamma) \,. \tag{3.13}$$

Angular diffusion for a single passive dumbbell

Subtracting the Langevin equations (3.4) for the two beads, a stochastic equation is obtained for the vector $\mathbf{r}_{12} = \mathbf{r}_1 - \mathbf{r}_2$ whose modulus $r_{12} = |\mathbf{r}_{12}|$ is the elongation of the dumbbell and whose direction $\hat{\mathbf{r}}_{12}$ the direction of the axis of the molecule.

$$m\ddot{\mathbf{r}}_{12} = -\gamma\dot{\mathbf{r}}_{12} - 2\left[\frac{\partial U_{FENE}}{\partial r_{ij}} + \frac{\partial U_{WCA}}{\partial r_{ij}}\right]\hat{\mathbf{r}}_{ij} + \boldsymbol{\zeta}\ . \tag{3.14}$$

where $\boldsymbol{\zeta}(t) = \boldsymbol{\eta}_1(t) - \boldsymbol{\eta}_2(t)$ is once again a white noise with the following distribution properties:

$$\langle\zeta_a(t)\rangle = 0\ , \quad \langle\zeta_a(t)\,\zeta_b(t')\rangle = \gamma k_B T\delta_{ab}\delta(t-t')\ , \quad a,b = x,y\ . \tag{3.15}$$

For the sake of simplicity of our notation we renamed r_{12} as R and we restrict the analysis that follows in a 2-dimensional space. In $d = 2$ we recover a simple form for the equation of the direction in terms of the unit vectors $\hat{\mathbf{u}}_{\parallel}$, parallel to the direction of the dumbbell, and $\hat{\mathbf{u}}_{\perp}$, perpendicular to it, whose time derivatives satisfy the relation

$$\frac{\mathrm{d}\hat{\mathbf{u}}_{\parallel}}{\mathrm{d}t} = \frac{\mathrm{d}\theta}{\mathrm{d}t}\hat{\mathbf{u}}_{\perp}\ , \tag{3.16}$$

where θ is the angle between the axis of the molecule and the x axis of the frame of reference. With such notation one obtain:

$$\dot{\mathbf{r}}_{12} = \dot{R}\hat{\mathbf{u}}_{\parallel} + R\dot{\theta}\hat{\mathbf{u}}_{\perp} \tag{3.17}$$

and

$$\ddot{\mathbf{r}}_{12} = \left[\ddot{R} - R\dot{\theta}^2\right]\hat{\mathbf{u}}_{\parallel} + \left[\frac{1}{R}\frac{\mathrm{d}}{\mathrm{d}t}\left(R^2\dot{\theta}\right)\right]\hat{\mathbf{u}}_{\perp} \tag{3.18}$$

whose expressions, inserted in the equation of motion (3.14), give:

$$m\left(\ddot{R} - R\dot{\theta}^2\right) = -\gamma\dot{R} - 2\left[\frac{\partial U_{FENE}}{\partial R} + \frac{\partial U_{WCA}}{\partial R}\right] + \zeta_{\parallel}\ , \tag{3.19a}$$

$$\frac{m}{R}\frac{\mathrm{d}}{\mathrm{d}t}\left(R^2\dot{\theta}\right) = -\gamma R\dot{\theta} + \zeta_{\perp}\ . \tag{3.19b}$$

where we have separate the motion along the parallel and the perpendicular direction and we have decomposed the noise

$$\boldsymbol{\zeta}(t) \equiv \zeta_{\parallel}(t)\hat{\mathbf{u}}_{\parallel}(t) + \zeta_{\perp}(t)\hat{\mathbf{u}}_{\perp}(t)\ . \tag{3.20}$$

It is easy to show that the two scalar stochastic processes $\zeta_\parallel$ and $\zeta_\perp$ are mutually independent and are separately white noises with zero mean and delta-correlated in time, with the same strength as in (3.15).

As we have discussed in section 2.3, physical realization of swimming at low Reynolds numbers (2.33) is the more adherent to reality. From the point of view of the equations of motion this condition reads as an overdamped regime assumption, that practically sets up, in a strict analogy with the low-Re assumption, when the inertial terms in the equations can be neglected with respect to the damping ones. We will illustrate later how to set our model parameters to realize an overdamped motion. Within this approximation, equations (3.19) simplify as follows:

$$\gamma\dot{R} = -2\left[\frac{\partial U_{FENE}}{\partial R} + \frac{\partial U_{WCA}}{\partial R}\right] + \zeta_\parallel \,, \tag{3.21a}$$

$$\gamma R\dot{\theta} = \zeta_\perp \,. \tag{3.21b}$$

Equation (3.21a) do not depends on θ and can solved for the elongation R. The time derivative of R reduces on average, after a certain transient, to zero

$$\gamma\langle\dot{R}\rangle = -2k\langle\frac{\partial U_{FENE}}{\partial R} + \frac{\partial U_{WCA}}{\partial R}\rangle \,, \tag{3.22}$$

therefore $\langle R\rangle$ evolves toward a stationary constant value that, for a proper choice of the parameters of the model (see later), is easy to shown to be $\langle R\rangle \to R_\infty \simeq \sigma$. If we assume to neglect the displacements of R from its mean value (and this is actually the case), we can replace R with its (constant) mean R_∞, and move on to solve the equation (3.21b) for the angular motion.

The time correlation for the angular velocity can be calculated:

$$\langle\dot{\theta}(t)\dot{\theta}(t')\rangle = \left(\frac{1}{\gamma R_\infty}\right)^2\langle\zeta_\perp(t)\zeta_\perp(t')\rangle = \left(\frac{1}{\gamma R_\infty}\right)^2\gamma k_B T\delta(t-t') \,, \tag{3.23}$$

and than the mean-square angular displacement

$$\langle\Big(\theta(t)-\theta(t')\Big)^2\rangle = 4k_BT\gamma\Big(\frac{1}{\gamma R_\infty}\Big)^2(t-t') \equiv 2D_R(t-t') \,. \tag{3.24}$$

As stated before, although no specific dynamics for the angular motion of the dumbbell has been added to the equations, effective rotational motion is generated here by the random torque due to white noises acting independently on the two beads. This results in a diffusive rotational dynamics with diffusive constant $D_R = 2k_BT/(\gamma R_\infty^2)$.

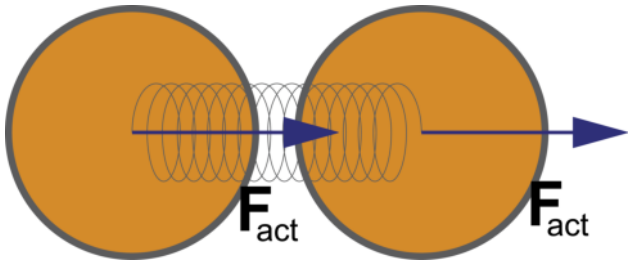


Figure 3.1: A sketch of an active dumbbell molecule. From [SGL+14]

3.1.2 How activity enters in the model

In section 2.2 we have have listed various cases of molecule-scale models that target to describe active matter systems, in which the autopropulsion of the constituents is implicitly modeled either as a constant velocity for the particles (equation (2.15) and equation (2.39)) or by means of a phase-space dependent friction coefficient (equation (2.19)).

Here the choice consists to add, explicitly mimicking the autopropulsion at the molecule scale, an "active" autopropulsion force

$$\mathbf{F}_{act} = F_{act}\,\hat{\mathbf{n}}\,, \tag{3.25}$$

where $\hat{\mathbf{n}}$ is the direction of the straight line passing by the two centers of mass. The active force is therefore constant in modulus, is directed along the axis of the molecule and select in the dumbbell a head and a tail (figure 3.1).

The equations of motion for the auto-propelled dumbbell are than, from (3.4):

$$m\ddot{\mathbf{r}}_1 = -\gamma\dot{\mathbf{r}}_1 - \left[\frac{\partial U_{FENE}}{\partial r_{12}} + \frac{\partial U_{WCA}}{\partial r_{12}}\right]\hat{\mathbf{r}}_{12} + F_{act}\,\hat{\mathbf{n}} + \boldsymbol{\eta}_1\,, \tag{3.26a}$$

$$m\ddot{\mathbf{r}}_2 = -\gamma\dot{\mathbf{r}}_2 + \left[\frac{\partial U_{FENE}}{\partial r_{12}} + \frac{\partial U_{WCA}}{\partial r_{12}}\right]\hat{\mathbf{r}}_{12} + F_{act}\,\hat{\mathbf{n}} + \boldsymbol{\eta}_2\,, \tag{3.26b}$$

where, according to the notation used for a 2-dimensional space,

$$\hat{\mathbf{n}}(t) = \Big(\cos\theta(t), \sin\theta(t)\Big)\,. \tag{3.27}$$

Recalling the same reasoning lines followed for the passive case, combining the two equations in (3.26) one obtains the dynamics for the center of mass of the dumbbell and for its elongation.

Angular diffusion for a single active dumbbell

In the overdamped regime, neglecting the action of the noise on the scalar elongation, R drops to a constant $R_\infty \simeq \sigma$ (σ being the diameter of the two beads). The equation for the angular diffusion reads again:

$$\dot{\theta}(t) = \left(\frac{1}{\gamma R_\infty}\right) \zeta_\perp(t) \equiv \zeta_R(t) \,, \tag{3.28}$$

where

$$\langle \zeta_R(t) \rangle = 0 \,, \tag{3.29a}$$

$$\langle \zeta_R(t)\, \zeta_R(t') \rangle = \left(\frac{1}{\gamma R_\infty}\right)^2 4\gamma k_B T \delta(t-t') \simeq \left(\frac{1}{\gamma \sigma}\right)^2 4\gamma k_B T \delta(t-t') \tag{3.29b}$$

$$\equiv 2D_R \delta(t-t') \,, \tag{3.29c}$$

As obvious form the fact that that the active forces cancel in the equation for the elongation, we recover the same rotational diffusion coefficient of the passive case.

Center of mass diffusion for a single active dumbbell

Adding the two equations in (3.26), one obtains the equation for the single active dumbbell, in the overdamped regime

$$\dot{\mathbf{r}}_{CM} = \frac{F_{act}}{\gamma}\, \hat{\mathbf{n}} + \tilde{\boldsymbol{\xi}} \,, \tag{3.30}$$

where $\tilde{\boldsymbol{\xi}}$ is related to the process $\boldsymbol{\xi}$ of the passive case in (3.6) by

$$\begin{aligned} \tilde{\xi}_a(t) &= \frac{1}{2\gamma} \xi_a(t) \,, \\ \langle \tilde{\xi}_a(t) \rangle = 0 \,, &\qquad \langle \tilde{\xi}_a(t) \tilde{\xi}_b(t') \rangle = 2D^{p.d.}_{CM} \delta_{ab} \delta(t-t') \,, \end{aligned} \tag{3.31}$$

where $a, b = x, y$ and $D^{p.d.}_{CM}$ is the diffusion constant for the center of mass of the passive case (3.13).

The mean-square displacement associated to the center-of-mass motion, setting $\Delta \mathbf{r}_{CM}(t) = \mathbf{r}_{CM}(t) - \mathbf{r}_{CM}(t=0)$, is

$$\langle \Delta \mathbf{r}_{CM}(t)^2 \rangle = \sum_{a=1}^{2} \int_0^t \mathrm{d}t' \int_0^t \mathrm{d}t'' \left[\langle \tilde{\xi}_a(t') \tilde{\xi}_a(t'') \rangle + \left(\frac{F_{act}}{\gamma}\right)^2 \langle \hat{n}_a(t') \hat{n}_a(t'') \rangle \right]. \tag{3.32}$$

Here we are discarded all the $\langle \hat{n}\tilde{\xi} \rangle$ correlations, because these two processes are stochastically independent, as one can immediately check from the definitions of $\hat{\mathbf{n}}$ and $\tilde{\boldsymbol{\xi}}$. Calculating the correlations for the process $\hat{\mathbf{n}}$ in (3.32) and solving the integral we obtain:

$$\langle \Delta \mathbf{r}_{CM}(t)^2 \rangle = 4D_{CM}^{p.d.} t + \left(\frac{F_{act}}{\gamma}\right)^2 \frac{2}{D_R}\left(t - \frac{1 - e^{-D_R t}}{D_R}\right). \tag{3.33}$$

According to this result a new time scale emerges,

$$t_A \equiv \frac{1}{D_R}\,, \tag{3.34}$$

that we call *active time* and that was absent in the passive context. With the aim to consider which is the scenario that sets up here, we stress that we are working in the overdamped limit and all the results that follow will retain its physical meaning within this limit, i.e. for $t \gg t_I$, being t_I defined in (3.9).
If $t \ll t_A$, the exponential in (3.33) can be expanded around small times, resulting in

$$\langle \Delta \mathbf{r}_{CM}(t)^2 \rangle \simeq 4D_{CM}^{p.d.} t + \left(\frac{F_{act}}{\gamma}\right)^2 t^2\,. \tag{3.35}$$

Within this regime we can still distinguish two subregimes. For times shorter than $t^* = 4D_{CM}^{p.d.}\gamma^2/F_{act}^2$ the first term dominates and the dynamics id diffusive as in the absence of the active force. If, instead, times are longer than t^* the dynamics becomes ballistic again and it is controlled by the active force. For even longer times, going beyond t_A, a new diffusive regime establishes,

$$\langle \Delta \mathbf{r}_{CM}(t)^2 \rangle \simeq 4D_A t\,, \tag{3.36}$$

where the new diffusive constant is active-force dependent

$$D_A = D_{CM}^{p.d.} + \frac{1}{2}\left(\frac{F_{act}}{\gamma}\right)^2 \frac{1}{D_R}\,. \tag{3.37}$$

The reason why the dynamics slow down in this last regime although there is still the active force acting on the dumbbell is that the angular diffusive motion goes against the translational one. All the three regimes are summarized in

$$\underset{}{\text{ballistic}} \underset{t_I}{\longmapsto} \underset{}{\text{diffusive}} \underset{t^*}{\longmapsto} \underset{}{\text{ballistic}} \underset{t_A}{\longmapsto} \underset{}{\text{diffusive}}$$

However this rich dynamic behavior may not always be actually identified because, with respect to the choice of the parameters of the systems, some of the four regimes may overlap.

3.2 Numerical integrator for the Langevin equation

In this section will be given a brief description of the numerical algorithm employed to solve the Langevin equations for N active dumbbell in interaction. The equations will be given later (3.44). This method has been used in the previous works about the dumbbell model and represent the starting point for our numerical analysis. The algorithm core is the integration scheme for the Langevin equations, proposed by Vanden-Eijnden and Ciccotti [VEC06]. Such scheme consists in substituting a general Langevin equation of the kind

$$m\dot{v}(t) = F(r(t)) - \gamma v(t) + \sqrt{2k_B T\gamma}\xi(t) \tag{3.38}$$

with the following update rules for position and velocity:

$$\begin{aligned} r(t+\Delta t) &= r(t) + \Delta t v(t) + A(t)\,, \\ v(t+\Delta t) &= v(t) + \frac{\Delta t}{2m}\Big[F(r(t+\Delta t))F(r(t))\Big] + \lambda\sqrt{\Delta t}\phi + \\ &\quad - \frac{\gamma}{m}\Big[\Delta t v(t) + A(t)\Big]\,, \end{aligned} \tag{3.39}$$

where

$$\begin{aligned} \lambda &= \sqrt{2k_B T\gamma}/m\,, \\ A(t) &= \frac{(\Delta t)^2}{2m}\Big[F(r(t)) - \gamma v(t)\Big] + \lambda(\Delta t)^{3/2}\Big[\frac{\phi}{2} + \frac{\theta}{2\sqrt{3}}\Big]\,, \end{aligned} \tag{3.40}$$

and ϕ, θ are independent Gaussian random numbers with zero mean and unit variance. This discretization of the Langevin equation is exact to $(\Delta t)^2$, being Δt the timestep for the update.

Particular attention deserves the choice of the timestep size. First some relevant time scale of the problem have to be identified. The time scale for the oscillation of the free dumbbell is

$$\tau_{osc} = 2\pi\sqrt{m/k} = 2\pi\sqrt{k^*}(\sqrt{m\sigma^2/\varepsilon})\,, \tag{3.41}$$

where the second equality refers to the adimensional definition of the elastic constant k with respect to the units of the problem, as described in the next section 3.3.1. The choice adopted $k^* = 30$ gives $\tau_{osc} = 1.14$. In the same way, the inertial time scale defined in (3.9)

$$t_I = m/\gamma = 1/(\gamma^* \sqrt{m\sigma^2/\varepsilon}) \tag{3.42}$$

equals 0.1.
The time scale associated to the angular diffusion (3.34) is

$$t_A = \gamma\sigma^2/(2k_BT) = \gamma^*\sigma^2 \sqrt{m\sigma^2/\varepsilon}/(2\varepsilon k_BT^*) \, . \tag{3.43}$$

According to these time scales one has to choose $\Delta t = t_I/100 \sim 1/1000$ to see details of the ballistic regime and $\Delta t = \tau_{osc}/100 \sim 1/100$ to enter the later diffusive and active regimes. A good choice for the purpose of our numerical work is the latter, and we will generally use that, whether not differently specified.

Beside the choice of the timescale, the WCA forces represent another issues the algorithm should deal with, since their calculus requires, for each bead, the checking of all the other beads. It is an operation which scales as N^2, differently from the other operations which scale as N. However, as even in these cases, one can generally takes advantages of the short range of the WCA forces, and build, for each bead, a list of the beads closer than σ. The WCA forces are than computed only for beads belonging to the same list, and the N scaling is recover. Finally, in order to ignore the effects of the boundaries, periodic boundary conditions are implemented.
Other informations about different numerical tools used for this work, will be given later, when we will present our results.

3.3 Collective behavior of a homogeneous active dumbbell system

Having established the single-molecule stochastic model, a straightforward generalization allows to consider a system of N such biatomic molecules in interaction, immersed in a bidimensional space. The dynamic equations for each of the N dumbbell in the system are the follows:

$$
\begin{aligned}
m\ddot{\mathbf{r}}_i &= -\gamma\dot{\mathbf{r}}_i - \frac{\partial U_{FENE}}{\partial r_{i,i+1}}\,\hat{\mathbf{r}}_{i,i+1} - \sum_{j=0,j\neq i}^{2N}\frac{\partial U_{WCA}}{\partial r_{ij}}\,\hat{\mathbf{r}}_{ij} + F_{act}\hat{\mathbf{n}}_i + \boldsymbol{\eta}_i\,, \\
m\ddot{\mathbf{r}}_{i+1} &= -\gamma\dot{\mathbf{r}}_{i+1} + \frac{\partial U_{FENE}}{\partial r_{i,i+1}}\,\hat{\mathbf{r}}_{i,i+1} - \sum_{j=0,j\neq i+1}^{2N}\frac{\partial U_{WCA}}{\partial r_{i+1,j}}\,\hat{\mathbf{r}}_{i+1,j} + F_{act}\hat{\mathbf{n}}_{i+1} + \boldsymbol{\eta}_{i+1}\,,
\end{aligned}
\tag{3.44}
$$

where $i = 1, 3, \ldots, 2N-1$ and $\mathbf{F}_{act}$ is directed from the colloid i (tail) to the colloid $i+1$ (head).
Any analytical strategy fails in facing this many-body problem, because the repulsion interaction terms $U_{WCA}(r_{ij})$ in the above equations involve all the beads in the system. However, collective behaviors for this system has been largely investigated in the previous works [SGL$^+$14, SGMO14, CGS15, GLS14] by means of a numerical approach. The details of the numerical integrator have been given in the previous section, because the earliest attempts in our analysis have been made use of the same computational methods.

Interesting phenomena, intrinsically related to activity, have been observed to arise for this model, some of which have been described from a general point of view in the first two chapter of this thesis. In particular, active dumbbell systems exhibit a transition between a homogeneous phase at small activity and a phase with stable aggregates of dumbbell as activity increases. This collective behavior is what we have previously called, and what the literature refers to as "motility-induced phase separation". Recalling our plans, we are mainly interested here to deeply investigate these kinds of activity-driven phase transitions for systems of active dumbbell-like constituents in interaction. Therefore it is convenient to summarize the present knowledge about the setting of the phase separation and its features, defining by now the collective variable relevant for its description. This is what the rest of this chapter will be concerned with.

3.3.1 MIPS for the dumbbells

In the motility-induced phase separation, a positive feedback mechanism of non-equilibrium crowding processes is shown to induce accumulation in compact clusters that, in certain conditions, steadily coexist with a homogeneous gaseous phase. In section 2.1 we have quantitatively described, from a field theory kinetic viewpoint, how, according to this feedback, particles decelerate where they are more concentrated and accumulate where

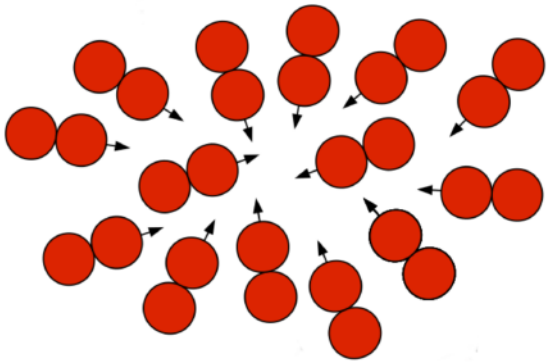


Figure 3.2: Aggregation mechanism: The arrows represent the direction of active forces. If activity is sufficiently large, these also represent the direction of motion. Then, when a group of dumbbells collide moving toward a common center, active forces nullify each other and a small cluster can be formed.

they go slower. This character is strictly activity-dependent and turns on regardless of the kind of the interaction among the constituents of the system, allowing the separation to take place even with a pure repulsive inter-particle interaction.

Figure 3.2 sketches how dumbbells can eventually begin to form an aggregate. During the Brownian motion, small, compact clusters form spontaneously since, when a group of dumbbells collide moving toward a common center, active forces cancel out. Although, due to these events, generally unstable clusters form, the arrival of more dumbbells could make them more stable, allowing aggregates to grow up and the system to separate.

The emergent physical picture is thus that of a simple self-trapping mechanism: two or more dumbbells that collide head-on are blocked due to the persistence of their orientations. Hence, a dumbbell situated at the edge of a cluster has to wait a time $\sim 1/D_R$ (being D_R the diffusive constant related to the angular diffusion) until rotational diffusion points its orientation outward to become free again. While the time to leave the cluster is independent of the swimming speed, a larger swimming speed implies a larger probability for other dumbbells to collide with the cluster, leading to its growth. The size of clusters is determined by the flux balance of incoming and outgoing dumbbells.

According to these picture, some relevant quantities manifestly take part in the macroscopic clustering phenomenon: the density of the system, the activity sources and the damping ones. In the 2-dimensional dumbbell system, the number density is taken into account with the so-called *surface*

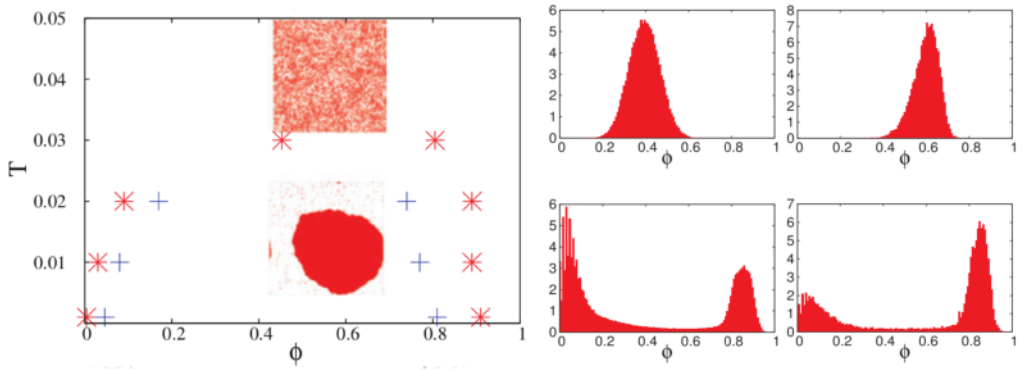


Figure 3.3: (a) Phase diagram for an active dumbbell suspension (stars), in the density-temperature plane, together with snapshots of the system in the uniform (top) and phase separated (bottom) regimes. (b)–(e) Probability distribution functions for finding a given local density ϕ. Plots are shown for parameters corresponding to the following points on the phase diagram in panel (a): (b) $T = 0.1$ $\phi = 0.4$, (c) $T = 0.1$ $\phi = 0.6$, (d) $T = 0.01$ $\phi = 0.4$, (e) $T = 0.01$ $\phi = 0.6$. From [SGMO14].

fraction

$$\phi = N\frac{2\pi(\sigma/2)^2}{S} = \frac{N\pi\sigma^2}{2S}\,, \tag{3.45}$$

where N is the total number of dumbbells and S the surface available. The *Péclet number* is a dimensionaless number that accounts for the balance between advective and diffusive transport:

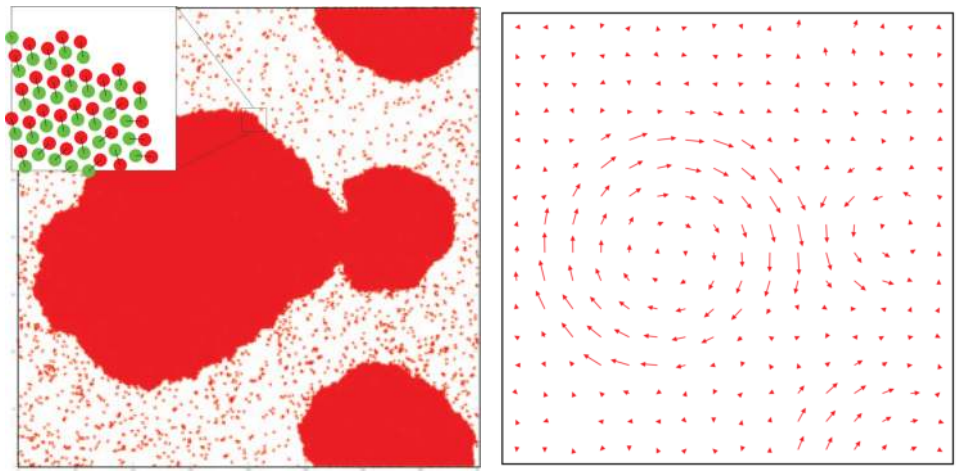
$$\mathrm{Pe} = \frac{Lv}{D} \tag{3.46}$$

with L a typical length, v a typical velocity and D a typical diffusion constant. Obvious choices are here $L \sim \sigma$, $v \sim F_{act}/\gamma$ and $D \sim k_B T/(2\gamma)$ the translational diffusion constant for a single passive dumbbell, as in (3.13). With these values we have:

$$\mathrm{Pe} = \frac{2\sigma F_{act}}{k_B T}\,. \tag{3.47}$$

Another important parameter is the active Reynolds number

$$\mathrm{Re} = \frac{mF_{act}}{\sigma\gamma^2}\,, \tag{3.48}$$



(a) (b)

Figure 3.4: (a) Snapshot of a phase separated active dumbbell fluid with three clusters (two of which are touching). The inset shows a detail of the dumbbell configuration; red and green beads indicate the tail and head of each dumbbell and are connected by a line. (b) Coarse-grained velocity field corresponding to the snapshot in (a), obtained by local averages on a square mesh. From [SGMO14].

defined in analogy with the usual hydrodynamic Reynolds number $\mathrm{Re} = Lv/\mu$ where μ is the viscosity of a given fluid. Expression (3.48) results by setting $\mu \sim \gamma\sigma^2/m$. The Reynolds number has to be fixed to small values, as we explained above, in order to keep the overdamped approximation in the Langevin equations.

Gonnella, Suma *et al.* in [SGMO14] studied for the first time how MIPS is related to these parameters in a suspension of active dumbbells. Before to summarize their results, we spend a few words about the parameters that remain fixed during simulations. Their numerical values have to be chosen appropriately to reproduce a set of physical conditions, suitable for the problem under investigation. The units of mass and length are respectively the mass m of a colloid and its diameter σ, whereas the unit of energy is the energy scale ε of the Lennard-Jones inter-particle interaction. All the other parameters are referred to these three quantities: the adimensional elastic constant is defined as $k^* = k\sigma^2/\varepsilon$, the maximum extension length in the FENE potential is rendered adimensional as $r_0^* = r_0/\sigma$, the thermal energy as $k_BT^* = k_BT/\varepsilon$ and the friction constant as $\gamma^* = \gamma/\sqrt{\varepsilon m/\sigma^2}$. The FENE parameters are set to $k^* = 30$ and $r_0^* = 1.5$, preventing the dumbbell to extends excessively and to vibrate. The friction constant has to be high enough for the overdamped limit to be valid (namely such that $\mathrm{Re} \ll 1$)

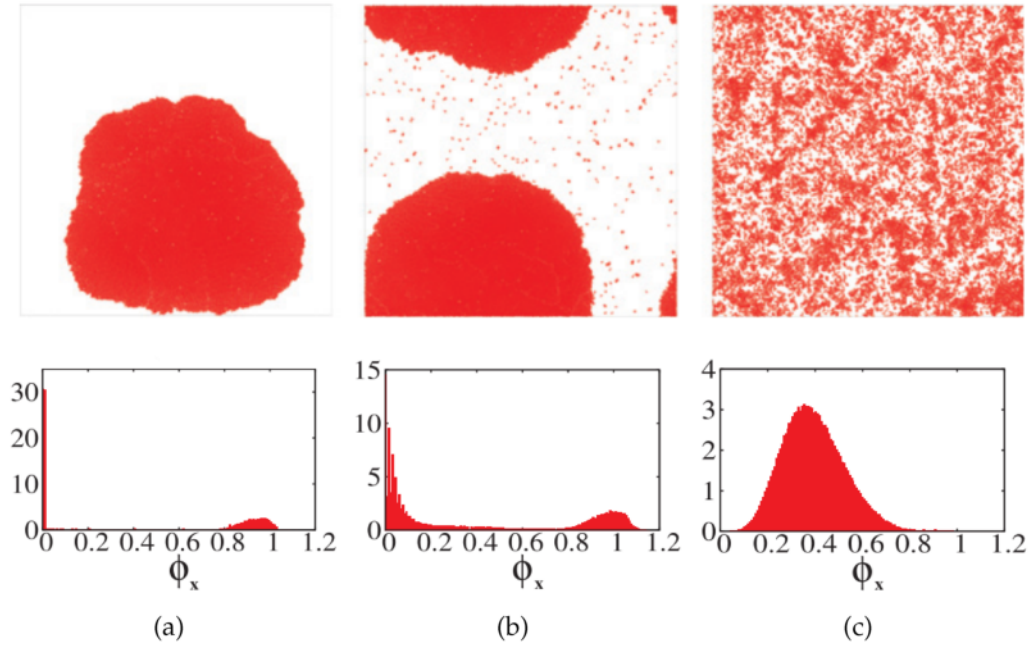


Figure 3.5: (a,b,c) - Snapshots of an active dumbbell fluid at $\phi = 0.4$, $T = 0$, and F_{act} equal to 3 (a), 5 (b) and 7 (c). The figures in the lower line show the corresponding probability distribution functions for the local densities. In (a) the system is phase separated, whereas in (c) it is in the uniform fluid phase. In (b) it is still phase separated but close to crossover to the uniform phase at large F_{act}. From [SGMO14].

and $\gamma^* = 10$ is used. Once all parameters are expressed in terms of reduced units one can effectively set $m = \sigma = k_B = \varepsilon = 1$. These are the choices generally adopted in [SGL+14, SGMO14, CGS15, GLS14] and within this work, unless differently stated.

Having three relevant parameters (ϕ, Pe and Re), a generally followed strategy is to take one fixed, varying the others, with the aim to lay out how activity, density and friction mutually couple in the process of motility-induced phase separation. In [SGMO14], for example, one set of analysis is carried out, taking Re fixed, varying the surface fraction and the Péclet number to characterize whether the separation triggers. Increasing the surface fraction at fixed temperature the active dumbbell fluid phase separates. A $(T - \phi)$ phase diagram results, as shown in figure 3.3, observing the peaks of the probability distribution function of the local value of surface fraction in the separated phases. Recasting this phase diagram in the $(\phi - \mathrm{Pe})$ plane, results are shown to be extremely sensitive to the actual value of F_{act}, since varying F_{act} leads to variations in two of the three dimensionaless number we identified before.

Moreover phase separation is observed to be suppressed when the active force increases as T and ϕ are kept constant, as is shown in the figure 3.5. This evidences the fact that not only the active Péclet number, but also the active Reynolds number (3.48) matters in the phase separation phenomenon. Local ordering within the high-density clusters is also inspected, and has been demonstrate that there is both local nematic and hexatic order, the former being unique to the case of non-spherical swimmers.

These results represent the starting point for the program of our work. The complex phase transition phenomenology presented here, along with local orientational order in the dense dumbbell phase, suggest to question whether such phase separation can be related to an equilibrium phase separation, as the active force continuously goes to zero, arising for a solid-liquid-like equilibrium phase transition. In the next chapters we will present more details about both equilibrium transitions and active phase separation for our dumbbell system, and we will explore the possibility for an interplay between them.

Chapter 4

Phase transitions in the passive dumbbell system

We dedicate this chapter to the analysis of the ordering transition in our two dimensional passive dumbbell system, since it does deviate from a standard melting transition picture, due to the low dimensionality of the system.
We will present in the first two section the general classic background for two dimensional melting, describing the problems concerning with it, outlining the possible schemes existing for its description, and after showing some answers to open questions, coming from the more recent numerical works. After we will show our numerical results for the dumbbell system.

4.1 No long-range order in one and two dimensions

Macroscopic physical properties of matter depend on the interactions between atoms or molecules, on their spatial arrangement and on temperature. A balance between the internal energy and entropy dictates the thermodynamic phase behavior of the bulk material. Depending on temperature, pressure or density different phases may appear with completely different response to external solicitation: response functions such as mechanical compressibility or shear modulus may greatly differ in the high and low temperature phase. As a rule the high temperature phase is always more symmetric than the low temperature phase. In a fluid, for instance, the positions of the atoms are randomly distributed and no position is more likely than any other. At macroscopic scales the fluid therefore

looks the same at every position, indicating continuous translational and orientational symmetry. By lowering the temperature T of the fluid, translational degrees of freedom of individual particles become restricted. The system can lower its free energy $F = E - TS$ by introducing order. The corresponding loss of entropy S (that enters free energy F with a negative sign thereby leading to an increase of free energy) is overcompensated by the reduction of the internal energy E: potential energy wins against thermal energy.
Symmetry is broken due to ordering: atoms arrange in closed packed periodic structures where continuous translational and orientational symmetries are broken in favor of discrete ones. It is a general feature of phase transitions, that high symmetry in the high temperature phase is broken in one or several steps until a low temperature phase with low symmetry occurs.

The concept of macroscopic symmetry breaking does not tell us anything about how a particular system manages to do so on the atomic scale. In fact, the microscopic processes involved both in melting and freezing are still poorly understood in many systems. As a general concept, during heating of the system, increasing amounts of defects in the ordered phase and dynamical (vibrational) modes provide the tools to restore symmetry. The dynamical modes depend strongly of the phase itself and are connected to the corresponding response functions which are thus strongly dependent on temperature. In a liquid, for instance, there is no transverse sound but longitudinal one since there is no shear but a compression modulus.

Since the beginning of the twentieth century, in the middle of the debate about the building of a statistical mechanics language for the phase transition phenomena, Peierls [Pei32] and Landau [Lan37] realized that phase transitions strongly depended on the system's dimensionality. They argued, for example, that there can not be one- or two-dimensional crystalline long-range order. In the argument from Peierls, a crystal is assumed to exists, his vibrations are studied within the classical harmonic approximation [AM76], and the mean square displacement of a particle is computed. When this mean square displacement is found to become infinite in the thermodynamic limit, the existence, previously assumed, of the crystalline order is discarded. These arguments were followed by some numerical studies, the most important of which was conducted by Alder and Wainwright [AW62], that indicated a transition to a two-dimensional crystalline ordered state, casting some doubt on the validity of the results from Peierls and Landau in two dimensions. Mermin and Wagner [MW66, Mer68], reviewed this question formulating what is generally called *Mermin-Wagner*

theorem, that excludes symmetries to spontaneously break at finite temperature in systems with sufficiently short-range interactions in dimensions $d \leqslant 2$. This practically allows for long-range fluctuations to be created with little energy cost and to destroy the long-range crystalline order. A detailed presentation of the Mermin argument [Mer68], goes beyond the purpose of this thesis, but, since an outline of the results may be useful for a deeper understanding of the discussion that follows, we discuss them in appendix A.

4.2 Melting scenarios for two-dimensional systems

In 2D systems a microscopic theory of melting was developed in the 70th by Kosterlitz, Thouless, Halperin, Nelson, and Young (KTHNY-theory). We rapidly summarize here the results of this theory, postponing to the next section a detailed illustration of the quantities used and their behavior. Melting is said to be driven by the emergence, in the crystalline phase, of a class of topological defects, namely thermally activated dislocations pairs which dissociate at the melting temperature T_m [KT72, KT73, You79] [†]. This gives rise to a softening of the crystal's compressibility and shear elasticity, resulting in a second order phase transition. A few years later the arising of this scheme, Nelson and Halperin predicted that the fluid phase above T_m still exhibits quasi-long-range orientational order with a sixfold symmetric field [HN78, NH79]. The orientational correlation function in this phase decays algebraically which is associated with a non-vanishing elastic modulus of the orientational stiffness. Finally, at a temperature $T_i > T_m$, the orientational symmetry is broken upon the origination of a second class of topological defects. Some of the dislocations dissociate into free disclinations leading to another second order transition and an exponential decay of the orientational correlation function above T_i [‡]. The fluid shows ordinary short range rotational and positional order as a characteristic of any isotropic liquid. The intermediate thermodynamic phase, located between the isotropic liquid and the crystalline solid, (which is unknown in

[†]A dislocation in a two-dimensional crystal is a defect that arises from the insertion of half lattice lines into the otherwise perfect lattice. Dislocations result as couples of a particle with five nearest neighbors and a particle with seven neighbors. Such pairs can evolve from local lattice displacements.

[‡]Disclinations arise from the complete decomposition of a dislocation into an isolated five-fold coordinated site and another seven-fold coordinate site.

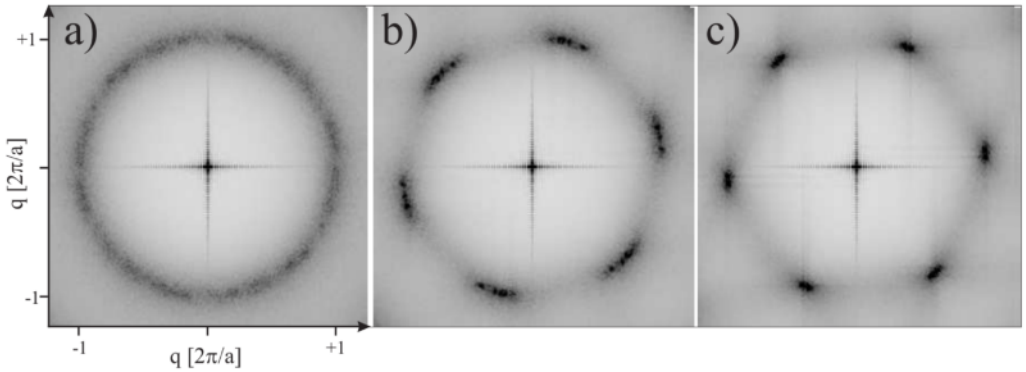


Figure 4.1: Structure factor, as defined in (A.3), of a colloidal systems in the various phases of the KYHNY transition: (a) - isotropic liquid, (b) - hexatic phase and (c) - crystal. $a = 1/\sqrt{\eta}$ is the average inter-particle distance, with η being the 2D-density.

3D-systems) is called *hexatic*. In order to visualize the different symmetries, the structure factors (A.3) of all the three phases are shown in figure 4.1.

We are not interested here in a detailed illustration of the defects-unbinding mechanism, for at least one fundamental reason. While the constituents of our system are dumbbell-like molecule, two-dimensional positional and orientational order involves each bead individually (this will be clear once all the variables related to the order in the system will be defined). More specifically, the constraint requiring two beads in a dumbbell to be stiffly bonded, strongly affects the characterization of the possible topological defects, and it changes for sure their binding/unbinding dynamics. Although there would not be possible for us to strictly refer to defects-unbinding-driven transitions, the dumbbell system seems anyway to undergo a melting protocol that presents many details in common with the KTHNY's one. Then we will describe in the next section the general features of the three phases in the KTHNY two-step melting transition, and later we will show a recent representative results about some of its particular interesting aspects. For anyone who is interested in the formal treatment of the microscopical KTHNY theory, namely how different type of defects can break translational or rotational symmetries and drive the transition, the works of Kosterlitz, Thouless, Halperin and Nelson provide an exhaustive explanation of all the phenomena involved.

4.2.1 Observables and correlations for the KTHNY melting scenario

As we have described before, according to the KTHNY scheme, a two-stage continuous transition correctly reproduces the melting behavior of a two-dimensional system.
We begin to describe here the properties of the crystalline phase. We stress that in two-dimensional crystals, translational symmetry does not correspond to a true long-range order. However, since the fluctuations of position weakly diverge at long distance, one generally speaks about a *quasi-long-range* positional order. This positional order is conveniently described in terms of the follow *positional correlation function*

$$C(r) = \langle \rho(\mathbf{r}_1)\rho(\mathbf{r}_2)\rangle_{|\mathbf{r}_1-\mathbf{r}_2|=r} \,. \tag{4.1}$$

In order to describe how this correlation behaves in the quasi-long-range ordered crystal, we suppose that the displacements due to thermal fluctuation $\mathbf{u}$ vary only slightly over scales of the order of the lattice spacing. The fluctuating density can than be written as $\rho(\mathbf{r}) = \rho^{(0)}[\mathbf{r} - \mathbf{u}(\mathbf{r})]$, where $\rho^{(0)}$ is the perfect periodic density. An expansion in Fourier series can be made as follows:

$$\rho^{(0)}(\mathbf{r}) = \sum_{\mathbf{K}} \rho_{\mathbf{K}}\, e^{i\mathbf{K}\cdot\mathbf{r}} \,, \tag{4.2}$$

where $\mathbf{K}$ are the reciprocal lattice vectors. Substituting this expansion in the definition (4.1) of the positional correlation function we obtained

$$C(r) = \sum_{\mathbf{K}} |\rho_{\mathbf{K}}|^2\, e^{i\mathbf{K}\cdot\mathbf{r}} \,\langle \exp(-i\mathbf{K}\cdot(\mathbf{u}_1 - \mathbf{u}_2))\rangle \,, \tag{4.3}$$

where we have written $\mathbf{u}(\mathbf{r}_1) = \mathbf{u}_1$ and $\mathbf{u}(\mathbf{r}_2) = \mathbf{u}_2$. Using the same strategy adopted in appendix A to calculate the mean square fluctuations, we can perform the statistical average in (4.3) obtaining:

$$C(r) \propto \frac{1}{r^{\nu}} \,, \tag{4.4}$$

for large distances r, with $\nu \propto k_B T$. This algebraic decay is the characteristic feature of what we have called quasi-long-range order. The correlation length diverges in this phase, though correlations decrease to zero at long distances, differently from the three-dimensional true long-range where correlation reach a nonzero constant value.

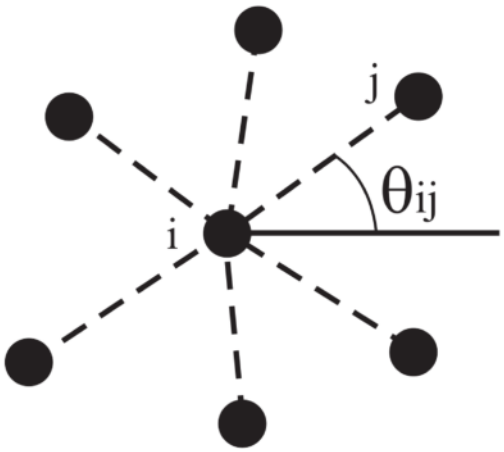


Figure 4.2: "Bonds" (dashed lines) joining a central particle i to its six nearest neighbors j. Each bonds make an angle θ with a fixed reference axis.

As suggested by the Mermin-Wagner theorem, a long-range order actually exists in the crystalline phase, regarding the directions of the bonds between particles.
In the case of spherical constituents for the systems, bonds in the ordered state are arranged about a triangular lattice. The bond orientational order is than usually quantified using the following *orientational correlation function*

$$C_6(r) = \langle \psi_6(\mathbf{r}_1)\psi_6(\mathbf{r}_2)\rangle_{|\mathbf{r}_1-\mathbf{r}_2|=r} , \tag{4.5}$$

where $\psi_6(\mathbf{r})$ is a local orientational order parameter, called *hexatic* from their hexagonal symmetry properties, defined for each particle position as

$$\psi_6(\mathbf{r}_i) = \frac{1}{n_i}\sum_{j=1}^{n_i} e^{\mathrm{i}6\theta_{ij}(\mathbf{r}_i)} , \tag{4.6}$$

where n_i are the number of the nearest neighbors of the particle i and $\theta_{ij}(\mathbf{r}_i)$ is the angle that the "bonds" between particle i with its j-th neighbor forms with a fixed reference axis (figure 4.2). For a perfect triangular lattice, all the angle θ_{ij} are the same, and therefore $|\psi_6| = 1$. We use here the misleading term "bond" regardless the actual potential between constituents. However the definition is the same also when, as in our dumbbells, there is not any real bond between particles, in which case it refers simply to the segment connecting two neighbor particle's centers of mass. As stated before in section 4.1 for an analogous orientational correlation function, in a two-dimensional crystalline phase this correlation

function can be shown to be constant for large distances, indicating a true long-range orientational order.

	Solid	**Hexatic**	**Liquid**
Position	quasi-long	short	short
Orientation	long	quasi-long	short

Table 4.1: Positional and orientational ordering in the KTHNY theory.

Starting from the crystalline phase, a first continuous transition breaks the translational symmetry. This transition, in the KTHNY theory, does not lead to the disordered liquid phase, but to a new phase, called hexatic. In the hexatic phase the positional order is short ranged, identified with an exponential decay of the positional correlation function define in (4.1), whereas the orientational order in quasi-long ranged and the associated correlation function $C_6(r)$ falls to zero with a power law. Finally, a second continuous transition melts the haxatic phase and the isotropic liquid phase settles. Liquid is a disordered phase where both the positional and the orientational correlations decay exponentially, establishing a finite correlation length. Table 4.1 summarizes the ordering displayed in the three phases involved in the KTHNY scheme for melting in two dimensions.

4.2.2 Two-step first order melting for hard disks

We have mentioned before in section 4.1 that the existence of an ordered crystal phase in two dimensions was established for the first time to exist by Alder and Wainwright [AW62] for a two-dimensional system of hard disks. The features of two-dimensional crystal has been previously discussed and a widely accepted scenario for the melting in two stages has been described in section 4.2. Instead the order of the two transitions is a debated argument even at present. According to the KTHNY description, the breaking of the positional order in the crystal and next of the orientational one in the hexatic solid are transitions of second order. We review now a series of work by Krauth, Bernard, Kapfer *et al.* that have been found a different significant result: their numerical Monte Carlo investigations have revealed that, depending of the inter-particle potential, within the general framework of KTHNY, the hexatic-to-liquid transition is a first order transition, exhibiting a phase-coexistence region.
This feature was already observed in [AW62] from numerical experiments, and even though their simulations was less accurate than the more recent

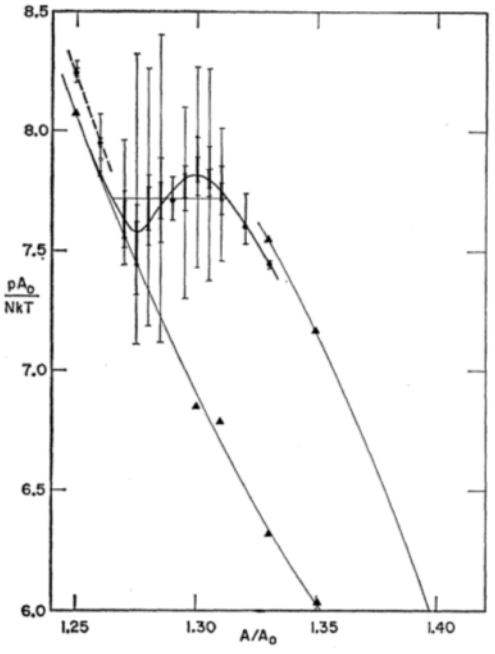


Figure 4.3: The equation of state of hard disks in the phase transition region. The heavy vertical lines indicate the estimated accuracy of the average pressure determination at each density. As can be seen, the fluctuations are much larger in the phase transition region than in the pure solid ($A/A_0 < 1.26$) and pure fluid ($A/A_0 > 1.33$) phases and they are also larger in the middle of the phase transition region than near the ends. A/A_0 is the reduced area with respect to the area A_0 of the system at close packing. This figure is obtained from [AW62], from a simulation of 870 hard-disks.

ones, the presence of a loop in the phase diagram, showed in figure 4.3, had allowed to indicate a discontinuity in the transition, preventing the question about the order of the transition to be answered with certainty. As explained by Mayer and Wood [MW65], this loop is a result of finite simulation sizes and therefore differs conceptually from a classical van der Waals loop, which is derived in the thermodynamic limit. The branches of the Mayer-Wood loop are thermodynamically stable, but vanish in the limit of infinite size. It is known that the presence of a Mayer-Wood loop in the equation of state is observed in systems showing a first-order transition as well as systems showing a continuous transition. However, the behavior of these loops with increasing system size is different. For a first-order transition, the loop is present in the coexistence region and is caused by the interface free energy F. In two dimensions, the interface free energy per disk $\Delta f = \Delta F/N$ scales as $f \propto N^{-1/2}$. In contrast, for a continuous transition, f decays faster, normally such that F is constant, that is $f \propto N^{-1}$, and the equation of state becomes monotonic for large enough systems.
In [BK11] the first-order nature of the transition involving the liquid is established by the visual evidence of phase coexistence (4.4), the $\propto \sqrt{N}$ scaling of the interface free energy per disk, and the characteristic shape of the equation of state in a finite periodic system.

Hard-disks model study represents often an accessible strategy to understand general behaviors of systems with short-range interactions. The

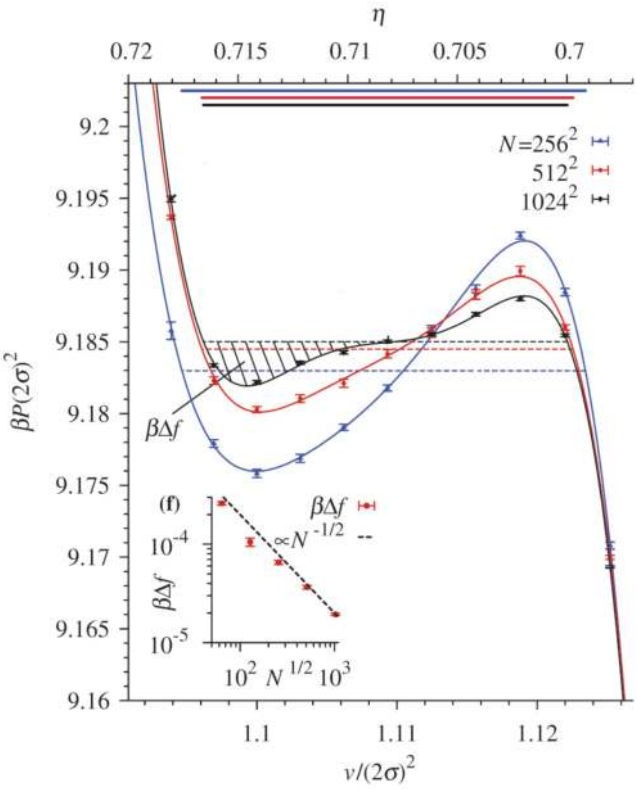


Figure 4.4: Equilibrium equation of state for hard disks. The pressure is plotted vs volume per particle ($v = V/N$) (lower scale) and density η (upper scale). In the coexistence region, the strong system-size dependence stems from the interface free energy. The Maxwell constructions (horizontal lines) suppress the interface effects (with a convex free energy) for each N. The interface free energy per disk $\beta\Delta f$ (hatched area) scales as $1/\sqrt{N}$ (f). From [BK11]

first order nature of the two-dimensional solid-to-hexatic transition for hard disks finally seems to be a certainty, after what accurately stated in a lot of works, among which the works of Krauth *et al.*. However, out of the hard-disks context, if one considers, as in our case, more real short-range interactions (for example power-law repulsive potentials), some complications arise. Even the nature of the low-density transition in the two-step KTHNY melting, becomes less clear, and anyway it suffers a strong dependence from the specific form of the potential.

Kapfer and Krauth [KK15] investigate this dependence, systematically studying, using computer simulations, the KTHNY transition for a wide range of repulsive power-law and Yukawa potentials in two dimensions. As anticipated, they find that the extension in the phase-space of region in which liquid and hexatic phases coexist (and consequently the first order character of the transition) strongly depends on the choice of the potential. In figure 4.5 is reported a graphical summary of their work, that shows how the coexistence region spreads and shrinks, varying the exponent in the power-law repulsive pair interaction and how the equation of state of the system in the transition region, change its behavior, eventually losing (referring to the Mayer-Wood loop) evidences of a first-order transition.

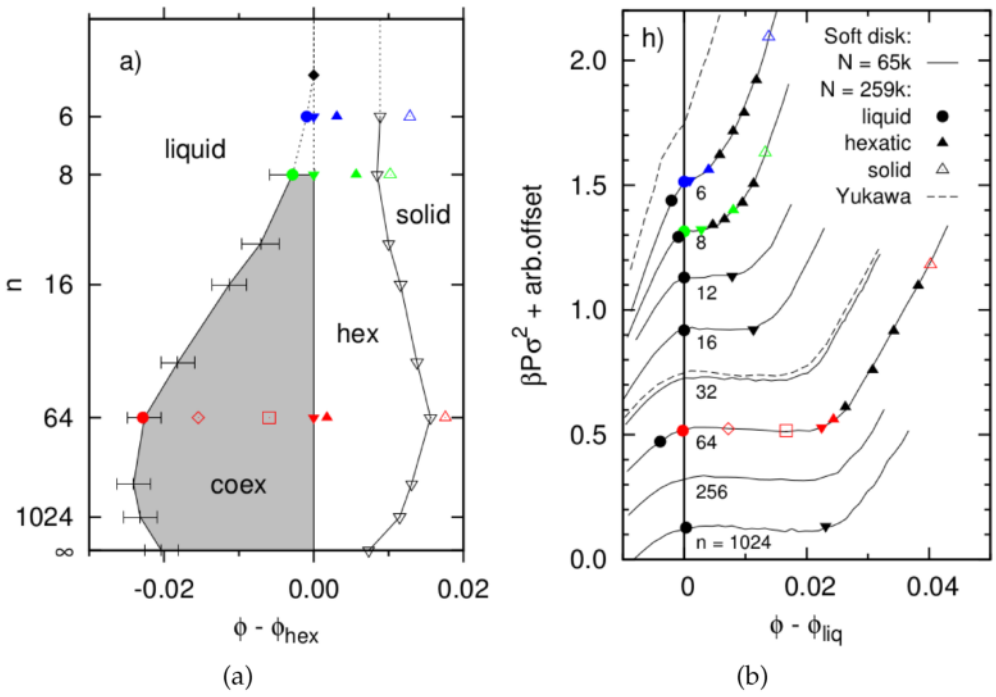


Figure 4.5: Phase behavior of r^{-n} soft disks for $n \geqslant 6$. (a) Phase diagram as a function of density ϕ relative to the density ϕ_{hex} of the pure hexatic at coexistence. The non-monotonic liquid-hexatic coexistence interval vanishes around $n = 6$. Symbols match the following figures: bullets are liquid states, filled triangles hexatics, of which downward filled triangles the hexatic at ϕ_{hex}; empty triangles are solids. (b) Equations of state with n from 6 through 1024 (solid lines correspond to $N = 65000$ soft disks, symbols correspond to $N = 259000$, ϕ_{liq} is the liquid density at coexistence, dashed lines are for Yukawa particles). From [KK15]

In particular, always within a two-step melting scenario (that is therefore strongly confirmed, regardless how much soft the particles are), the analysis in [KK15] shows that to different scenarios sets up depending on the steepness of the pair repulsion. Denoting with n the exponent in a $U(r) \propto (\sigma/r)^n$ potential (σ being the characteristic size of the system, for example the diameter of the particles), at large n values a hard-disk-like behavior is present, with a first-order hexatic-liquid transition, even with a coexistence region that becomes smaller as the exponent decreases. How n is further decreased, a new scenario is shown to emerge, in which the hexatic-to-liquid transition is of second order, and the two phase can not coexist together.

We start from these results, with the aim to understand how the KTHNY transition takes place in our soft dumbbell system. As we will be described

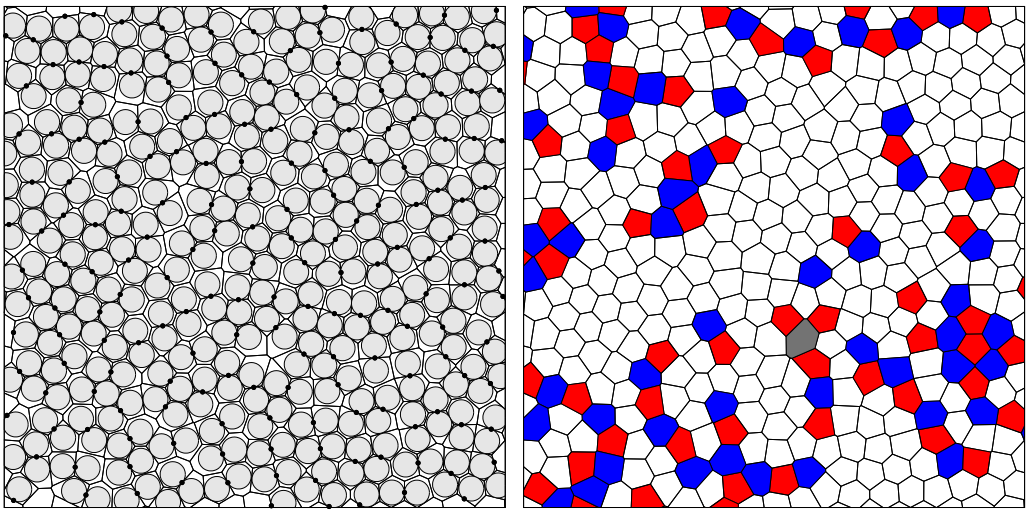
later, the weakness of the first order nature of the low-density transition, has resulted to be evident even for the dumbbells. Therefore some insights that come from the these analysis of spherical colloids systems are demonstrate to be helpful for our purpose, that, as explained throughout the thesis, goes beyond the understanding of the features of the passive system only, and is specifically aimed in the characterization of the transitions of the system driven out of equilibrium by activity.

4.3 Observables for the dumbbell system

We will explain in this section how the observables in the system are evaluated, and which graphical strategies are adopted to visualize them. Our numerical studies involve a system of dumbbell in interaction through a repulsive pair potential, as described in detail in chapter 3. Although in this chapter we limit our considerations to the passive case, the observables and the methods used for understanding their behavior will be essentially the same even throughout the investigation of the system with activity, which will follow in this thesis. Among the considerable quantities in the context of the liquid-to-solid transition, the local hexatic parameter $\psi_6(\mathbf{r}_i)$, as defined in (4.6), and its sample average are strongly sensitive from a methodological viewpoint about how they are evaluated, and are the less widely used in the condensed matter literature. For these reasons they deserve a particular attention and a detailed description. This section it essentially devoted to it.

4.3.1 Voronoi diagram

The more relevant trouble that can arise if one look to the definition (4.6) of the local hexatic parameter, is about the choice of the nearest-neighbors network in a system in which particles positions are displaced from the nodes of a perfect triangular lattice, of an amount that depends on the ordering in the system. A way to unambiguous define which particles are nearest to any other is making use of the so-called *Voronoi tessellation*. Generally speaking, given a set (finite for simplicity) of points $\mathbf{p}_1, \ldots, \mathbf{p}_M$ in some d-dimensional space, Voronoi rule establishes a partitioning of the space with M regions $D_1, \ldots, D_M$, one for each point. The region D_i, associate to the point $\mathbf{p}_i$, contains all the points of the space that are closer to $\mathbf{p}_i$ than to any other $\mathbf{p}_j$ ($j \neq i$). In figure 4.6 is showed an example of what we have described about the Voronoi tessellation strategy.

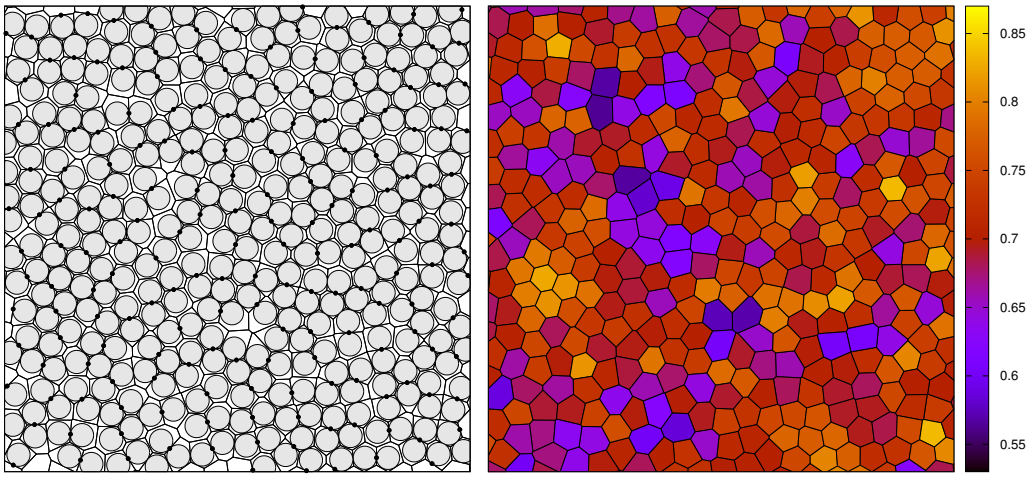


(a) (b)

Figure 4.6: (a) - Voronoi tessellation for a dumbbells configuration. Each colloid has its Voronoi region, that delimits the portion of space around the colloids of the points that are closer to it than to any other. All the beads are shown in gray. Black spots are the centers of mass of the dumbbells. (b) - The Voronoi construction defines colloids neighborhood. Taking the i-th disk and its cell, we choose as its neighbors all other disks whose cell have at least one side in common with the i-th cell. We have colored in red the cells with five neighbors, in blue the cells with seven neighbors and in gray all the other cases. Cells with six nearest neighbor are not colored.

Thanks to the Voronoi tessellation, the definition of nearness relations between particles comes straightforwardly. Two particles are defined to be neighbors if their Voronoi cells share at least one of their sides. We specify that the points used as seeds for the Voronoi construction, are the centers of mass of each colloid. This choice, alternatively to the possibility of taking as seeds the centers of mass of the dumbbells, is quite obvious, since in our system the hexatic order has to be sought in the high packed configurations, in which the single colloids occupy the nodes of a triangular two-dimensional lattice.
Note that this definition of the neighbors network may cause particles to have a variable number of neighbors. Figure 4.6-(b) shows how it is possible, once the Voronoi regions are drawn, to individuate the neighbors of a given particles and how to count them.

The Voronoi diagram gives also a useful possibility to estimate the local surface fraction of the system. In fact, since every bead has its Voronoi region, one can easily evaluate the local value of the surface fraction at the position $\mathbf{p}_i$ of a bead, taking the ratio between the surface of the bead



(a) (b)

Figure 4.7: (a) - Voronoi tessellation for a dumbbells configuration. (b) - The local values of the surface fraction, as defined in the text, are plotted using the color gradient shown on the right.

$S_i^{(\text{beads})}$ and the surface $S_i^{(\text{cell})}$ of the corresponding Voronoi cell

$$\phi(\mathbf{p}_i) = \frac{S_i^{(\text{beads})}}{S_i^{(\text{cell})}} = \frac{\pi(\sigma/2)^2}{S_i^{(\text{beads})}}\,, \tag{4.7}$$

where σ is, as previously defined, the diameter of the beads and the $S_i^{(\text{cell})}$s are quite simple to be calculated, since they are the surfaces of irregular convex polygons. In figure 4.7 is shown an example for this procedure.
For all the practical purposes, this estimation of the local density of the system has an extreme local nature, and than results in a strongly fluctuating density profile. When the estimation of the density is made through this method, a successive coarse-graining procedure has to be performed, within a given scale, in order to suppress the larger fluctuations and recover a smooth density profile.

4.3.2 Local hexatic order

We have previously anticipated that a useful graphical strategy has been used, with the purpose to have a practical way to visualize the local hexatic order parameter, defined in (4.6), which, as explained before, plays a fundamental role in the study of the crystallization of colloidal two-dimensional systems.

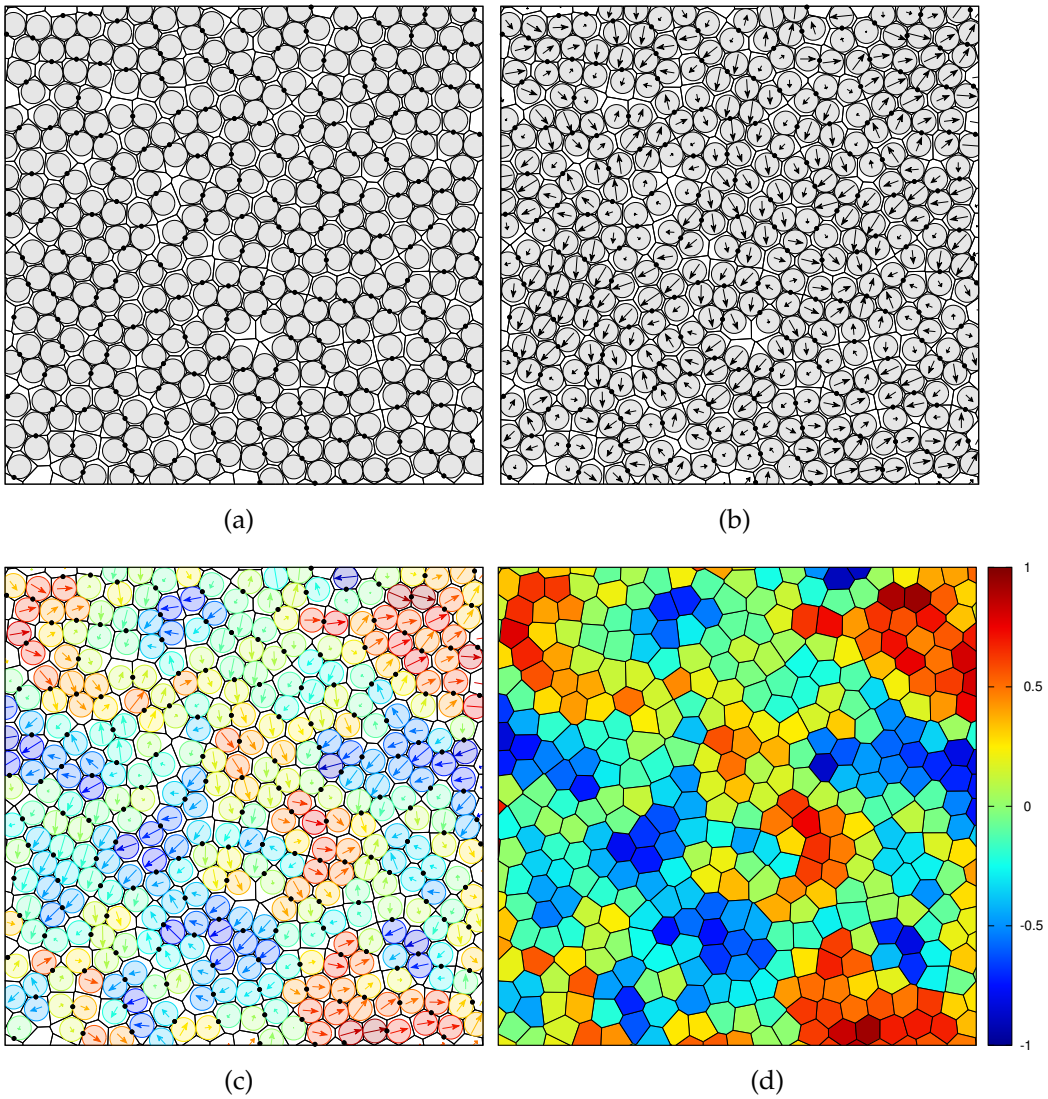


Figure 4.8: (a) - Voronoi tessellation for a dumbbells configuration. (b) - For each particle, the value of the local hexatic parameter, which is a complex number by definition, is plotted as an arrow in the complex plane with the real axis oriented as the x (horizontal) axis of the configuration. (c) - A color code is chosen, which represents the projection of the local hexatic parameter on the sample orientation (see text). (d) - The beads disappear and the colors are assigned to the corresponding Voronoi cells. This is what finally we really plot.

From (4.6), one can immediately recognize that $\psi_6(\mathbf{r}_i)$ (than from now on we abbreviate with $\psi_{6,i}$) lies on a complex plane and can therefore be identified with its absolute value $|\psi_{6,i}|$ and its phase $\arg(\psi_{6,i})$. One can easily check that, if the neighbors of particle i are arranged on a perfect triangular

lattice, $\psi_{6,i}$ has its maximum (unit) modulus and its phase rotates by 2π as the lattice is rotated by an angle of $\pi/3$, taking fixed the reference axis for the angles θ_{ij} in the definition. This property comes obviously from the $\pi/3$-periodicity for an hexagon under rotation on the plane. For a non-periodic arrangement of nearest neighbors, one have $|\psi_{6,i}| \leqslant 1$, and the orientation in the complex plane does not generally have a simple relation with the orientation of the bonds. However, we gain an acceptable representation of $\psi_{6,i}$ (we lose some information of course), considering the projection of $(\mathrm{Re}\,\psi_{6,i}, \mathrm{Im}\,\psi_{6,i})$ onto the direction $\hat{\Psi}_6$ of the *sample-averaged orientation*

$$\Psi_6 = \frac{1}{N}\sum_{i=1}^{N} \psi_{6,i}\ , \tag{4.8}$$

where N is the number of colloids in the system. If correctly normalized, the projection is a number between -1 and 1 and it can therefore be translated, as shown with details in figure 4.8, on a color scale. Another quantity that will be useful for some of the following analysis is the sample-average of the absolute values of the local hexatic order parameter, defined as

$$\Gamma_6 = \frac{1}{N}\sum_{i=1}^{N} |\psi_{6,i}|\ . \tag{4.9}$$

As we will see later, the sample-averaged orientational order parameter defined in (4.8) may lead to misleading results in the case of a configuration where different ordered regions have different orientation directions that cancel out in the sum. In such cases Γ_6 will allow to prevent this effects, returning more correct informations about ordering in the system.

4.3.3 Large systems simulation methods

In section 3.2 we have described the numerical integrator used to solve, here and in the previously works on the dumbbell system, the Langevin equations for N interacting dumbbells. Facing the purpose of an accurate analysis of the collective phases involved in a low-to-high density transition, we have been forced to large-size system simulations. Generally speaking, a lower bound for the size of system in a simulation is the largest scale involved in the phenomenon of interest. Studies about order-disorder transitions are obviously much severe with this bound, since they frequently involve correlation length that diverge in the system. On the other hand, in our dumbbell system, as said, only short-range interactions are present and such other feature surely reduced the requests about the

minimal size of simulations. It has been clear, from the beginning of our work, that an acceptable choice for the system size, should have been greater than what any previously numerical implementation could have achieved. More details about the choices made for the size of the system used in the numerical analysis will be give later, and will be motivated with respects to the direct observations of the results obtained.

The numerical program previously used is strongly limited, essentially due to the fact that it works as single-CPU program. For this reason, LAMMPS software [†] has been largely used to produce almost all the results that we will presents. LAMMPS is a free, open-source software for parallel computing, that includes implementation of a number of different possibility for molecular dynamics simulations. For our particular purposes, we have used a velocity-Verlet algorithm in the NVE ensemble, keeping the system at constant temperature with a Langevin-type stochastic thermostat [Tuc10]. The set of parameters used in the simulations, where not differently specified, are the same of that given in section 3.2.

Simulations with LAMMPS, were also given the opportunity to modify the interactions within a single dumbbell. Recalling the definition of the model given in chapter 3, the two beads in the molecules was bonded together by means of a spring-like finitely extensible interaction, whose elastic constant was appropriately chosen in order to preserve the rigidity of the dumbbell. This strategy was advantageous since the spring-like interaction can be described in terms of a potential, that has only to be "dynamically" added in the equations of motion, and has therefore a limited computational cost. In the LAMMPS numerical scheme, we have introduced an explicit constrained dynamic in which the dumbbells are rigid object, made of two beads held at a constant distance σ during their evolution. The constraint implementation is based on the RATTLE scheme, described in [Tuc10].

4.4 First order ordering transition for passive WCA-interacting dumbbells

We are going to start illustrating, from now to the end of this chapter, our results about the possibility for a two-dimensional passive dumbbell system to order and aggregate. The main purpose of this first part of the work was to be able to decide whether our passive dumbbells crystallize in a

[†]Large-scale Atomic and Molecular Massively Parallel Simulator (LAMMPS) official web page: `http://lammps.sandia.gov/`

two-step KTHNY transition or not. To achieve this goal, we have mainly observed the behavior of the local hexatic parameter, since, recalling the general description of the two-dimensional phase transition outlined before, the orientational order is the more suitable feature that distinguishes the liquid phase, the hexatic phase and the crystalline one. Along with the recognition of the phases, another fundamental step of our analysis, is to gain an indication about the nature of the liquid-hexatic transition. As we have shown before, the more recent studies about this topic seem to ensure that a first order transition occurs in colloidal systems with short-range interactions. A hallmark of a first-order transition is the presence of a region in the space of the parameters in which the two extreme phases coexist. Therefore our efforts, in the context of the passive system, point to find coexistence between a disordered (liquid) phase an ordered (hexatic) one, possibly establishing which are the limits of the region where the coexistence settles.
With this aim, we have simulated the dumbbell system, at increasing values of constant surface fraction, with a constant-temperature Langevin dynamics (see sections 3.2 and 4.3 for technical details about the simulations), to see how the system orders as the particle density increases. Each different constant-density configuration has been simulated starting from differently ordering conditions, to allow to correctly estimate when the system would have reached equilibrium.

The first starting configuration used was a configuration in which the simulation box has been partially filled with a close packed arrangement of N dumbbells (the close-packing arrangement for two-dimensional disk is the perfect triangular one, whose surface fraction is $\phi_{CP} \approx 0.907$), adjusting N to obtain the desired total surface fraction. The dumbbell orientations in the initial dense package, have been largely randomized before the simulation started, repeatedly exchanging couples of the dumbbell forming colloids that occupy the sites of the perfect lattice. Figure 4.9 illustrate an example of such initial configuration, with a detail of the order. Obviously, since N is fixed from the value of the total surface fraction (from the definition (3.45)), depending on the surface fraction assigned, a certain fraction of the total available volume is occupied as the free evolution starts. Therefore when this particular initial condition is chosen, the first part of the evolution is dominated by a sudden expansion of the system that, being the particle purely repulsive, begins to take all the volume of the box. We anticipated that the results found have been demonstrated this particular initial condition to be very useful for the analysis carried out. In fact it gives the opportunity of immediately discriminate between (low) densities that allows the initial crystal to “melts“ due to the expansion,

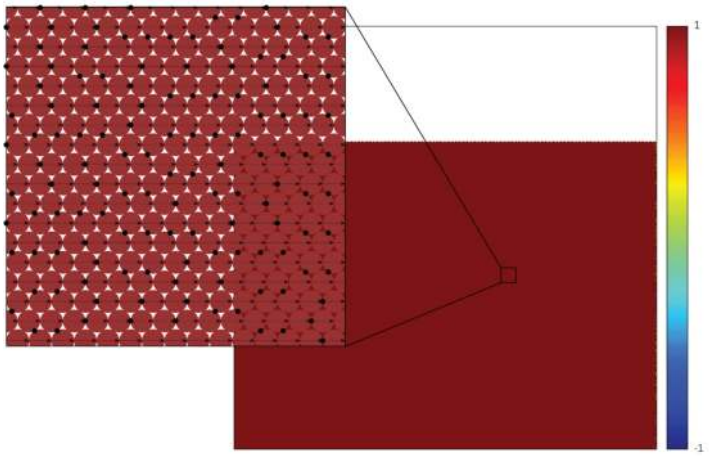


Figure 4.9: (a) - A simulation box partially filled with a close-packed configuration of a given total surface fraction. All the beads in the dumbbells occupy the sites of a perfect triangular lattice, with spacing equal to the diameter σ of the beads. The dumbbell's directions are taken randomly among the three different directions allowed for the lattice (passive dumbbell are completely symmetric with respect to their principal axis). A detail of the close-packed structure is plot in (b) where the centers of mass of the molecules are indicate, to distinguish the orientations.

and (high) densities for which the crystal partially dissolves and partially is rearranged retaining its ordered structure.

As previously mentioned, the equilibrium behavior for each considered value of the surface fraction is extracted comparing results for different starting points. Therefore, together with the first initial condition described before, a disordered, randomly initialized, configuration is evolved. Even if the true equilibration times are not explicitly measured, a clear indication of their order of magnitude is immediately taken for such comparison. Since the two starts have opposite features with respect the ordering, as the two evolutions fall into similar stationary conditions, equilibrium is supposed to be reached.

In order to be sure to catch the real properties of the system and not to be mislead from finite size effects, we have initially compared simulation of different sizes and, examining the typical correlation lengths involved in the range of parameters under investigation, we have chosen the best compromise between the suppression of errors due to finite size and an accessible simulation time. Obviously the lower limit of a reasonable box size increases as the density is increased, because the system begin to be long-range correlated; a useful choice is finally estimate to be 500σ. However we

decide to carry out the full simulation of the Lennard-Jones system within a box of 1000σ of linear size with periodic boundary conditions, with the aim to observe the size-dependence of our results.

4.4.1 Disordered liquid phase

Low-density systems are observed to evolve toward a disordered configuration, regardless of the initial configuration chosen. In figure 4.10 are shown some snapshots taken from the whole simulation, for a system that evolves, starting from the two different conditions illustrated before, at fixed $\phi = 0.64$ surface fraction, that is the higher surface fraction value at which the system is observed to have such behavior. The figures display, as we have described in the previous section, the local hexatic order parameter (4.6) projected along the global orientation (4.8) and graphically represented through a color code. Since the regions of the system which are orientationally ordered (in the sense described in section 4.2.1) result to be uniformly colored, such representation allows us to easily distinguish the typical spatial extension of the orientationally ordered domains the system is able to sustain.

Observing the snapshots in figure 4.10, it is clear that at $\phi = 0.64$, the equilibrium state of the dumbbell system is a short-ranged orientationally ordered configuration. We recall, for clarity of the discussion, that "short-range orientational order" means that the bonds between the beads in the system have not ordered orientations (in other words, the orientations of the bonds are finite-size correlated with respect to the size of the system). Therefore, according to our general description about ordering in the two-dimensional thermodynamic phases, we can state our dumbbells to be in an isotropic liquid phase for values of the surface fraction at least up to $\phi = 0.64$.

4.4.2 Ordered phase

As the surface fraction of the system is increased, a disorder-to-order transition is notice to occurs, as it clear from the two runs at constant $\phi = 0.68$, starting again from the two opposite conditions, shown in snapshot in figure 4.11.
As it is quite evident in the upper line of figure 4.11, the evolution of the initial ordered condensed phase towards its equilibrium, drives the system first to fill the entire simulation box, and than to reorder in the whole available volume. Until the last figure, corresponding to 4×10^7

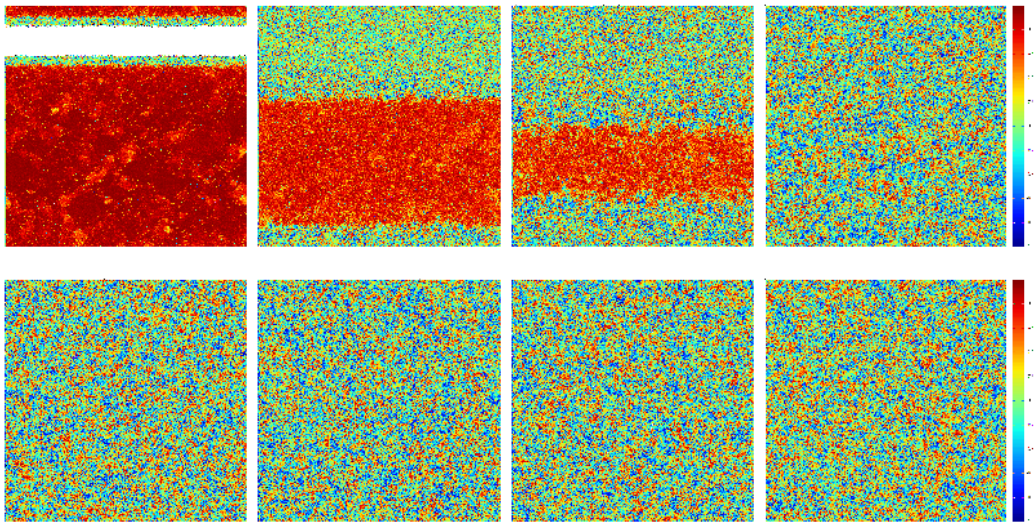


Figure 4.10: The snapshots in the upper line are taken from one single run at fixed $\phi = 0.64$ surface fraction, started from the dense packed phase. The lower-line snapshots are taken from one run at the same density, started from a random initialized phase. The four figures in both the two lines correspond (from left to right) to 1×10^6, 1×10^7, 2×10^7 and 4×10^7 timesteps of simulation.

timesteps of simulation, the system does not succeed to form a uniform ordered domain, in facts little spots of different colors are still present. However these regions are orientationally ordered, even within a finite-size domain, along a different direction with respect to the direction of the bigger (red) domain. The hexatic orientation of the bigger domain prevails in the sample-averaged orientation, along which we project any local value of the hexatic parameter, to extract the color code.

For the random initial condition the situation is comparable to the previous case. The system starts from a completely disordered phase, and undergoes an ordering dynamics, reaching a stationary condition in which many ordered domains are present. Maybe such configuration is not the true equilibrium of the system (equilibrium should be a single uniformly ordered domain) because at such high densities, when the system starts to crystallize, the mobility of the particle becomes very low and the dynamics drastically slow down, preventing the system to reach the true equilibrium within a reasonable time. As we will see later, how the hardness of the colloids is increased by changing the interaction potential, it becomes more easily for the particles to move with respect to each other, even at higher densities.
The elongated shape of the dumbbells is probably another factor, of a steric

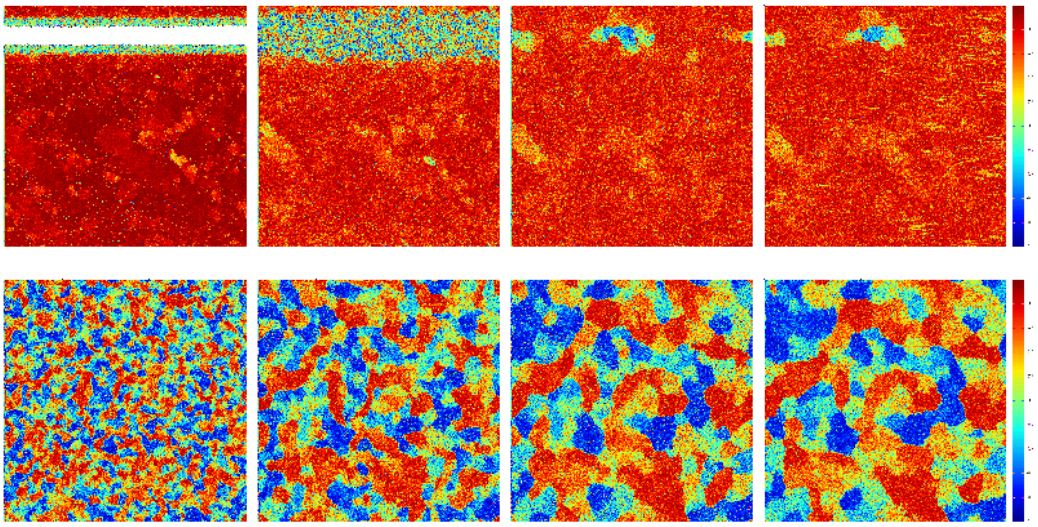


Figure 4.11: Snapshots from the run at fixed $\phi = 0.68$ surface fraction, started from the dense packed configuration (upper line) and from the random configuration (lower line) at 1×10^6, 1×10^7, 2×10^7 and 4×10^7 timesteps of simulation.

nature, that inhibits the particle's movements, and that results in situations (of the kind shown in figure 4.11) in which they are stuck together in such multi-domain arrangement. This is perhaps the first indication about the differences between our dumbbell system and systems (some example is given above) of spherical colloids.

According to this considerations we can state that, for values of the surface fraction greater than $\phi = 0.68$ our soft dumbbell system is orientationally ordered, and therefore, within the KTHNY transition scenario, it is situated above the first liquid-to-hexatic transition.
A second step, in the study of the passive system, would be to site where the second transition (from a orientationally oriented hexatic phase to a positionally ordered crystal) occurs; then it would be necessary to distinguish whether the system is characterized by short-range positional order and quasi-long-range orientational order (as in the hexatic phase) or by quasi-long range positional order and long-range orientational order (as in the crystal). However such part of the problem has been left out, since, as we will see in the next chapter, it is not of fundamental importance in the comprehension of the features of the active counterpart of the passive dumbbell crystallization. Furthermore, due to the softness of our colloids with respect to hard-disks makes this work extremely problematic. We will try to deeply investigate the high-density second step of the KTHNY crystallization in the context of harder colloids, since its collective behavior

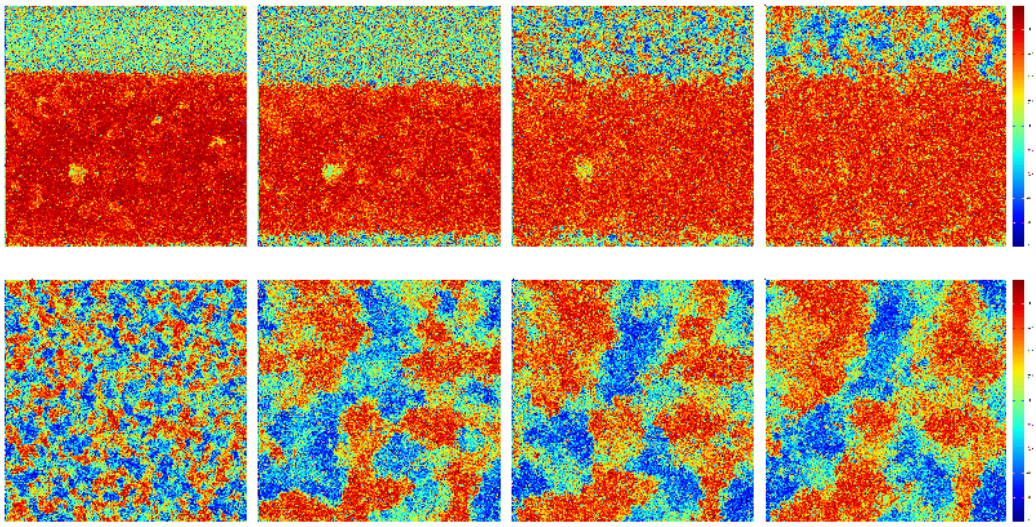


Figure 4.12: Snapshots from the run at fixed $\phi = 0.66$ surface fraction, started from the dense packed phase (upper line) and from the random phase (lower line) at 5×10^6, 1×10^7, 2×10^7 and 4×10^7 timesteps of simulation.

resembles a bit more the behavior of a pure hard-disk system, for which a great detailed characterization is known.

4.4.3 First evidences of liquid-hexatic coexistence

After having established an upper bond for the liquid phase and a lower bond for the hexatic one, we illustrate what happens to the WCA dumbbell system within these two limits, where the transition occurs, with the purpose to find some evidence for the determination of the order of the transition.

Figure 4.12 shows the summary of a single run at fixed $\phi = 0.66$ of the solid phase (snapshot in the first line) and the liquid one (snapshot on the second line) and actually indicates that the system does not evolve towards a single liquid or solid phase, but the colloids arrange in two differently ordered aggregates, that persist even at the largest time reached by the simulation. This behavior suggests, almost with no doubt, that a coexistence establishes, between a short-range ordered phase, the liquid, and an orientationally ordered one, which, on the basis of what previously described about the generalities of two-dimensional KTHNY crystallization scenario, we can claim to be an hexatic phase.

The code color in this case may be misleading in the recognition of the phases in the system. In fact, the last snapshot in the lower line of figure 4.12

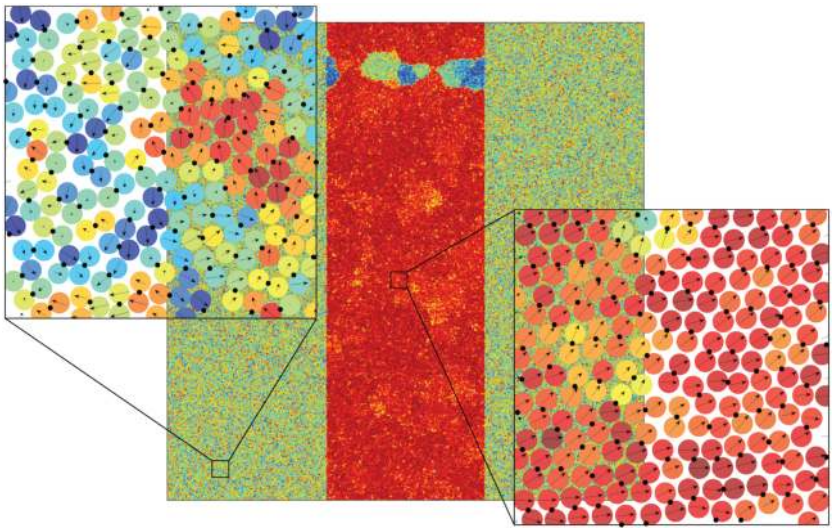


Figure 4.13: The coexisting start is shown in details. The central vertical (red) stripe of the box is a piece of previously equilibrated configurations, at a so high surface fraction that it has reached a completely ordered arrangement. The remaining volume of the box is initialized with dumbbells whose positions and orientations are extracted from a uniform distribution, and are than both randomly selected. The two squares on the left side of the figure contain a detailed plot of the the two pieces.

is apparently pretty similar to the corresponding snapshot of figure 4.11 which, as we have claimed before, represents a configuration of the system with a number of orientationally ordered domains. Differently from what deduced previously, we are saying now that some orientationally ordered part of the system coexists with disordered liquid regions.

We have deeply investigate the coexistence region, performing other simulations at different values of surface fraction (within the estimated coexistence interval) with more appropriate starting configurations. Since one can be able to discriminate whether, at fixed global density, two different phase are allowed to coexist in the system, we have prepared an initial configuration, in which the two phases that are supposed to coexist are already present in an undoubted separated adjustment. In particular, the "coexistence" initial state has been prepared as follows: we have extrapolate a stripe of dumbbells from a previously evolved solid system at a density not too far above what we have estimate to be the upper limit of the coexistence region; then we have randomly initialized the remaining empty portion of the box, satisfying a required global density. Since we have chosen the densities of the two phases nearby (on the two opposite sides) the transition region, we have created an almost equilibrated two-phase system. Such system is shown in figure 4.13 with details about the

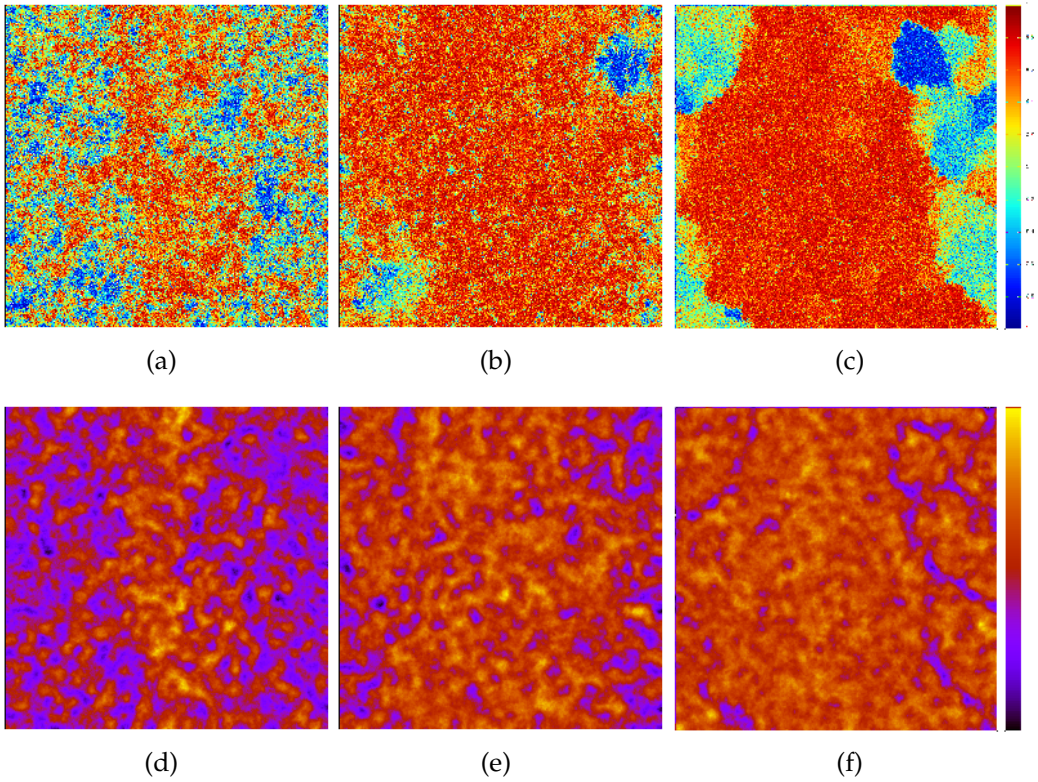


Figure 4.14: Final configurations of the run at densities $\phi = 0.65$ (a), $\phi = 0.66$ (b) and $\phi = 0.67$ (c), at 6×10^7 timesteps of simulation, starting from the coexistence system of figure 4.13. Since in the high density peace of the initial configuration the density is fixed, the total surface fraction is obtained opportunely chosen the density of the disordered part. (d), (e) and (f) are the corresponding density profile of the three cases.

ordering of the two phases.

The final configurations for three intermediate values of the surface fraction $\phi = 0.65$, $\phi = 0.66$ and $\phi = 0.67$ can be viewed in figure 4.14 for simulations started from the coexistence condition. We show here both the local hexatic parameter of the configurations and the corresponding local density profile. One immediately observe that, for $\phi = 0.65$, a disordered low-density phase prevails over small residual high-density hexatic regions. For $\phi = 0.66$ the situation is exactly the opposite: the high-density ordered phase coexists with a little bubble of liquid. At $\phi = 0.67$ the two phases of different density are not observed to coexist anymore. The low-density regions that appear in the surface fraction profile at $\phi = 0.67$ correspond to the interstices between differently oriented high-density domains. Therefore this value of the surface fraction can be rule out from the

coexisting region.

Measuring the two coexisting densities, and observing that two cases at $\phi = 0.65$ and $\phi = 0.66$ are extremal cases with a strong majority of one phase with respect to the other one, we refine our estimation of the limits of the coexisting region. We have concluded our analysis of the Lennard-Jones passive transitions, with another check for the coexistence. We have performed two simulations of the system at two new intermediate values of the surface fraction $\phi = 0.654$ and $\phi = 0.656$, starting again with two coexisting phase, placed by hand in the box, at the two new extremal densities $\phi \sim 0.65$ and $\phi \sim 0.66$ of the transition. The results from this check are positive, since the two phase are observed to remain separated during the evolution of the system.

Chapter 5

Phase coexistence in passive and active dumbbell system

In our original system, constituents interact through the soft WCA potential, obtained from the truncation of the attractive branch of the Lennard-Jones one. Due to its softness, this potential can allow small interpenetration of disks and disfavor the dense phase formation. According to the results of Kapfer and Krauth [KK15], the hardness of the potential can heavily affect the density interval of the coexistence region, and eventually completely inhibit any coexistence, allowing a continuous transition to replace the first-order one (see figure 4.5). Various indications can be found about the strong dependence of the nature of the phase transition on the form of the pair interaction potential that rules the repulsion between the constituent of the system. In particular, it emerges that the first-order character of the liquid-to-hexatic transition becomes more evident when the potential steeply diverges as the particles approach. Such behavior has been tested in our numerical experiments, comparing the results for the original Lennard-Jones potential and a different, harder power-law potential. In the previous section we have summarized the results for Lennard-Jones potential, showing how the different phases set up, varying the total density of the system, and how the phases can be immediately characterized with respect to their orientational order.

Within this chapter a more complete analysis of the crystallization transition will be give for dumbbells interacting through the so-called *Mie potential*, since, as we will see, this potential get the system closer to an hard-disks system, in which the features of the phases, and also the first-order nature of the liquid-hexatic transition, are more evident, and is therefore easier to give an unambiguously interpretation of the results. Such new set of simulation have been performed using a box size of 500σ with pe-

riodic boundary conditions, with a fixed time step of of 0.008 time units. We remember that time units of our problem refer to the fundamental parameters of the models, i.e. the mass m of the colloids, their diameter σ and the energy scale of the interacting potential ε through the relation $t = t^* \sqrt{m\sigma^2/\varepsilon}$. A smaller box size is chosen, deducing from the Lennard-Jones simulations that 500σ is enough to observe typical lengths scale for aggregation phenomena and coexistence, without any strong finite size effects. Mie potential is defined as

$$U_{\text{Mie}}(r) = \left(\frac{n}{n-m}\right)\left(\frac{n}{m}\right)^{\frac{m}{n-m}} \varepsilon\left[\left(\frac{\sigma}{r}\right)^n - \left(\frac{\sigma}{r}\right)^m\right]. \tag{5.1}$$

This potential is a generalization of the Lennard-Jones potential where therefore ε is an energy scale and σ a length scale (in our case σ is the diameter of the the beads) which remain, as before, respectively the energy unit and the length unit of the system, $\varepsilon = 1 = \sigma$. Analogously to the WCA procedure, we can truncated this potential at its minimum

$$r_{min} = \left(\frac{n}{m}\,\sigma^{n-m}\right)^{1/(n-m)}, \tag{5.2}$$

and lift it up such that $U_{\text{Mie}}(r_{min}) = 0$. In order to get closer to hard core disks, we choose $n = 64$ and $m = 32$.

5.1 Coexistence in passive Mie-interacting dumbbells

We begin the illustration of the results that come from simulating this system, analyzing the details of the transition region and presenting what we have found about the coexistence between phases.

With this aim, as a first evidence, we show in figure 5.1 a snapshot of the simulation of the system at fixed surface fraction $\phi = 0.740$, starting from the hard-packed aggregate which does not completely filled the box and, as described before for the Lennard-Jones case, immediately expands. It is quite noticeable from the surface fraction profile of the configuration that, after a very long time of evolution, two phases of different densities remain strongly separated. Such evidence is clearly confirmed by the probability density of the surface fraction which develops a bimodal shape with two distinct peaks, that correspond to the two coexisting phases. Furthermore, comparing the density profile with the plot of the local hexatic parameter one notices that the high-density phase is orientationally ordered, whereas

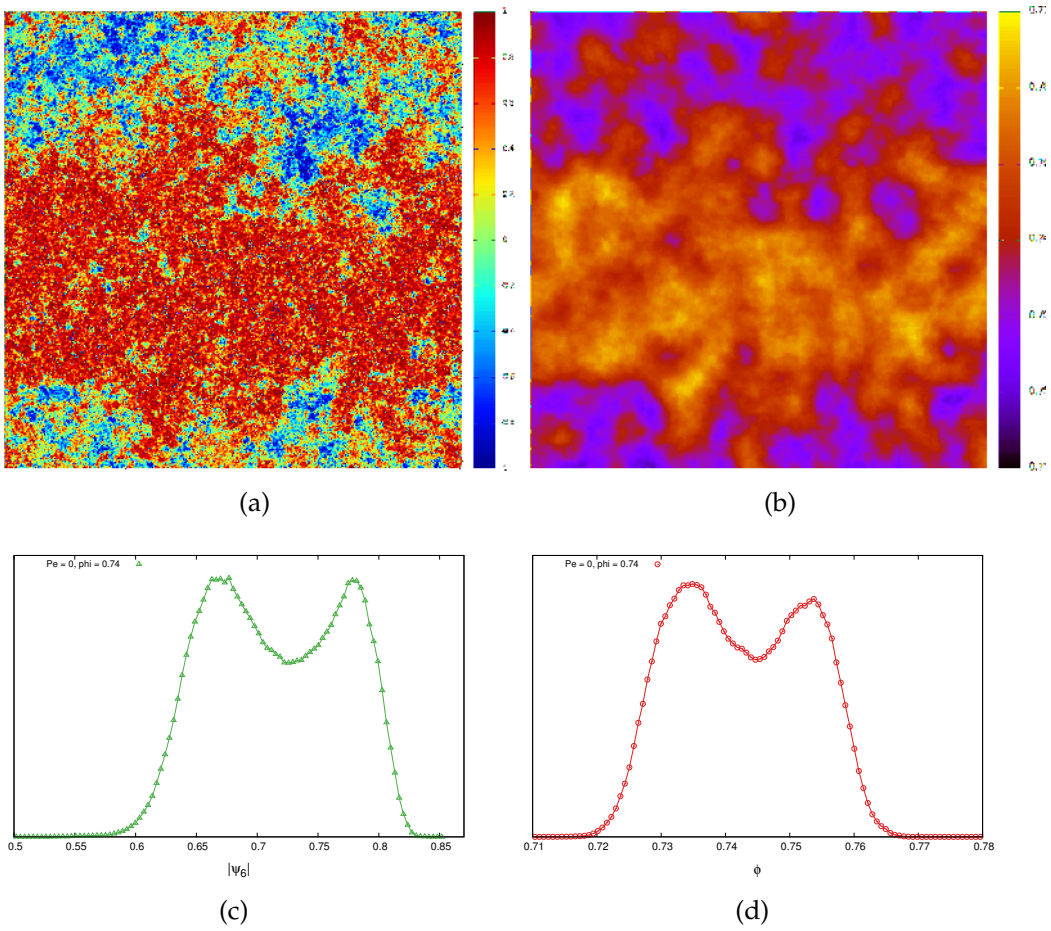


Figure 5.1: (a),(c) - Color representation of the local hexatic parameter for $\phi = 0.740$ at 1×10^8 timestep of the simulation and the probability density of its modulus. (b),(d) - Plot of the corresponding local surface fraction profile and its probability density.

the low-density one is disordered. The correlation between hexagonal order and density in the two phases is unambiguous. As for the surface fraction, we have extrapolate a probability density of the absolute value of hexatic order parameter, shown in figure 5.1, which confirms again the presence of two differently ordered phase in the system.
Results from other simulations at $\phi = 0.740$ that start from different initial conditions are completely comparable with the first one. See figure 5.2 for a complete comparison.

We have repeated such analysis for a range of values of the total surface fraction in order to place accurate limits to the coexistence region between the liquid phase and the hexatic solid one. Such limits are established from

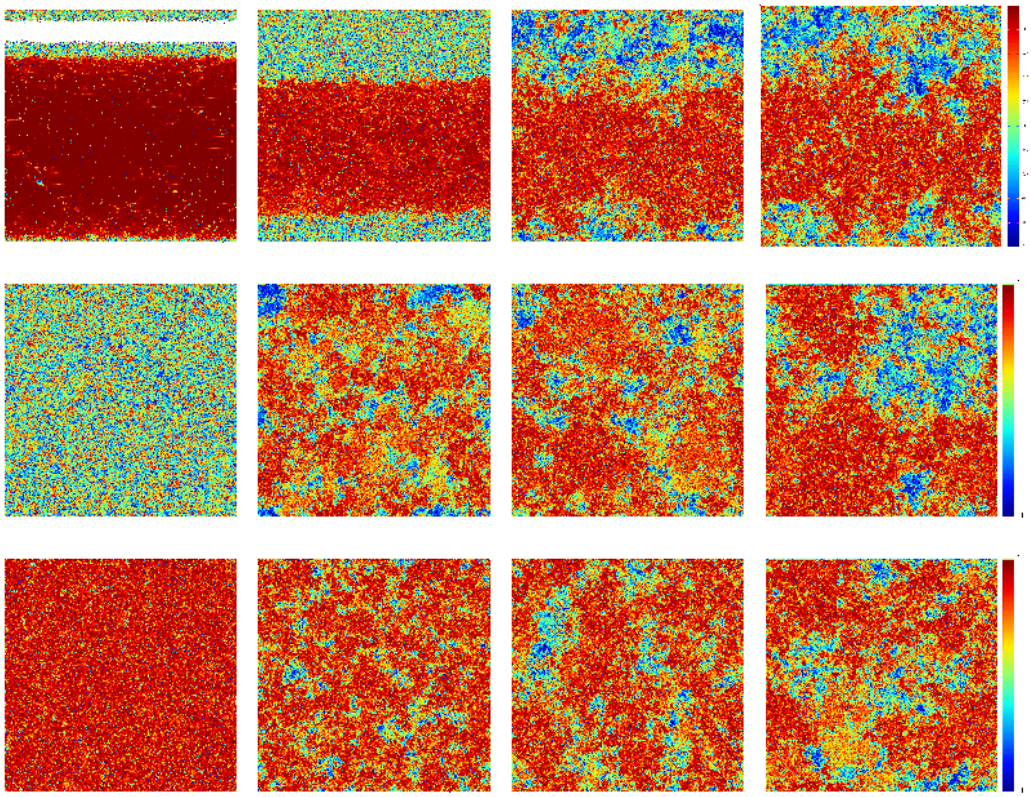


Figure 5.2: This figure contains three different simulations of the system at $\phi = 0.740$ for different starting points. In the first line are shown four snapshots at 1×10^6, 1×10^7, 5×10^7 and 1×10^8 timesteps of the simulation that starts from a close packed configuration. In the second line snapshots at 0, 1×10^7, 5×10^7 and 1×10^8 timesteps for the random disordered start. In the third line snapshots at 0, 1×10^6, 1×10^7 and 5×10^7 timesteps for the ordered solid start.

different informations. Firstly, the visual observation of the hexatic parameter configuration and of the density profile of the system have allowed us to make a first estimation about the presence of two coexisting phases, whose local orientational order and the local surface fraction have a strong correlation between theme, as for the case at $\phi = 0.740$. In particular, this kind of visual inspection indicates which one of the two phase prevails in the system and provides then a qualitative method to find the borders of the interval where the two phase coexist. In our case, convinced that liquid and solid coexist somewhere, the upper end of such region would be characterized by droplets of liquid in the prevailing hexatic phase, whereas at the lower limit some bubble of hexatic persist in "sea" of liquid. This is a typical feature of first-order transitions, as described for example

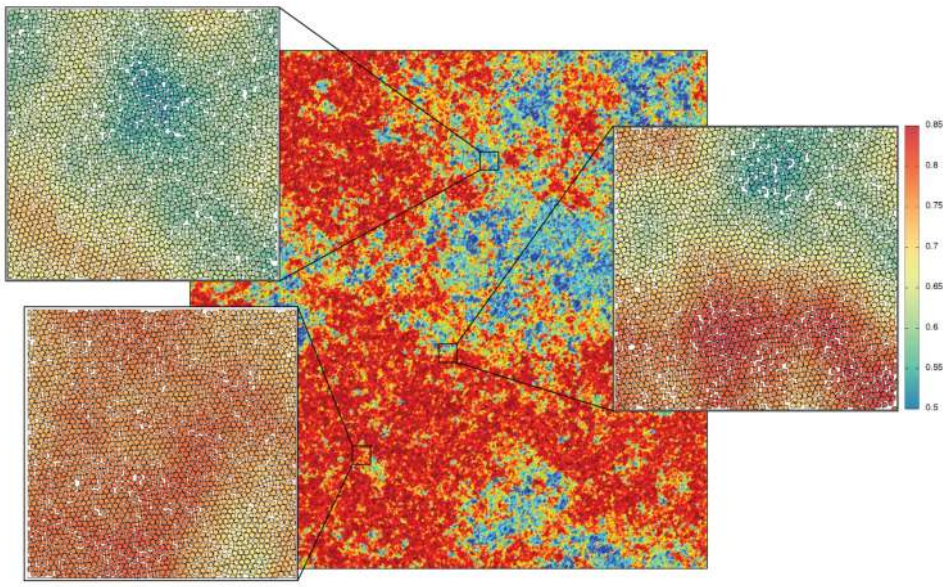
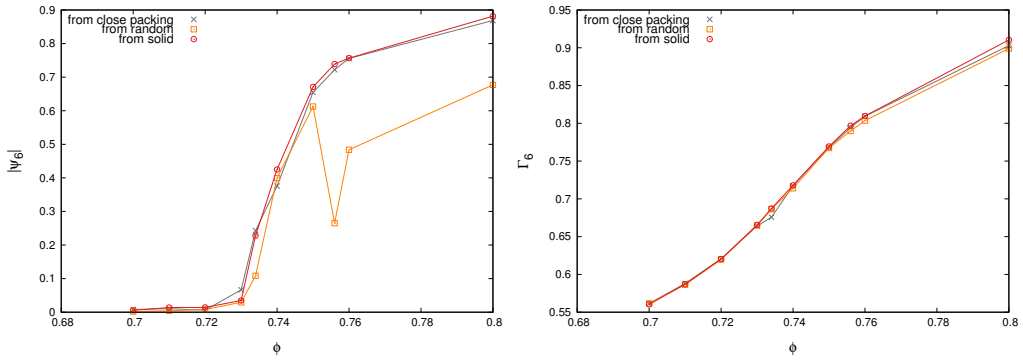


Figure 5.3: A coexisting configuration from the simulation of the passive dumbbell system at $\phi = 0.74$ with details of the modulus of the local hexatic parameter for different phase in the system.

in [MW65], where, starting from such construction, Mayer and Wood determined the scaling behavior of the free energy associated to the interfaces between the two coexisting phases in a first-order transition.
Along this qualitative strategy, one can consider a more rigorous tool for the determination of this two limits. Since in the first-order phase transition scheme, the two phase that coexist separately preserve its nature, one can access the surface fraction values of two bounds of the coexistence region measuring the surface fraction of the two phase within the coexistence range. The probability density of the surface fraction provides a means to quantitatively extract such values, that locate in correspondence of the two peaks of the distribution.

Performing all these measures on the dumbbell system we have found that, starting from the liquid phase and increasing the surface fraction, the hexatic phase begin to appear and the two phase begin to separate, approximately at $\phi \sim 0.734$. Whereas at $\phi \sim 0.756$ coexistence quits and an hexatic ordered phase settle. We will show below a summary of these results, after having illustrate in more details the feature of the phase in which our system appears within the range of our simulations.

Figure 5.3 shows some details of a coexisting configuration at $\phi = 0.74$,



(a) (b)

Figure 5.4: (a) - Sample average of the local hexatic parameter define in (4.8) plotted against the total surface fraction of the system for all the three starting points used. In gray is shown the case of the close-packed initial condition, in red the case in which the simulation started from a solid configuration, and in yellow the random one. (b) - The same plot for the sample average of the modulus of the local hexatic parameter.

where a direct comparison has been made between the local dumbbell arrangement in the space and the corresponding local values of the modulus of the hexatic parameter $|\psi_{6,i}|$. One can easily distinguish different ordering characters of the two phase that coexist in the system.

5.1.1 Passive two-step phase transition

To complete this part of the work, we discuss some global quantity of the system, which appears to be useful for general confirmations of what we have claimed so far, and that will be of fundamental importance in the comparison of these results with the discussion that will follow, about the active system. One of these global parameters is the sample-average orientation (4.8) that we have previously used as the direction to project the local hexatic parameter, in order to extract our color code. Taking its absolute value, gives a global information about how the ordered is the system. The plot on the left in figure 5.4 shows the behavior of such parameter how the total surface fraction is increased. Three different cases are plotted, corresponding to the three different starting condition used: the partially filled box of a close-packed structure, the random initialized configuration and an ordered (solid) one, that homogeneously occupy all the volume of the box. Note that for the close-packed start and the solid one, the behavior of this parameter is almost the same: as we aspect it is zero in the low-density region where the system is disordered, and increases

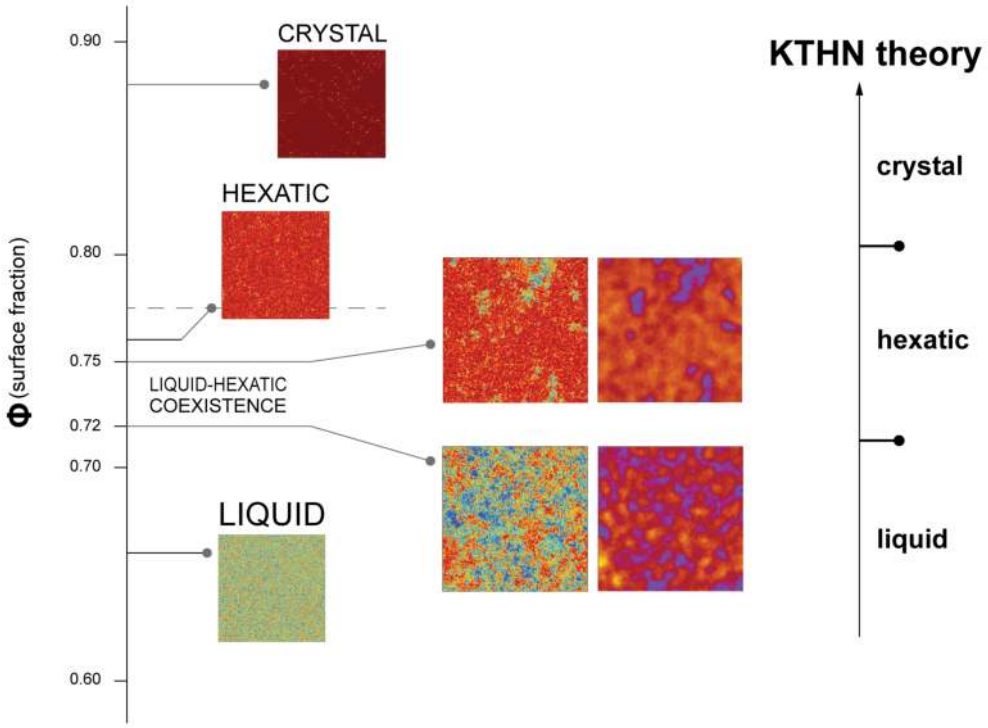


Figure 5.5: This figure summarizes how our system is observed to undergo a crystallization phase transition within the framework of the two-step KTHNY transition. Some example are shown for the various phases at different surface fraction. In particular in the diagram are indicated the two limits of the coexistence region. The lower limit is place at $\phi \sim 0.720$ where a minimal coexistence is displayed between some small ordered aggregate and a large liquid region. At the upper limit, near $\phi \sim 0.750$, the situation is reversed, with a small liquid droplet that breaks the dominating hexatic structure.

with density as the system globally orders, reaching a maximum value (near to unity) above the transition. The random initialized run differs from such behavior in the high-density regime. It is immediate to understand the causes of such deviation, looking at the ordered configurations resulting from the evolutions of a random phase: as we have already explained, the system freezes in a multi-domain arrangement. All the domain are ordered by themselves, but differently oriented one from each other, and therefore they do not contributes coherently to the sample averaged, preventing the latter to rise.

We can easily compensate such eventually, taking the average of the modulus of the hexatic parameter defined in (4.9).
As one can observe in the plot on the right of figure 5.4, Γ_6 restores the equivalence among the the different initial conditions.
The utility of such result is threefold. First of all it is a confirmations that,

regardless of the domain structure, the solid configurations found before are ordered at the same way. It establishes a coherent order parameter to characterize the transition, which not depend anymore from the initial condition. Moreover, the extraordinary similarity of the three curves in figure 5.4 ensures that our simulations have reached the equilibrium, since has converged, starting from oppositely ordered conditions.

We end this chapter with a schematic summary of the results achieved. Figure 5.5 outlines all the results found about the crystallization phase transition in the passive dumbbell system. As explained before, the two borders of the coexistence region are characterized by two symmetric situations in which one phase strongly prevails to the other. Although all the profound differences between our molecular system and a system of hard spherical colloids, passive dumbbells seem to crystallize within the classical scenario due to Kosterlitz, Thouless, Halperin and Nelson in which two different orders in the system are separately restored as the density increases: at the first transition the system orders from an orientationally point of view and at the second transition the system truly crystallizes. Differently from the KTHN scenario the first of the two transitions, are seen to present strong evidences of a coexistence region which selects, as in a number of recent studies, a transition of first order nature.
Knowing some of the properties of the dumbbell system in which the molecules are self-propelled, we now start to investigate how the activity modifies this scenario and whether some of the intriguing phenomena that belong to the active out-of-equilibrium context, are related to the features described about the equilibrium crystallization phase transition.

5.2 Phase separation and crystallization in the active dumbbell system

Throughout the rest of the thesis, we purpose to illustrate how the crystallization scenario, described in the previous sections for the passive dumbbell system, changes when each single dumbbell is allowed to auto-propel, driving the system out of equilibrium. Many details about active dumbbells are given in chapter 3, where we have described the model, and after we have illustrate some general interesting, activity-dependent, collective behaviors. In particular, we recall, dumbbells display an active-driven phase separation (MIPS), therefore, under favorable conditions, they are able to aggregate in ordered clusters, that separate from the rest of system, which in turn appears to remain in a disordered phase.

As demonstrated in previous works about the MIPS in dumbbell system [SGL+14, SGMO14, CGS15, GLS14], the aggregation mechanisms, and consequently the clustering process, closely depend on the surface fraction ϕ of the system and the Péclet number, which have been defined by (3.46) and (3.47) and accounts for the balance between activity in the system and its diffusive properties.
Our work develops in three different perspectives:

- relate two different phase separation phenomena: the equilibrium phase separation in the coexistence region for the passive system and the non-equilibrium phase separation induced in the system by the activity;
- understand whether the self-propelled dumbbells are allowed to crystallize in an ordered phase despite the fact that energy is injected incessantly in the system and, if so, how the activity modifies the KTHN passive phase transition scheme;
- delineate the phase diagram for the active system in the Pe-ϕ parameter space.

5.2.1 Effects of the active force on the phases of the passive system

In order to suitably face the first point of the list above, we have to deeply understand how the ability of the dumbbells to "swim" by themselves can affect the phase separate arrangement, that we have found to exist within the coexistence region of the the first-order passive phase transition. The phase separation that settles in coexistence region is between the disordered liquid phase and the ordered hexatic one, and arises from purely entropic effects. Therefore the truly relevant question here concerns the balance between such equilibrium causes for aggregation and the activity driven ones. We have already seen in section 3.3.1 that, within the mechanisms at the base of the motility induced phase separation, activity competes against entropic features, and we have stated that cluster formation has triggered within a cooperation between self-propulsion strength and, for example, the density of the system.
While one can mistakenly think that activity is the unique element that drives such macroscopic aggregation phenomena, the question is more subtle, and it is undoubtedly evident that phase separation and clustering are grounded, even far from equilibrium, on such interplay.

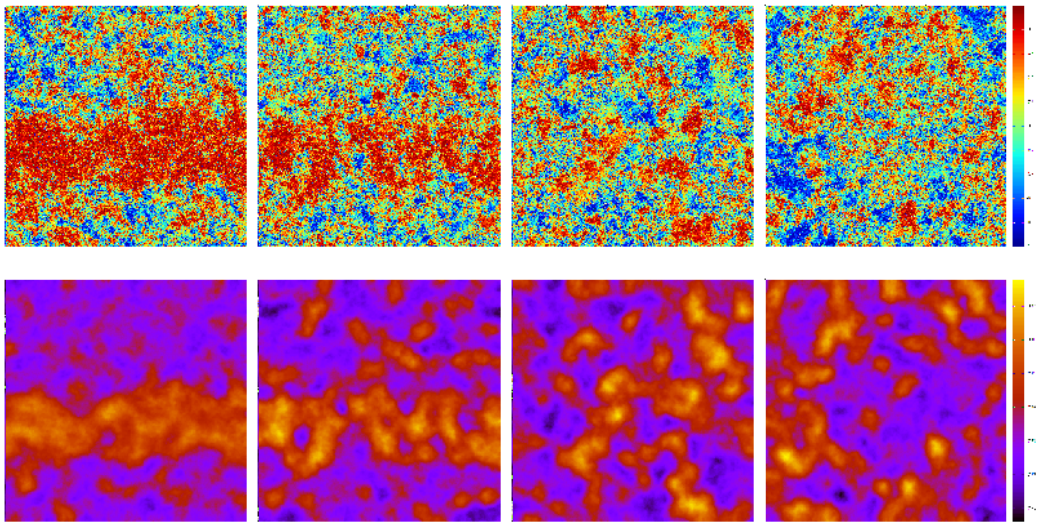


Figure 5.6: Snapshots for the local hexatic parameter for a simulation at $\phi = 0.734$, starting from the last configuration of the passive run at $\phi = 0.734$ that have started from the close-packing configuration, showed in the first snapshot from left. The other three figure are at 1×10^6, 1×10^7, 5×10^7 timesteps of simulation. The second line the corresponding surface fraction profile of the system is shown at the same time.

For all these reasons, our work plays a fundamental role in the general comprehension of activity-driven nonequilibrium aggregation phenomena, since it is placed into a favored context: we are considering the effects of the activity on a system that already phase separate at equilibrium, and that is known for sure to phase separate even out of equilibrium.

The first step of the strategy we adopt to examine our problem from its ground is to slightly drive the system out of equilibrium, exploring then what happens at low Péclet numbers, within the range of surface fraction where we have previously observed two phase coexist in the system.

Figure 5.6 shows a summary of the evolution of the system at constant surface fraction $\phi = 0.734$ with Pe $= 2$ and it displays the first interesting result of such analysis. In the characterization of the passive phase transition, we have observed the system at $\phi = 0.734$ to equilibrate in a phase-coexisting way. Starting from the finishing point of the passive run, we have let the dumbbells to swim at low Pe. In this case the activity has the net effect to disrupted the ordered region and therefore to disfavor the phase separation. At $\phi = 0.760$, as is evident in the snapshots in figure 5.7, the situation is reversed. We consider, at $\phi = 0.760$, the condensed single-phase configuration resulted from an ordering dynamics of the passive system. This configuration immediately starts to phase separated at

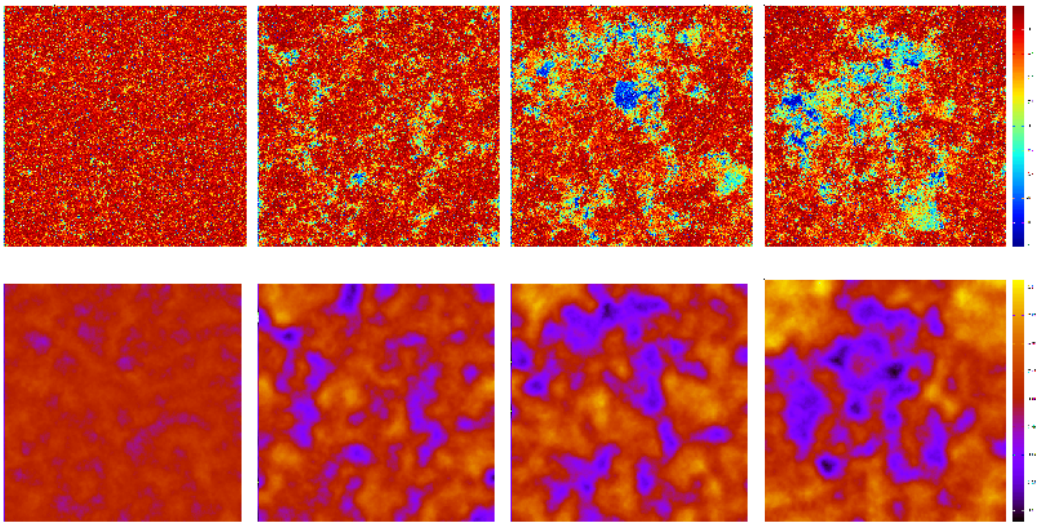


Figure 5.7: In the first line the local hexatic parameter for a simulation at $\phi = 0.760$. Snapshot at 0 (initial configuration taken from the last timestep of the passive run at $\phi = 0.760$), 1×10^6, 1×10^7, 5×10^7 timesteps of simulation. In the second line the surface fraction profiles of the system at the same time.

Pe = 2, due to the effect of the activity. Here, while for the passive system the phase separation region is already passed and the ordered phase has settled, due to self-propulsion two phases separate again.

We only give, at this level, a phenomenological description of these two cases. At not to high global densities, although some ordered aggregate is present in the passive system, it has a highly rough interface. This is for example the case we have shown at $\phi = 0.734$, which in the passive phase transition is placed slightly above the lower limit of the coexistence region. As the dumbbells acquire motility, such interfaces are easily broken and the ordered phase dissolves. The stationary situation yet present some small dense ordered region, but they are not observed to be stable. They move, dissolve and reaggregate, without forming any persistent cluster. As the global surface fraction is increased the passive phase separation ceases, in favor of the ordered solid. Switching on the self-propulsion, the dumbbell start to closer aggregate in stable ordered clusters, leaving low density disordered region in the available volume.

Although at the two mentioned cases the activity have an opposite effects on the phase separation (it opposes to the separation at $\phi = 0.734$ and favors it at $\phi = 0.760$), at both values of surface fraction it drives the system towards a less ordered configuration. At $\phi = 0.734$ the system, being partially ordered in the absence of activity, disorders due to the disruption

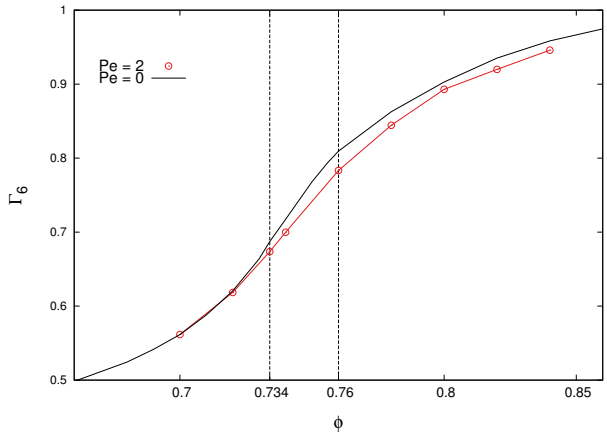


Figure 5.8: Sample average of the absolute value of the local hexatic parameter (4.9). Black line is the result already showed in figure 5.4-b at Pe = 0. An average over the runs at different starting point is made. Red circles refer to the same Γ_6 at Pe = 0. We have used again an average over the last timestep configuration of the simulation at each value of the surface fraction. Differently from the study at Pe = 0, we have not used different initial condition for the active system, but we have initialize the system with the arrival point of the corresponding passive run started from the close-packing condition.

of the dense phase. At $\phi = 0.760$ the passive hexatically ordered configuration separates, and a disordered liquid region appear. This features have their confirmation in the plot of figure 5.8, where we compare the global values of the modulus of the hexatic parameter (4.9) at Pe = 2 with their passive counterparts. As it clear from the figure , the global ordering behavior as function of the surface fraction of the dumbbell system deviates from the behavior of its passive counterpart, as it is slightly driven out of equilibrium by the self-propulsion. In particular, starting approximately from the lower bound of the passive coexistence region, activity lowers the ordering in the system.
However, also in presence of the activity, dumbbells order as the surface fraction of the system increases. In the next section we will examined how this ordering arise in the active case, even at higher values of the Péclet number.

5.3 Low-density limit of the phase separation region

In the previous section we have observed the main effects of weak activity on the aggregation properties of the dumbbells. The results illustrated, as

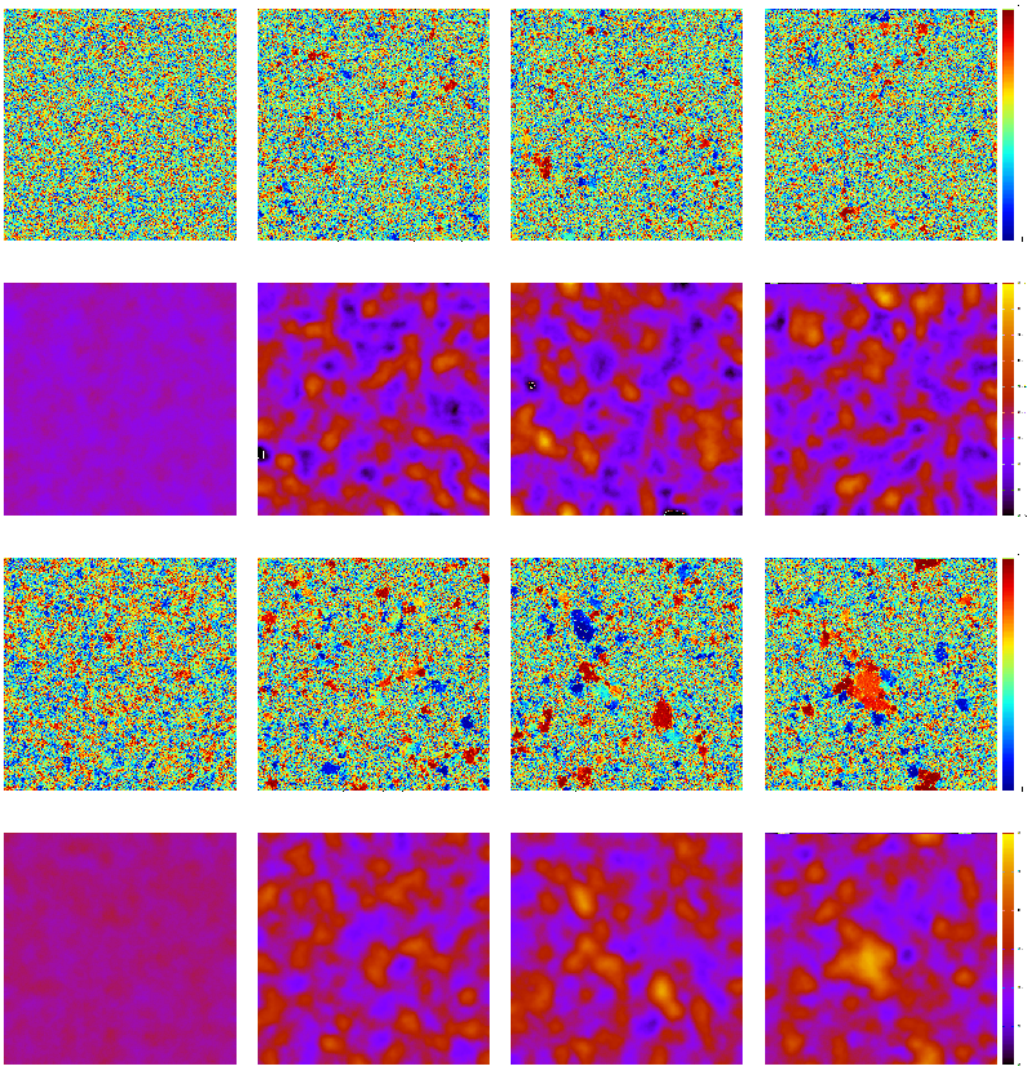


Figure 5.9: Local hexatic parameter for the Pe = 10, $\phi = 0.70$ (above) and $\phi = 0.72$ (below) systems at 0, 1×10^6, 1×10^7, 5×10^7 timesteps of simulation. The surface fraction profiles of the system at the same times is also shown.

we have discussed above, have allowed us to consider the phase separation as both an activity-driven and an "entropic-driven" phenomenon. This fact was already well known from previously studies about active systems, but our viewpoint deeply enters in the question of the balance between such driving effects.
Beside this more profound question, simulation at Pe = 2 immediately stimulates another interesting point. Since the system separates even at low Péclet number, it is possible to look at the variations of the phase

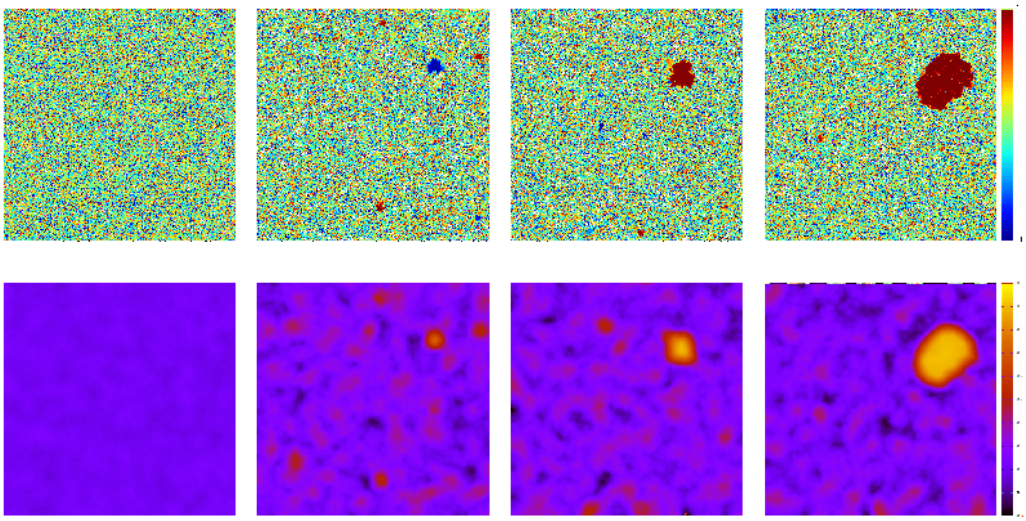


Figure 5.10: Local hexatic parameter (above) and the local surface fraction (below) for the Pe = 20, $\phi = 0.54$ systems at 0, 1×10^7, 2×10^7, 5×10^7 timestep of simulation.

separation region with continuity, starting from the coexistence at Pe = 0 and arriving in the far-from-equilibrium regime, where the MIPS has well established features?

We decide to face this question in steps. Therefore within this section we first hold our attention to the displacement, at increasing values of the activity, of the low-density limit of the phase separation region.
Having decide the starting point at Pe = 0 to coincide with the low-density bound of the coexistence region, the results of the previous section immediately indicate that, at the beginning of the active region, such lower limit slightly rises towards higher values of the surface fraction. We refer for such statement again to the system at $\phi = 0.734$. Although the system separate in the passive case, when particles are allowed to weakly propel, the two separated phases seem to melt, driving the system towards a more disordered state, as figure 5.8 clearly evidences. This is the more unexpected result, since one generally thinks that particles motility would favor ordering collective behavior and, in certain conditions, the phase separation, regardless the global density of the system. Indeed the very high activity regime was already known to deviate from such rule, since high active forces was demonstrated to destroy clusters, disfavoring phase separation. Our considerable claim consists to have observed such anomalous behavior even at the very low activity regime.

Once the strength of the active forces in increased, the more predictable rule settles, and activity begin to strongly drive phase separation. At

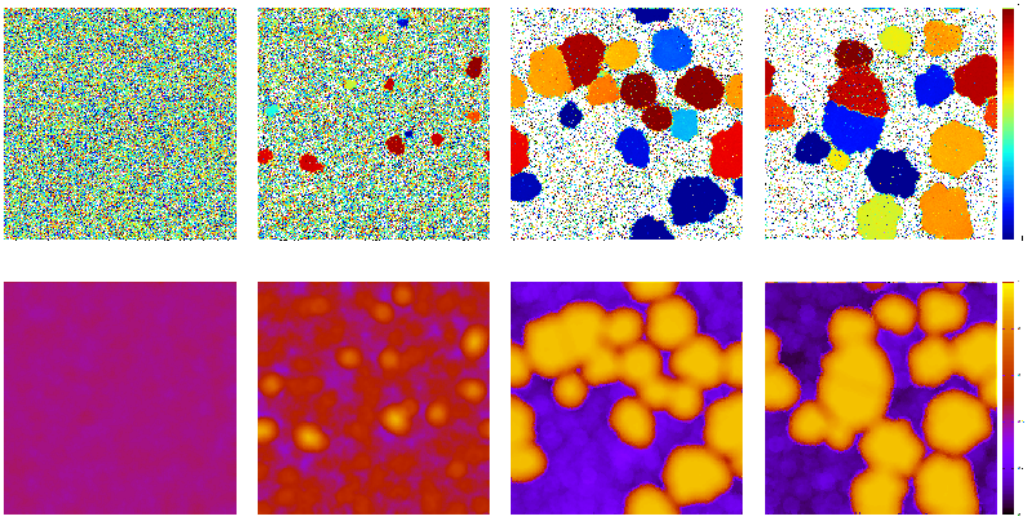


Figure 5.11: Local hexatic parameter (above) and the local surface fraction (below) for the Pe = 40, $\phi = 0.40$ systems at 0, 1×10^6, 1×10^7, 5×10^7 timestep of simulation.

Pe = 10 the value of the surface fraction where the system start to separate can be placed between $\phi = 0.70$ an $\phi = 0.72$. As shown in figure 5.9, at $\phi = 0.70$ small ordered regions begin to form within a disordered liquid phase. However such structures do not succeed to become stable, and continuously aggregate, melt and fluctuate in their positions. At $\phi = 0.72$ clusters of considerable size appear to arise and to gain stability. We say that the system succeeds to phase separate.

At higher values of activity the system starts to phase separate at lower values of surface fraction, since the self-propulsion effects continue to heavily dominate the aggregation mechanisms, against the entropic tendency of the system to disorder at low densities. At Pe = 20 the system separates at $\phi = 0.54$. At this value of surface fraction, we recover a standard motility-induced cluster formation dynamics. As is shown in figure 5.10, a little aggregate of dumbbells happens to form in the system, and subsequently it succeeds to grow and stabilize due to other dumbbells that swim towards it.

At Pe = 40 a similar situation is observed to already arise at $\phi = 0.40$, as shown in figure 5.11, where a number of large clusters form and begin to move and rotate in the system, leaving the rest of the box at a very low density.

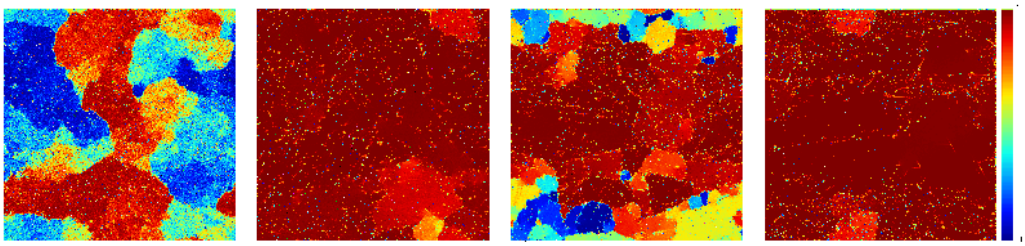


Figure 5.12: Local hexatic parameter for the high-density transition between phase-separate state and hexatically ordered state. From left to right: (Pe = 2, ϕ = 0.80), (Pe = 10, ϕ = 0.88), (Pe = 20, ϕ = 0.88) and (Pe = 40, ϕ = 0.90).

5.4 High-density limit of the phase separation region

For each considered value of the Péclet number, and increasing the value of the total surface fraction, the system phase separates approximately at the values established in the previous section, and it remains in a phase separated state. However at high densities phase separation ceases, and is replaced by an hexatically ordered single-phase state. As we have described before, the effect from which separation arise for active systems at high densities is quite clear. As, due to its activity, swimmers begin to accumulate is some region of the available volume, they empty some other region in the system, where dumbbells completely disorder, allowing for the coexistence of the two phases. Such kind of aggregation process gives us the possibility of understand how the upper bound of the coexistence region displaces, with respect to the global surface fraction of the system and the strength of the auto-propulsion force. As the activity rises, the ordered regions become denser, and they leave more free space to the disordered part of the system, globally favoring the coexistence of the two phases, even at higher values of the total density. For the same reason, at higher values of Pe, the ordered phase is allowed to occupy the entire box at increasing values of the global surface fraction. Since the single ordered phase settles provided no more free space is leaved to low-density disordered regions, as ordered cluster become denser, more dumbbell are needed for such condition to occur.

In figure 5.12 are shown, for each value of the Pe number, the lower density configurations at which the coexistence id observed to disappear.

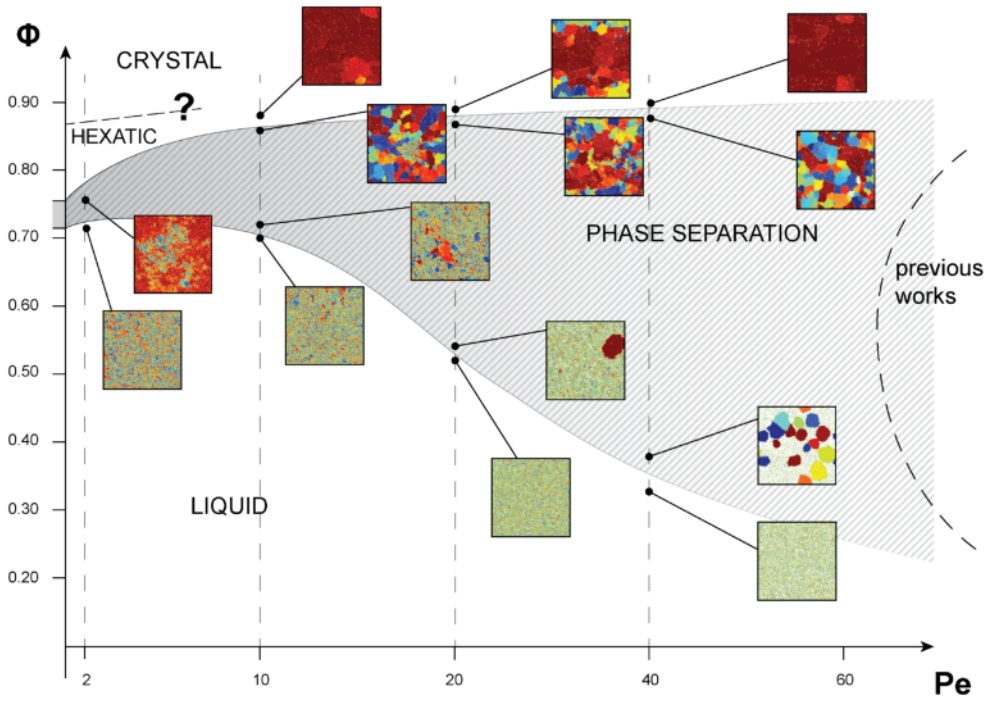


Figure 5.13: Phase diagram in the (Pe − ϕ) plane. The passive coexistence interval is indicate, and a sketch of the two bounds for the phase separation region is shown.

5.5 Phase diagram

Summarizing all the observations made, we can state that we do not see any discontinuity between the behavior of the system at Pe = 0 and at Pe > 0 at the densities at which there is phase co-existence in the passive limit. As in a conventional liquid-vapor transition it is very hard to establish where the first-order transition lies with high precision. Therefore, examining the results of long simulations within a large set of points in the (Pe − ϕ) plane, we have approximately established either in the passive case, or in the active one, where the limits of the coexistence region are placed. By means of such investigation, we have sketched a (Pe − ϕ) phase diagram for the dumbbell system for the low-Pe region. The phase diagram is shown in figure 5.13 and it includes some representative snapshots from simulation at different Péclet numbers, that clearly indicate where, starting from low densities, phase separation arises from the disordered phase and where, at higher densities, it ceases in favor of a hexatically ordered phase.

Conclusions and perspectives

As anticipated in the questions made at the opening of this thesis, our work has been dealt with an deep investigation about aggregation phenomena in the active dumbbell system. We have widely described two different kinds of aggregation.

- In the passive dumbbell two-dimensional system parameter space is observed to exist a coexistence region. As for the classical phase transitions framework, coexistence is generally associate to a first-order transitions. Since the constituents in our system interact by means of purely repulsive forces, a phase coexistence behavior, in which aggregation plays a fundamental role, is a first interesting result for the passive case, where there is no activity effects that would drive the collective behaviors. Such result slightly deviates from the main confirmed KTNHY scenario for melting in two dimensions, whereas it agrees with recent numerical results for the ordering transitions in 2D hard-disk systems. It then represents the first evidence of such first-order transition scheme for asymmetric repulsive-interacting two-dimensional systems.

- The active dumbbell system is known in turn to strongly phase separate due to activity, undergoing what is generally called motility-induced phase separation (MIPS). Within such context, we have achieved another important result. Active dumbbells are able to strong phase separate even at low values of activity strength. Therefore we have claimed that phase separation is not a pure far-from-equilibrium phenomenon, but it exists even at slightly perturbed equilibrium conditions.
  Such behavior represents a new step in the study of the motility-driven aggregation phenomena, that inspires a number of questions and some unexplored theoretical attempt, relative to a deep understanding of the physics of the active systems. Thanks to this feature,

for example, it has been possible to investigate, at least qualitatively, the interplay between the phase separation phenomena outlined above. We have thus slightly driven the system out of equilibrium, allowing for the particles in the system to weakly auto-propel, starting from the equilibrium coexistence conditions, and we have observed how such perturbation modifies the aggregation properties. We have found that activity intervenes differently, depending to the total surface fraction of the system. At low values of surface fraction, near the lower limit of the passive coexistence region, auto-propulsion breaks the ordered regions, that begin to "melt" starting from their rough interfaces, and therefore globally disfavor the phase separation. At high densities, in the surface fraction regime where the passive coexistence begin to cease, activity forces the dumbbells to densely pack in some region of the available volume, leaving the rest of the system in a low-density disordered phase, having the net effect of separating the two phases.
In conclusion, such careful study of the low Péclet parameter space region has provided the possibility to understand how the ordering transition evolves from the equilibrium scenario to the active one. As summarized in figure 5.13, we have described phase separation in a strictly continuity with the equilibrium phase coexistence. Such viewpoint is unique in the literature about the dumbbell system, and also about any other active Brownian system. An article that contains these new observations has been already submitted to a physics journal.
This qualitative characterization of the effects of the activity provides some first insights that will be developed in the future, in order to quantitative describe how pure entropic equilibrium properties and particle motility compete in the collective phenomena of aggregation and phase separation, that represent the ground of a number of fascinating events in active matter.

Appendix A

Two-dimensional positional order. The Mermin-Wagner thorem

Following the original works by Mermin and Wagner [MW66, Mer68], let us considered N classical particles interacting through a pair potential $\Phi(\mathbf{r})$, supposed to form a crystal with a lattice generated by the base vectors $\mathbf{a}_1$ and $\mathbf{a}_2$ (the argument is given in two dimensions; the one-dimensional case follows with the same strategy). The significative quantity are the Fourier components of the density defined by

$$\hat{\rho}_{\mathbf{k}} = \frac{1}{N}\langle \rho_{\mathbf{k}} \rangle \,, \tag{A.1}$$

where

$$\rho_{\mathbf{k}} = \int \mathrm{d}\mathbf{r}\, e^{-i\mathbf{k}\cdot\mathbf{r}} \rho(\mathbf{r}) = \sum_{i=1}^{N} e^{-i\mathbf{k}\cdot\mathbf{r}_i} \,, \tag{A.2}$$

with density concentrated at the particle's positions $\rho(\mathbf{r}) = \sum_{i=1}^{N} \delta(\mathbf{r} - \mathbf{r}_i)$. The so-called *static structure factor* is obtained from these quantities as

$$S(\mathbf{k}) = \frac{1}{N}\langle \rho_{\mathbf{k}}\, \rho^*_{\mathbf{k}} \rangle \,. \tag{A.3}$$

If $\mathbf{k}$ is a vector of the lattice reciprocal to that generated by $\mathbf{a}_1$ and $\mathbf{a}_2$, then $\hat{\rho}_{\mathbf{k}}$ will in general be nonzero, whereas it will vanish in the thermodynamic limit if $\mathbf{k}$ is not a reciprocal-lattice vector. The following criterion is than adopted for the crystal to exist:

(i) $\lim \hat{\rho}_{\mathbf{k}} = 0$ for $\mathbf{k}$ not a reciprocal-lattice vector;

(ii) $\lim \hat{\rho}_{\mathbf{k}} \neq 0$ for at least one nonzero reciprocal-lattice vector $\mathbf{k}$.

where "lim" denotes the theromdynamic limit. Mermin demonstrated that, if the interaction potential is sufficiently short-range, the second condition cannot be satisfied for $d \leqslant 2$. He actually showed that, if one chose $\mathbf{k}$ to be a reciprocal-lattice vector, in the thermodynamic limit would result

$$\begin{aligned} \hat{\rho}_{\mathbf{k}} &\leqslant 1/(\ln N)^{1/2} \quad \text{in two dimensions,} \\ \hat{\rho}_{\mathbf{k}} &\leqslant 1/\sqrt{N} \qquad \text{in one dimension.} \end{aligned} \tag{A.4}$$

A significant point of the Mermin theorem is that the bonds in (A.4) are weaker than bonds found for a harmonic model of crystal (used for example in the Peierls argument):

$$\begin{aligned} \hat{\rho}_{\mathbf{k}} &\sim N^{-k^2} \quad \text{in two dimensions,} \\ \hat{\rho}_{\mathbf{k}} &\sim e^{-Nk^2} \quad \text{in one dimension.} \end{aligned} \tag{A.5}$$

The weakness of the bonds allows for some other kind of ordering to be present even in two dimensions. If one supposes, within a two-dimensional harmonic crystal approximation, that equilibrium sites are $\mathbf{R} = n_1\mathbf{a}_1 + n_2\mathbf{a}_2$ and the actual instantaneous position of the particles are $\mathbf{r}(\mathbf{R}) = \mathbf{R} + \mathbf{u}(\mathbf{R})$, then the absence of long-range crystalline order is reflected in the divergence of the displacement correlation function

$$\langle [\mathbf{u}(\mathbf{R}) - \mathbf{u}(\mathbf{R}')]^2 \rangle \sim \ln|\mathbf{R} - \mathbf{R}'| \,, \text{ as } |\mathbf{R} - \mathbf{R}'| \to \infty \,.$$

We outline now a proof of this charactiristic divergence, that actually reveals that positional long-range order does not exist. In particular we show how thermal fluctuations in two-dimensional solids can destroy long-range crystalline order. The argument is inspired by [LLP80].
Consider an oredered configuration of particles in a two-dimensional system. This configuration can be completely described by a periodic density function, $\rho(x, y) = \sum_{\text{sites}} \delta[\mathbf{r}(x, y) - \mathbf{r}_{\text{sites}}]$ for a density concentrated at each lattice site. At finite temperatures, one expects each particle to vibrate about its equilibrium lattice position. Let $\mathbf{u}(x, y)$ denote the displacement field vector due to the thermal fluctuations of some small region labeled by the two-dimensional position vector $\mathbf{r}(x, y)$.

We are interested in mean-square displacements of the form $\langle [\mathbf{u}(\mathbf{r}) - \mathbf{u}(\mathbf{r}')]^2 \rangle$. Taking advantage of the periodicity of the lattice, $\mathbf{u}$ can be expanded as a Fourier series

$$\mathbf{u}(\mathbf{r}) = \sum_{\mathbf{k}} \mathbf{u}_{\mathbf{k}} e^{i\mathbf{k}\cdot\mathbf{r}} \,, \tag{A.6}$$

where the components of the vector $\mathbf{k}$ take both positive and negative values, and the coefficients $\mathbf{u}_\mathbf{k}$ are related by $\mathbf{u}_{-\mathbf{k}} = \mathbf{u}^*_\mathbf{k}$, since $\mathbf{u}(\mathbf{r})$ is real. The series includes terms with wave numbers $k \leqslant 1/d$, where d is the linear dimension of the region previously defined.
The harmonic crystal approximation consists of an expansion of the potential at each lattice site, up the second order in the displacements from equilibrium positions, the first order terms being indentically zero since its coefficients are the forces calculated in the equilibrium positions. Within this approzimation, one can perform the statistical average taking a probability density $w \propto \exp(-\beta U^{(\mathrm{harm})})$, where

$$\begin{aligned} U^{(\mathrm{harm})} &\propto \sum_{\mathbf{k}} \chi_{ijlm} k_l k_m u_{i,\mathbf{k}} u^*_{j,\mathbf{k}} \\ &\equiv \sum_{\mathbf{k}} \lambda_{ij}(\mathbf{k}) u_{i,\mathbf{k}} u^*_{j,\mathbf{k}} \,, \end{aligned} \tag{A.7}$$

where we have made use of the Fourier expansion and the indices i,j,l,m denote the cartesian components.

Because the probability density is Gaussian, one can immediately calculate the mean square fluctuations of the Fourier components of the displacements vector:

$$\langle u_{i,\mathbf{k}} u^*_{j,\mathbf{k}} \rangle \propto \frac{1}{\beta}\, \lambda^{-1}_{ij}(\mathbf{k}) \,, \tag{A.8}$$

where $\lambda^{-1}_{ij}(\mathbf{k})$ are the components of the tensor inverse to λ_{ij}. Because, from its definition in (A.7), $\boldsymbol{\lambda}$ is quadratic in k, one can write explicitly such dependence with $\lambda^{-1}_{ij}(\mathbf{k}) = \tilde{\lambda}_{ij}(\hat{\mathbf{k}})/k^2$.
FInally, summing over $\mathbf{k}$ and changing the discrete sum to an integral over $\mathbf{k}$, the mean square value of the displacement field is obtained:

$$\langle |\mathbf{u}|^2 \rangle \propto \frac{1}{\beta} \int \frac{\tilde{\lambda}_{ii}(\hat{\mathbf{k}})}{k^2}\, \mathrm{d}^d\mathbf{k} \,. \tag{A.9}$$

Note that in the limit of large distances (small wave numbers) the integral above diverges linearly for $k \to 0$ in one dimension, it diverges logarithmically in two dimensions and it not diverges for $d \geqslant 3$. As a rule, we can say that once, for large enought distance, $\sqrt{\langle u^2 \rangle} \gtrsim a$ (a being the lattice spacing) the long-range periodicity is lost.

However, as indicated in [Mer68], *directional* long-range order can establishes in two-dimensional systems, as suggests the evaluation of the following correlation for a field corresponding to the relative position of

two neighboring particles:

$$\begin{aligned}&\langle[\mathbf{r}(\mathbf{R}+\mathbf{a}_1)-\mathbf{r}(\mathbf{R})]\cdot[\mathbf{r}(\mathbf{R}'+\mathbf{a}_1)-\mathbf{r}(\mathbf{R}')]\rangle\\&=a_1^2+\langle[\mathbf{u}(\mathbf{R}+\mathbf{a}_1)-\mathbf{u}(\mathbf{R})]\cdot[\mathbf{u}(\mathbf{R}'+\mathbf{a}_1)-\mathbf{u}(\mathbf{R}')]\rangle\to a_1^2\end{aligned}$$

as $|\mathbf{R}-\mathbf{R}'|\to\infty$. If the particles were "frozen" to their equilibrium sites this would be a_1^2 identically. If, at non-zero temperature, thermal fluctuation suppressed long-range propagation of the local crystalline orientation, it would vanish at large $|\mathbf{R}-\mathbf{R}'|\to\infty$. In fact this is not the case, because such correlation approaches the finit non-zero value a_1^2.
We will illustrate in the next section how such ordering possibility allows to build a theoretical frame that has the purpose to describe what "crystallization" means, even in a two-dimensional space.

Bibliography

[AM76] N. W. Ashcroft and N. D. Mermin. ***Solid State Physics***. 1976.

[ASR02] R. Aditi Simha and S. Ramaswamy. **Hydrodynamic Fluctuations and Instabilities in Ordered Suspensions of Self-Propelled Particles**. *Phys. Rev. Lett.*, 89:058101, Jul 2002.

[AW62] B. J. Alder and T. E. Wainwright. **Phase Transition in Elastic Disks**. *Phys. Rev.*, 127:359–361, Jul 1962.

[BBK+13] I. Buttinoni, J. Bialké, F. Kümmel, H. Löwen, C. Bechinger, and T. Speck. **Dynamical Clustering and Phase Separation in Suspensions of Self-Propelled Colloidal Particles**. *Phys. Rev. Lett.*, 110:238301, Jun 2013.

[BJST+94] E. Ben-Jacob, O. Shochet, A. Tenenbaum, I. Cohen, A. Czirok, and T. Vicsek. **Generic Modelling of Cooperative Grouth Patterns in Bacterial Colonies**. *Nature*, 89:46, 1994.

[BK11] E. P. Bernard and W. Krauth. **Two-Step Melting in Two Dimensions: First-Order Liquid-Hexatic Transition**. *Phys. Rev. Lett.*, 107:155704, Oct 2011.

[BM09] A. Baskaran and M. C. Marchetti. **Statistical mechanics and hydrodynamics of bacterial suspensions**. *Proceedings of the National Academy of Sciences*, 106(37):15567–15572, 2009.

[BNK03] D. L. Blair, T. Neicu, and A. Kudrolli. **Vortices in vibrated granular rods**. *Phys. Rev. E*, 67:031303, Mar 2003.

[BSR01] M. Beekman, D.J.T. Sumpter, and F.L.W. Ratnieks. **Phase Transition between Disordered and Ordered Foraging in Pharaoh's Ants**. *PNAS*, 98:9703, 2001.

[CCD+07] L. H. Cisneros, R. Cortez, C. Dombrowski, R.E. Goldstein, and J.O. Kessler. **Fluid dynamics of self-propelled microorganism, from individuals to concentrated populations**. *Exp. Fluids*, 43:737, 2007.

[CGS15] L. F. Cugliandolo, G. Gonnella, and A. Suma. **Rotational and translational diffusion in an interacting active dumbbell system**. *Phys. Rev. E*, 91:062124, Jun 2015.

[FM12] Y. Fily and M. C. Marchetti. **Athermal Phase Separation of Self-Propelled Particles with No Alignment**. *Phys. Rev. Lett.*, 108:235702, Jun 2012.

[GLS14] G. Gonnella, A. Lamura, and A. Suma. **Phase segregation in a system of active dumbbells**. *International Journal of Modern Physics C*, 25(12):1441004, 2014.

[GMST15] G. Gonnella, D. Marenduzzo, A. Suma, and A. Tiribocchi. **Motility-induced phase separation and coarsening in active matter**. *Comptes Rendus Physique*, 16(3):316–331, 2015.

[GPBC10] F. Ginelli, F. Peruani, M. Bär, and H. Chaté. **Large-Scale Collective Properties of Self-Propelled Rods**. *Phys. Rev. Lett.*, 104:184502, May 2010.

[HN78] B. I. Halperin and David R. Nelson. **Theory of Two-Dimensional Melting**. *Phys. Rev. Lett.*, 41:121–124, Jul 1978.

[KK15] S. C. Kapfer and W. Krauth. **Two-Dimensional Melting: From Liquid-Hexatic Coexistence to Continuous Transitions**. *Phys. Rev. Lett.*, 114:035702, Jan 2015.

[KLVT08] A. Kudrolli, G. Lumay, D. Volfson, and L. S. Tsimring. **Swarming and Swirling in Self-Propelled Polar Granular Rods**. *Phys. Rev. Lett.*, 100:058001, Feb 2008.

[KT72] J. M. Kosterlitz and D. J. Thouless. **Long range order and metastability in two dimensional solids and superfluids. (Application of dislocation theory)**. *Journal of Physics C: Solid State Physics*, 5(11):L124, 1972.

[KT73] J. M. Kosterlitz and D. J. Thouless. **Ordering, metastability and phase transitions in two-dimensional systems**. *Journal of Physics C: Solid State Physics*, 6(7):1181, 1973.

[Lan37] L. D. Landau. *Phys. Z. Sowjet*, 11:26, 1937.

[LLP80] L. D. Landau, E. M. Lifshitz, and L. P. Pitaevskii. ***Course of Theoretical Physics. Vol.5 - Statistical Physics 1***. 1980.

[Mer68] N. D. Mermin. **Crystalline Order in Two Dimensions**. *Phys. Rev.*, 176:250–254, Dec 1968.

[MW65] J. E. Mayer and Wm. W. Wood. **Interfacial tension effects in finite, periodic, two-dimensional systems**. *The Journal of Chemical Physics*, 42(12):4268–4274, 1965.

[MW66] N. D. Mermin and H. Wagner. Absence of ferromagnetism or antiferromagnetism in one- or two-dimensional isotropic heisenberg models. *Phys. Rev. Lett.*, 17:1133–1136, Nov 1966.

[NH79] David R. Nelson and B. I. Halperin. **Dislocation-mediated melting in two dimensions**. *Phys. Rev. B*, 19:2457–2484, Mar 1979.

[NMR06] V. Narayan, N. Menon, and S. Ramaswamy. **Nonequilibrium steady states in a vibrated-rod monolayer: tetratic, nematic, and smectic correlations**. *Journal of Statistical Mechanics: Theory and Experiment*, 2006(01):P01005, 2006.

[NRM07] V. Narayan, S. Ramaswamy, and N. Menon. **Long-Lived Giant Number Fluctuations in a Swarming Granular Nematic**. *Science*, 317(5834):105–108, 2007.

[PDB06] F. Peruani, A. Deutsch, and M. Bär. **Nonequilibrium clustering of self-propelled rods**. *Phys. Rev. E*, 74:030904, Sep 2006.

[Pei32] R. E. Peierld. *Helv. Phys. Acta*, 7:81, 1932.

[Pur77] E. M. Purcell. **Life at low Reynolds number**. *American Journal of Physics*, 45(1):3–11, 1977.

[Ree00] S.G. Reebs. **Can a minority of informed leaders determine the foraging movements of a fish shoal?** *Animal Behaviour*, 59:403, 2000.

[Rey87] C.W. Reynolds. ***Computer Graphics***. 1987.

[Sch93] M. J. Schnitzer. **Theory of continuum random walks and application to chemotaxis**. *Phys. Rev. E*, 48:2553–2568, Oct 1993.

[SGL+14] A. Suma, G. Gonnella, G. Laghezza, A. Lamura, A. Mossa, and L. F. Cugliandolo. **Dynamics of a homogeneous active dumbbell system**. *Phys. Rev. E*, 90:052130, Nov 2014.

[SGMO14] A. Suma, G. Gonnella, D. Marenduzzo, and E. Orlandini. **Motility-induced phase separation in an active dumbbell fluid**. *EPL (Europhysics Letters)*, 108(5):56004, 2014.

[TT95] J. Toner and Y. Tu. **Long-Range Order in a Two-Dimensional Dynamical** XY **Model: How Birds Fly Together**. *Phys. Rev. Lett.*, 75:4326–4329, Dec 1995.

[TT98] J. Toner and Y. Tu. **Flocks, herds, and schools: A quantitative theory of flocking**. *Phys. Rev. E*, 58:4828–4858, Oct 1998.

[Tuc10] M.E. Tuckerman. ***Statistical Mechanics. Theory and Molecular Simulation***. 2010.

[VCBJ+95] T. Vicsek, A. Czirók, E. Ben-Jacob, I. Cohen, and O. Shochet. **Novel Type of Phase Transition in a System of Self-Driven Particles**. *Phys. Rev. Lett.*, 75:1226–1229, Aug 1995.

[VEC06] E. Vanden-Eijnden and G. Ciccotti. **Second-order integrators for Langevin equations with holonomic constraints**. *Chemical Physics Letters*, 429:310–316, Sep 2006.

[WSC+08] A. J. W. Ward, D. J. T. Sumpter, I. D. Couzin, P. J. B. Hart, and J. Krause. **Quorum decision-making facilitates information transfer in fish shoals**. *Proceedings of the National Academy of Sciences*, 105(19):6948–6953, 2008.

[You79] A. P. Young. **Melting and the vector Coulomb gas in two dimensions**. *Phys. Rev. B*, 19:1855–1866, Feb 1979.